

## Final Technical Report

15 November 1982 - 30 December 1984

FREQUENCY DEPENDENCE OF Q IN THE MANTLE  
UNDERLYING THE SHIELD AREAS OF EURASIA

by

Z.A. Der, A.C. Lees, V.F. Cormier  
L. Anderson, J. Burnetti, and M. MarshallTeledyne Geotech  
Alexandria Laboratories  
P.O. Box 334  
Alexandria, VA 22313DTIC  
ELECTE  
MAR 18 1985  
S D ESponsored by  
Advanced Research Projects Agency (DOD)  
ARPA Order No. 4493  
Monitored by AFOSR/NP Under Contract #F49620-83-C-0040

The views and conclusions contained in this document are those of the authors and should not be interpreted as necessarily representing the official policies, either expressed or implied, of the Defense Advanced Research Projects Agency or the U.S. Government.

Approved for public release;  
distribution unlimited.

AD-A151 367

DTIC FILE COPY

Unclassified

SECURITY CLASSIFICATION OF THIS PAGE

## REPORT DOCUMENTATION PAGE

1a. REPORT SECURITY CLASSIFICATION		1b. RESTRICTIVE MARKINGS	
2a. SECURITY CLASSIFICATION AUTHORITY		3. DISTRIBUTION/AVAILABILITY OF REPORT Approved for public release distribution unlimited.	
2b. DECLASSIFICATION/DOWNGRADING SCHEDULE			
4. PERFORMING ORGANIZATION REPORT NUMBER(S) AL-85-1		5. MONITORING ORGANIZATION REPORT NUMBER(S) AFOSR-TR- 85 - 0240	
6a. NAME OF PERFORMING ORGANIZATION TELEDYNE GEOTECH Alexandria Laboratories		7a. NAME OF MONITORING ORGANIZATION Air Force Office of Scientific Research	
6b. OFFICE SYMBOL (If applicable)		7b. ADDRESS (City, State and ZIP Code) Building 410 Bolling AFB, D.C. 20332	
6c. ADDRESS (City, State and ZIP Code) P.O. Box 334 Alexandria, Virginia 22313		7c. ADDRESS (City, State and ZIP Code)	
8a. NAME OF FUNDING/SPONSORING ORGANIZATION DARPA		8b. OFFICE SYMBOL (If applicable)	
9. PROCUREMENT INSTRUMENT IDENTIFICATION NUMBER F49620-83C-0040		10. SOURCE OF FUNDING NOS.	
11. TITLE (Include Security Classification) (See Block 16)		PROGRAM ELEMENT NO. 61101E	
12. PERSONAL AUTHOR(S) Der. Z.A., Lees, A.C., Cormier, V.F., Anderson, L., Burnett, J., Marshall, M.		PROJECT NO. 4493	
13a. TYPE OF REPORT Final		TASK NO. 00 <del>Task A</del>	
13b. TIME COVERED FROM 11/15/82 TO 12/30/84		WORK UNIT NO. Task A	
14. DATE OF REPORT (Yr., Mo., Day) 85-01-11		15. PAGE COUNT	
16. SUPPLEMENTARY NOTATION Frequency Dependence of Q in the Mantle Underlying the Shield Areas of Eurasia			
17. COSATI CODES		18. SUBJECT TERMS (Continue on reverse if necessary and identify by block number)	
FIELD	GROUP	SUB. GR.	
		Q Frequency Dependence of Q Attenuation	
19. ABSTRACT (Continue on reverse if necessary and identify by block number) Part I: Analyses of Short and Intermediate Period Data The results of short and intermediate period data analyses for the determination of a frequency dependent Q model of the mantle under the shield areas of Eurasia are presented. The spectra of short period P waves from nuclear explosions in the 1-8 Hz frequency range give $t_p^* \sim 0.15-0.2$ seconds. Using recordings of Soviet nuclear explosions at NORSAR, P wave profiles were assembled to study Q in the upper mantle under the Russian-Fennoscandian shield. Analyses of the relative amplitudes and frequency contents of the various upper mantle arrivals support the existence of an upper mantle low Q layer in this region, but the Q in this layer is high, around 700, compared to well studied tectonic regions of the western United States. A variety of measurements were used in the 0.3-1 Hz intermediate frequency band including S-wave periods, P and S rise times, ScS-ScP periods, and S-SS periods, giving $t_s^* \sim 1.8$ seconds, or $t_p^* \sim 0.45$ seconds.			
20. DISTRIBUTION/AVAILABILITY OF ABSTRACT UNCLASSIFIED/UNLIMITED <input checked="" type="checkbox"/> SAME AS RPT. <input type="checkbox"/> DTIC USERS <input type="checkbox"/>		21. ABSTRACT SECURITY CLASSIFICATION Unclassified	
22a. NAME OF RESPONSIBLE INDIVIDUAL Dr. Kadoski		22b. TELEPHONE NUMBER (Include Area Code) (202) 767-4906	
		22c. OFFICE SYMBOL YIP	

DD FORM 1473, 83 APR

EDITION OF 1 JAN 73 IS OBSOLETE.

Unclassified  
SECURITY CLASSIFICATION OF THIS PAGE

85 02 28 023

*Part II presents*  
Part II: Analyses of Long Period Data:

Long period multiple S and ScS phases observed in northern Europe were analyzed to determine mantle attenuation in the 0.02 to 0.2 Hz range under the Eurasian shield. Two groups of events are used: deep Far-Eastern earthquakes and large earthquakes near the edges of the shield areas of Eurasia. The Q of the upper mantle under the Eurasian shield region was estimated in the time domain by taking amplitude ratios and in the frequency domain by taking spectral amplitude ratios among various arrivals and matching waveforms of synthetic seismograms and observed data. Under shield regions SS/S amplitude ratios give  $t_s^* \sim 2.5-3$  seconds and multiple ScS amplitude ratios give  $t_s^* \sim 4.2$  seconds. Under tectonic regions, multiple S amplitude ratios suggest  $t_s^* \sim 5$  seconds. The results show that the upper mantle Q under this shield area is larger than the global average, but less than the Q values inferred from our studies of short period data in the same area. Preliminary results also suggest that at frequencies around 0.02 to 0.2 Hz, there is a  $\Delta t_s^*$  differential of around 2 seconds between shield and tectonic regions.

*Part III provides*  
Part III: The Q Model:

A large set of broad band data was analyzed to determine the frequency and depth dependence of Q for P and S waves under the northern shield areas of Eurasia. A wide range of techniques utilizing spectra, amplitude ratios and waveform modeling were used to derive apparent and absolute  $t^*$  estimated for P and S waves covering the seismic band between 0.01 to 10 Hz. A Q model of the Eurasian shield was constructed on the basis of these results. The data require a model in which Q increases with frequency and which is characterized by Q values in the upper mantle that are generally higher than those of global average models. The model with the best fit includes a minimum in Q between about 100 and 200 km depth and high Q values of the order of thousands throughout the bulk of the mantle. The long period multiple ScS may require a low Q zone near the core-mantle boundary. Preliminary results suggest that  $t^*$  versus frequency in tectonic regions is higher and roughly parallel, or slightly divergent towards low frequencies, when compared to  $t^*$  versus frequency in shield regions, with a  $t_p^*$  differential of about 0.2 seconds.

*A supplement discusses*  
Supplement: Methodologies for Estimating  $t^*(f)$  from Short Period Body Waves and Regional Variations of  $t^*(f)$  in the United States. *Keywords include: Attenuation*

In this paper we discuss some aspects of estimating  $t^*$  from short period body waves and present some limits on  $t^*(f)$  models for the central and southwestern United States (CUS and SWUS). We find that for short period data, with frequencies above 1 or 2 Hz, while the average spectral shape is stable, the smaller details of the spectra are not; thus, only an average  $t^*$ , and not a frequency-dependent  $t^*$ , can be derived from such information. Also, amplitudes are extremely variable for short period data, and thus a great deal of data from many stations and azimuths must be used when amplitudes are included in attenuation studies.

The predictions of three pairs of models for  $t^*(f)$  in the central and southwestern United States are compared with time domain observations of amplitudes and waveforms and frequency domain observations of spectral slopes to put bounds on the attenuation under the different parts of the country. A model with the  $t^*$  values of the CUS and SWUS converging at low frequencies and differing slightly at high frequencies matches the spectral domain characteristics, but not the time domain amplitudes and waveforms of short period body waves. A model with  $t^*$  curves converging at low frequencies, but diverging strongly at high frequencies matches the time domain observations, but not the spectral shapes. A model with nearly-parallel  $t^*(f)$  curves for the central and southwestern United States satisfies both the time and frequency domain observations.

We conclude that use of both time and frequency domain information is essential in determining  $t^*(f)$  models. For the central and southwestern United States, a model with nearly-parallel  $t^*(f)$  curves, where  $\Delta t^* \sim 0.2$  seconds, satisfies both kinds of data in the 0.3-2 Hz frequency range.

Accession For	
NTIS GRA&I	<input checked="checked" type="checkbox"/>
DTIC TAB	<input type="checkbox"/>
Unannounced	<input type="checkbox"/>
Justification	
By _____	
Distribution/	
Availability Codes	
Dist	Avail and/or Special
A-1	



**Frequency Dependence of Q in the Mantle**  
**Underlying the Shield Areas of Eurasia,**  
**Part I: Analyses of Short and Intermediate Period Data**

by  
Zoltan Der  
Alison Lees  
Vernon Cormier\*  
and  
Lisa Anderson

Teledyne-Geotech  
314 Montgomery Street  
Alexandria, Virginia 22314

\* Earth Resources Laboratory  
Massachusetts Institute of Technology  
Cambridge, Massachusetts 02412

11 January 1985

AIR FORCE OFFICE OF SCIENTIFIC RESEARCH (AFSC)  
NOTICE OF TRANSMITTAL TO DTIC  
This technical report has been reviewed and is  
approved for public release under AFM APR 190-12.  
Distribution is unlimited.  
MATTHEW J. KENNEL  
Chief, Technical Information Division

### Abstract

The results of short and intermediate period data analyses for the determination of a frequency dependent  $Q$  model of the mantle under the shield areas of Eurasia are presented. The spectra of short period  $P$  waves from nuclear explosions in the 1-8 Hz frequency range give  $\bar{t}_P^* \sim 0.15-0.2$  seconds. Using recordings of Soviet nuclear explosions at NORSAR,  $P$  wave profiles were assembled to study  $Q$  in the upper mantle under the Russian-Fennoscandian shield. Analyses of the relative amplitudes and frequency contents of the various upper mantle arrivals support the existence of an upper mantle low  $Q$  layer in this region, but the  $Q_P$  in this layer is high, around 700, compared to well studied tectonic regions of the western United States. A variety of measurements were used in the 0.3-1 Hz intermediate frequency band including  $S$ -wave periods,  $P$  and  $S$  rise times,  $ScS$ - $ScP$  periods, and  $S$ - $SS$  periods, giving  $t_S^* \sim 1.8$  seconds, or  $t_P^* \sim 0.45$  seconds.

## Introduction

In order to determine the functional forms of frequency dependence of  $Q$  in the mantle under a specific region, broad-band measurements of attenuation must be made on seismic waves that traversed the mantle under the same region. Since the various kinds of methods for the estimation of  $Q$  are biased in different ways by other factors it is desirable to combine various methodologies rather than to rely on one method. Only  $Q$  models that are compatible all kinds of data can be accepted as valid representations of the Earth's structure. While the frequency dependence of  $Q$  is often asserted on the incompatibility of  $Q$  values from free oscillation studies and short period body wave measurements, it must be remembered that while free oscillations give globally averaged  $Q$  structures, attenuation estimates from body waves are specific to given paths. The discrepancies in the  $Q$  between the two kinds of methods can be explained in other ways. This study attempts to determine the frequency dependence under the Eurasian shield from broad-band analyses of teleseismic body waves confined to the shield area. The general plan of the study is to make  $Q$  estimates in several overlapping narrow frequency bands and piece together the best fitting model, frequency dependent if necessary, from a variety of measurements.

In this paper, we present results of a study of  $t^*$  under the Eurasian shield for frequencies between 0.5 and 8 Hz. The following paper presents results for frequencies between 0.3 and 0.5 Hz (Lees et al, 1984, hereafter referred to as Paper II) and the third paper presents the frequency dependent  $Q$  models that we have developed from this broadband study (Der et al, 1984a, hereafter referred to as Paper III).

Estimation of  $Q$  in the short period band is facilitated by the increasing availability of high quality digital data which enables one to measure the high frequency (3-8 Hz) content of teleseismic short period body waves. The sensitivity of short period body wave spectra to  $Q$  is such that very accurate estimates (to 0.1 seconds) of the attenuation parameter  $t_p^*$  may be obtained in spite of uncertainties in source spectra. Even

crude measurements of some obvious time domain signal characteristics such as rise times (Stewart, 1984) or dominant periods (Der et al, 1982) put stringent limits on the possible values of mantle  $Q$ . The mere observability of some short period arrivals, such as SS, is proof of high  $Q$  along the path (for example, SS at  $80^\circ$  with a period of less than 2 seconds and  $t_{SS}^* \sim 5$  seconds or  $t_S^* \sim 2.5$  seconds suggest an average  $Q_S \sim 350$  for the upper 900 km of the mantle). Clearly, the formerly accepted values of  $t_P^*$  of 1 second and  $t_S^*$  of 4 seconds are incompatible with the time and frequency domain characteristics of seismic waves in the intermediate and short period bands.

The northern parts of the Eurasian continent constitute a classical shield with high upper mantle velocities. Although recent work in tomographic inversions for laterally varying earth structure (Clayton and Comer, 1983; Nataf et al, 1984; Woodhouse and Dziewonski, 1984) are rapidly changing our concepts of tectonic classifications, the results do show that this part of the world is underlain by a deep high velocity "root". In contrast, the adjoining regions of Iran, Afghanistan, Korea, China, and Southeast Asia are characterized by low velocities in the underlying upper mantle. The shield areas of this continent are also bounded by the North American Plate east of the Lena river. The decompositions of the Earth velocity structure using low order spherical harmonics do not allow us to distinguish fine details, and many apparent fine structures may be side lobes produced by the analysis procedures (Tanimoto and Kanamori, 1984). Since we want to determine the  $Q$  model for the mantle under the shield area, we shall take special care not to mix data from various regions, but separate out the effects of propagation through the mantle under the adjoining tectonically active regions.

Previous work on attenuation in the short period band has yielded  $t_P^*$  around 0.15 seconds (Bache, 1984; Der et al, 1984b) for Soviet test sites on the Eurasian shield, and  $t_P^*$  around 0.15 seconds and 0.35 seconds for the eastern and western United States, respectively (Lay and Helmberger, 1981; Der et al, 1982; Der et al, 1984b).



Short and intermediate period P and S wave data from Soviet nuclear explosions and earthquakes in the Far East were analyzed using a variety of methods in the time and frequency domains. This study of the Q in the short and intermediate period band is followed by a study of attenuation in the long period band (Paper II). In each narrow frequency band we treat Q as a constant and all the pieces of information are collected in Paper III and a broad band, frequency dependent Q model is constructed. The reasons for not constructing an initial frequency dependent model from the short period data alone are given in a companion paper included with this final report (Der and Lees, 1984). Briefly stated, there is no convincing evidence for any rapid variation of Q with frequency, and the use of quasi-constant apparent Q in narrow frequency bands will thus introduce no appreciable errors in the final conclusions. In all of our data analyses we make a distinction between results for absolute  $t^*$  and apparent  $t^*$ ,  $\bar{t}^*$ ; for more detailed explanation of these terms the reader is referred to Part III of this paper.

### **Analyses of Short Period P Waves from Nuclear Explosions**

For the studies of attenuation at the highest frequencies, we have utilized P wave recordings from nuclear explosions in the Soviet Union obtained at NORSAR and other Scandinavian and Northern European stations. Typically, these explosions produce significant energy at frequencies up to 8 or 10 Hz at NORSAR. In spite of the limitations of the present system at NORSAR which employs gain ranging (Bungum, 1983), seismic energy in the 3-8 Hz range is present in most seismic P wave signals propagating through the mantle under shield regions. These high frequency arrivals were used to estimate  $t^*$  from spectra, P-wave profiles, and spectral ratios of the P branches.

Spectra of P waves were computed for the first arrivals of a suite of Soviet explosions, some examples of which are shown in Figure 1 for NORSAR recordings. The spectra were computed using a 12 second time window containing about 7 seconds of the

initial P wave, a Parzen taper, and 10 point smoothing on the power spectra. A noise window preceding the arrival was treated in a similar manner. The positioning of the signal window was designed to avoid an excessive distortion of the first arrival by tapering; the Parzen taper also has very small side lobes, thus preventing the leakage of the signal energy from low to high frequencies which may lead to the overestimation of high frequency energy in the signals. As typical of signal spectra from most USSR explosions recorded in Fennoscandia, these show high frequency energy above the noise level to frequencies of 6-8 Hz. In order to avoid problems with the artificial apparent high frequency energy generated by the variable quantization associated with gain ranging, all energy below 1% of the peak amplitude level is disregarded. Even with these conservative assumptions it appears that the range of valid signal frequencies extends to 6-8 Hz in some teleseismic signals at NORSAR. Due to the sensitivity of high frequency energy to  $Q$ , these spectra provide robust constraints on any frequency dependent  $Q$  models of the upper mantle almost irrespective of the uncertainties in the details of source spectra.

At NORSAR the assumption of a cube-root scaled source according to the von Seggern and Blandford (1972) model yielded the apparent  $t_p^*$  values from Soviet Peaceful Nuclear Explosions shown plotted on a map in Figure 2. Over the 1-8 Hz band,  $t^* \sim 0.1$ -0.25 seconds. These low values indicate a high  $Q$  upper mantle under the sources as well as under the NORSAR receivers. Although our choice of source spectral models has some effect on our  $t_p^*$  estimates, other plausible source models such as that proposed by Mueller and Murphy (1971) give essentially the same result over this wide frequency band. This is because both the von Seggern-Blandford and Mueller-Murphy models fall off as  $\omega^{-2}$  at high frequencies and the attenuation is estimated in the frequency range where the spectra fall off at the same rate. However, the models of Helmberger and Hadley (1981) and Lay et al (1984), which fall off as  $\omega^{-3}$ , would yield even lower, sometimes negative,  $t_p^*$  values, which in itself indicates that such models do not give an accurate description of the seismic source. This is not surprising since

near-field recordings of explosions, and most earthquakes as well, often require  $\omega^{-2}$  falloff in the deduced far-field spectra. Moment tensor inversions of near field data usually give spectral falloffs somewhat greater than  $\omega^{-2}$  (Stump and Johnson, 1984), but such methods tend to underestimate high frequency energy if, as is usually the case, it tends to be incoherent.

In addition to estimating  $t^*$  from individual spectra, we have estimated  $t^*$  from stacked spectra in order to estimate the variance in the  $t^*$  measurements. Figure 3 shows two of the stacked spectra with 95% confidence limits. Curves for several different  $t^*$  models are superimposed on the data, and it is clear that while the data can generally distinguish between  $t^*$  values, it cannot distinguish between models where  $t^*$  varies slowly with frequency and models with constant  $t^*$ . Bache (1984) found similar values of  $t_p^* \sim 0.14$  seconds from extensive spectral averaging at the British arrays in Scotland (EKA), India (GBA), and northern Canada (YKA) of Soviet nuclear tests at Kazakh. While Bache chose to fit his data with frequency dependent Q models, he noted that a variety of models are consistent with the observed data. Thus, in the short period band  $t_p^*$  is indistinguishable from a constant, as it has been previously suggested (Der et al, 1982; Shore, 1983; Der and Lees, 1984).

In addition to computing the spectra of first arrival P waves, we have assembled the NORSAR recordings of these events into profiles following the approach of Masse and Alexander (1974) and King and Calcagnile (1976). For each individual event several sensors at NORSAR were used to obtain a dense coverage with respect to epicentral distance. Since in this study we are not concerned with the velocity structure, we will use the previously published velocity structure of King and Calcagnile (1976) as a starting point and modify it as needed to match the amplitude and spectral characteristics of these profiles. Figures 4 to 7 show the profiles unfiltered and filtered into various frequency bands. The amplitudes of P waves in these profiles were normalized with respect to magnitude and increased proportionally with the square root of distance in order to improve readability. The travel time triplications according to King and

Calcagnile are superposed on each figure. Although the travel time branches shown in these figures may create the impression that they are largely derived by subjective interpretation, more detailed sections constructed from larger sets of sensors, in the manner of King and Calcagnile (1976) (Figures 8 to 10) show that, although the relative amplitudes of arrivals are variable, the arrivals themselves are quite distinct and continuous across the NORSAR array.

Inspecting the principal characteristics of the various arrivals in the time domain the following major features are apparent: the B branch extends to about  $32^\circ$  in distance and in the  $16\text{-}20^\circ$  range the arrivals on the A branch are about one half to one third the amplitude of arrivals on the BC and CD branches. Both the KCA velocity model of King and Calcagnile (1976) and the K8 velocity model of Given and Helmberger (1980) were compared with these observations. These two models is shown in Figure 11; the PREM model of Dziewonski and Anderson (1981) was used for the lower mantle in both cases. Figures 12 and 13 show sets of synthetic record sections computed by the WKB method (Chapman, 1978; Dey-Sarkar and Chapman, 1978) for the KCA and K8 velocity models, assuming an elastic earth, a von Seggern and Blandford source function (1972), and the short period NORSAR instrument response. The K8 model contains a low velocity zone in the upper mantle as seen in Figure 11, which gives low AB/CD amplitude ratios, actually smaller than observed, and a shortened B branch terminating at about  $23^\circ$  instead of  $32^\circ$ . Inspection of the data used by Given and Helmberger reveals that the data for the Novaya Zemlya explosions, which are included in the data set used to derive K8, is quite different from the data from explosions elsewhere in the USSR in that the B branch is weak or missing at distances beyond  $27^\circ$ . Thus the K8 model is inconsistent with observations from the Eurasian shield and we must conclude that paths involving Novaya Zemlya are not representative of our study area. The KCA model shows an extended B branch, but the AB/CD amplitude ratios around  $16\text{-}20^\circ$  are too large. However, this amplitude discrepancy can be explained by a low Q layer at the depth of about 150 km. Thus, the velocity structure can be kept identical to the

King and Calcagnile model (1976).

Inspecting Figures 4 to 7 reveals that there is not much change in the patterns of arrivals as functions of the changes in the frequency bands. This by itself is an indication of a high  $Q$  environment in the upper mantle. If the overall envelopes of all arrivals were the same in all frequency bands this would indicate an infinite  $Q$  throughout the upper mantle under the Eurasian shield.

To measure more subtle changes in the frequency content of the various travel time branches and to put further constraints on the upper mantle  $Q$  model, we have computed spectral ratios between some of the  $P$  travel time branches. This approach has the advantage that source and receiver effects cancel and using many traces one can assess the reliability of the results by comparing the spectral ratios between neighboring sensors. First, we need to consider the effect of upper mantle structure on the  $P$ -wave spectra, as any structural contribution to the spectra must be separated from the contributions of intrinsic attenuation. To investigate this problem, we computed suites of synthetic seismograms using the WKBJ method for the King and Calcagnile velocity model. Since no attenuation was included in producing the synthetics, spectral ratios between branches of the synthetics give an estimate of the structural contribution to the total measured attenuation. Spectral ratios at  $16^\circ$  and  $30^\circ$  are shown in Figure 14. For  $CD/AB$  at  $16^\circ$ ,  $\bar{t}^* \sim -0.02$  seconds and for  $AB/EF$  at  $30^\circ$ ,  $\bar{t}^* \sim 0.04$  seconds; thus at these high frequencies, upper mantle structure may have an observable effect on the spectra and should be considered when estimating the intrinsic attenuation. It may be also argued however, that these synthetic records may not be realistic and detailed enough to model fine spectral details. Indeed we have only included the directly returned rays in the calculations, and reverberations, which cause long ringing wavetrains were not modeled. Since the synthetics for the directly returned rays indicate spectral differences between the branches similar to those observed, as shown below, the limiting assumption that may be made is that all these differences are due to anelasticity. This would overstate the amount of attenuation in

the mantle.

Examples of observed spectral ratios, offset in absolute value to show the overall slopes better, are shown in Figure 15. Only a few are shown for clarity, but about ten were computed for each combination of travel time branches for the same event. These figures show that although the slopes are small they are fairly consistent and repeatable for the same combination of travel time branches, giving  $\bar{t}_P^* \sim -0.07$  seconds for CD/AB and  $\bar{t}_P^* \sim 0.07$  seconds for AB/EF, and give net  $\bar{t}_{PS}^*$  of -0.05 and 0.03 seconds for the CD/AB and AB/EF ratios, respectively, if the above estimate of the effect of upper mantle structure has been accounted for. If the Q were constant throughout the structures involved we would see the values of  $\bar{t}_P^*$  proportional to the travel times. The relative  $\bar{t}_P^*$  difference between the AB and BC-CD branches around 16° epicentral distance is just the reverse of this. Thus there must be some vertical variation in Q, consistent with the presence of a low Q zone as suggested above. A low Q layer would reduce the amplitudes of the A branch close to the observed values given the high dominant frequencies (around 2.5 Hz) of the P waves shown in Figures 4 and 7 to 10 assuming that the  $t^*$  in excess of the estimated structural effect is due to intrinsic attenuation. One could conceivably put a combination of slightly lower velocity and low Q at this depth. However, the presence of almost any sort of low velocity layer in the upper 400 km substantially reduces the distance to which the AB arrival extends on the travel time curves.

The Q-velocity model that reproduces our observations of relative amplitudes and spectra of upper mantle arrivals as well as the  $\bar{t}^*$  estimates from direct, first arriving P waves is shown in Figure 16. Although this model has a "low Q layer" in the upper mantle, the  $Q_P$  value there is about an order of magnitude higher than those derived for the same depth under the western United States (Der and McElfresh, 1977) and thus contains, actually, quite high Q values in the absolute sense. The Q values may actually be even higher if some of the spectral differences between the branches are due to struc-

ture. This Q model in conjunction with the KCA velocity model satisfies all the criteria, the extended B branch, the low amplitudes of the first arrivals in the 16-20° range, and the spectral ratios. In Figure 17 we show some representative  $t_p^*$  values, derived by raytracing through this model, that imply the kind of spectral differences in the upper mantle arrivals seen in the data. The typical  $t^*$ 's in this figure are about 0.1 second greater than the  $\bar{t}^*$ 's found previously from spectra. The reason for this can be seen in Paper III; our final Q model is frequency dependent, with  $t^*$  decreasing as frequency increases. Thus, the apparent  $t^*$ ,  $\bar{t}^* = t^* + dt^*/df$ , is less than  $t^*$ , and there is really no discrepancy between the  $\bar{t}^*$ 's from the spectral measurements and the  $t^*$ 's on Figure 17.

It must be noted that no low velocity layer is needed to match the observations. The data does not permit a more precise definition of the details of the depth distribution of Q. The depth of our postulated low Q layer may vary and it may not be homogeneous, but the data imply a weak low Q layer at a shallow depth as required by most proposed physical models of attenuation for high frequency seismic waves (Lundquist and Cormier, 1980; Anderson and Given, 1982). The P wave spectra and our analyses of the frequency contents of the various upper mantle arrivals provide the constraints for our frequency dependent shield Q model in the 1-8 Hz range.

### Data Analyses of Intermediate Period Phases

In the "intermediate" period band, 0.3-1 Hz, a variety of data analyses were done on P and S waves recorded at short period WWSSN stations in northern Europe and Fennoscandia. Rise times of P and S waves provide upper limits on  $\bar{t}^*$  at the appropriate frequencies. The relative periods of P-PP, S-SS, and ScP-ScS pairs also provide estimates of  $\bar{t}^*$ , and the relative amplitudes of short and long period S and SS give an estimate of  $\bar{t}^*$  at lower frequencies. Each of these approaches and the corresponding

results are discussed in the following sections.

### Rise Times of P Waves from Nuclear Explosions

A time domain approach to the estimation of  $Q$  for body waves is the matching of rise times (Stewart, 1984). The idea is that  $\bar{t}^*$  is the controlling factor that determines the overall gross shape of the initial swing of the short period P waveform as characterized by a "rise time". Other factors that may influence the rise time are the shape of the initial source pulse, the time lag between P and pP, and "stochastic dispersion" (Richards and Menke, 1983; McLaughlin et al, 1984). For nuclear explosions we have a reasonably good idea about the minimum rise times of the source pulses from near field measurements; these are the shortest for shots in hard rock. The minimum P-pP time lag may be obtained by assuming that the explosion was buried at a relatively shallow scaled depth ( $h=0.07Y^{1/3}$ , where the depth  $h$  is given in km and the explosion yield  $Y$  in kilotons) and assuming that the near surface velocities are high. Deeper burial depths and lower uphole velocities would give overly high, conservative upper limits for  $\bar{t}_p^*$ .

Rise time is usually defined as the time between the first maximum and the intersection of the tangent to the rising portion of the P waveform with the maximum slope with the zero amplitude level. Since the maximum slope is hard to measure we have used the time between the first break and the first maximum as rise time. We have used the same definition in our theoretical simulations and, therefore, this modification of the procedure has no effect on our conclusions. We have measured the rise times for a set of USSR nuclear explosions and one Indian nuclear explosion at NORSAR. The theoretical rise times were computed by using the cube-root scaled von Seggern and Blandford (1972) granite source model, the minimum scale depth, a range of apparent  $t^*$  from 0 to 1 seconds, a surface reflection coefficient of unity and an uphole velocity of 5.5 km/sec. The observed rise times are plotted against the apparent  $t^*$  values in Figure 18. The four curves in the figure correspond to the



theoretical values for four yields. Each observed rise time is plotted such that the ordinate is equal to the observed rise time, and the point is located between the curves to correspond to its  $m_b$ -estimated yield. The projection of each point on the horizontal axis gives an apparent  $t^*$  value which, in view of the conservative assumptions we have used, must be an upper limit. The results in Figure 16 indicate an overall upper limit for  $t_P^*$  in the range of 0.3-0.7 seconds with the mean value slightly higher than 0.5 seconds. These results agree with those of Stewart (1984) who obtained a similar mean value for USSR explosions at YKA, also a shield station. These observations effectively rule out models which have  $t^* \sim 1$  second around 1 Hz, since, with the NORSAR instrument response, the rise times should be much higher, in the range of 0.4-0.5 seconds, rather than the observed 0.15-0.3 seconds.

The estimate  $\bar{t}_P^* \sim 0.5$  seconds from rise times is significantly greater than the estimate  $\bar{t}_P^* \sim 0.15$  seconds from spectra. Theoretically, in a minimum phase, causal waveform, all frequencies arrive at the same time, so due to their shorter wavelength, the higher frequencies have most influence on the rise time and thus the rise time of the initial pulse is less than one fourth the period. However, observed rise times are often greater than one fourth the period, and it has been observed that often the higher frequencies in the P wave arrive somewhat later than the lower frequencies (McLaughlin and Anderson, 1984). The higher frequencies probably arrive later due to scattering along the ray path as opposed to intrinsic attenuation, and thus the longer rise times overestimate  $\bar{t}^*$  and serve as upper bounds on the attenuation. Recent theoretical work on stochastic dispersion (Richards and Menke, 1983; Frankel and Clayton, 1984; McLaughlin and Anderson, 1984; McLaughlin et al, 1984) also indicates that such upper limits for  $\bar{t}_P^*$  from rise times are probably overestimated, and therefore impose even more severe constraints on the admissible values of  $\bar{t}^*$  than previously thought, since the group delay due to the randomness of media increases with increasing frequency thus increasing the rise times independently of Q effects.

## Waveforms of Short Period S Waves

Short period S waves observed at WWSSN stations in Scandinavia from Far-Eastern deep earthquakes usually have very short periods (between 1 and 2 seconds) as shown in Figure 19. The waveforms and amplitudes of short period S waves should be quite sensitive to the  $Q$  in the upper mantle. However, the waveforms should give a more robust measurement of  $t_S^*$  than the amplitudes since the amplitudes are more affected by factors such as radiation pattern and earth structure than is the frequency content. We have estimated  $\bar{t}_S^*$  by comparing the periods of S waves with synthetic waveforms.

Synthetic waveforms for a range of source durations and  $t^*$ 's, as shown in Figure 20, were used to determine the  $\bar{t}_S^*$  values corresponding to the observed waveforms. In Figure 20, the amplitudes of the waveforms have been normalized. For a given source duration, the period of the waveform clearly varies significantly as  $t^*$  varies. Table I is a tabulation of the periods of such synthetics. In Figure 21, the period of synthetic waveforms like those in Figure 20 is plotted versus the  $t^*$  used in the simulation, for source durations ranging from an impulse to a triangle function of three seconds duration. On the right hand side of the figure, arrows correspond to the periods measured for short period S arrivals from deep Far Eastern events as recorded at Scandinavian stations. The  $\bar{t}_S^*$  that these observations correspond to depends on the choice of source duration. However, for reasonable source durations of 1 to 2 seconds, these arrivals suggest  $\bar{t}_S^* \sim 0.5$  to 1.5 seconds. Since these arrivals are from deep events, they only travel through the relatively attenuating upper mantle once. If the bulk of the attenuation is conservatively estimated to occur in the upper mantle, doubling the  $\bar{t}_S^*$  estimate above to 1 to 3 seconds should provide an upper bound on the  $\bar{t}^*$  estimate.

## Waveforms of Short Period S-SS Pairs

The waveforms and amplitudes of short period S and SS pairs should be quite sensitive to the  $Q$  in the upper mantle. We have made another estimate of  $\bar{t}_S^*$  by comparing the differences in the periods of S and SS phases from the same records. By

attributing the entire difference in period between the SS and S phases to attenuation, the estimate of  $\bar{t}^*$  is an upper bound.

As above, comparison of the measured periods with the periods of synthetic simulations such as those in Figure 20 and Table I were used to estimate  $\bar{t}_S^*$  for each of the S and SS. Consideration of different source durations for the synthetic waveforms puts bounds on the estimates of  $\Delta\bar{t}_S^*$  for each S-SS pair. The changes in period of around ten S-SS pairs that we have observed give  $\bar{t}_S^*$  differentials of less than 3 seconds for S and SS with frequencies in the 0.3-1 Hz range. This differential measurement gives the additional attenuation of the SS relative to the S from the passage of SS through the upper mantle to its surface reflection point and back down through the upper mantle. Thus the measurement corresponds to the  $\bar{t}_S^*$  for a double pass through the mantle in the region of the SS surface reflection point.

#### Rise Times of S Waves from Earthquakes

The rise times of the short period S arrivals from deep events can also be used to give an estimate of  $\bar{t}_S^*$ . As discussed earlier with relation to short period P waves,  $t^*$  measurements from rise times give upper bounds on estimates of  $t^*$  due to scattering of high frequency energy from the initial pulse into the coda and the resultant broadening of the initial part of the waveform.

We again estimate  $\bar{t}_S^*$  by comparison of the observed pulses with synthetic waveforms, such as those shown in Figure 20, generated for a variety of source durations and  $t^*$ s. Table II is a tabulation of the rise times of such synthetics. Figure 22 is a plot of  $t^*$  versus rise time for a range of source durations. The arrows on the right hand side of the figure correspond to the rise times measured from deep Far Eastern events as observed at Northern European and Scandinavian stations. For source durations of 1 or 2 seconds, these short periods cannot be reproduced for  $\bar{t}_S^*$  much larger than 1 to 2 seconds. Doubling this value one gets an upper limit for  $\bar{t}_S^*$  of 2-4 seconds

for a double passage of S through a Scandinavian type of upper mantle. Assuming losses entirely in shear deformation this is equivalent to a  $\bar{t}_P^*$  of 0.5 seconds.

#### Periods of P-PP Pairs

Comparison of the periods of P and PP on short period vertical records gives another estimate of  $\bar{t}_P^*$ . We found several instances where both phases were recorded at Scandinavian stations from deep earthquakes in the Far East and Hindu Kush. These are shown in Figure 23. Note that the change in the periods due to an additional double passage through the upper mantle is small, though there are complex changes in the waveforms, probably caused by crustal reverberations near the surface reflection point.

The analysis was done like that for determining  $\bar{t}_S^*$  from S-SS pairs. The periods of the P and PP phases were compared with the periods of simulations like those in Figure 20 and Table I, and indicated that the associated  $\bar{t}_P^*$  differential must be less than 0.5 seconds. This is in good agreement with the findings given in the previous section.

#### Amplitudes of Short and Long Period S-SS Pairs

Amplitude ratios of SS/S from corresponding long and short period records provide an estimate of  $\bar{t}_S^*$  across the 0.07-0.5 Hz frequency range. Figure 24 shows tracing of such long and short period S and SS from Far Eastern events recorded at Northern European stations. Even when the short period SS is not seen, this measurement can be made using the amplitude of the noise where the SS is expected as an upper bound on the SS amplitude. The amplitudes were adjusted for the appropriate short or long period WWSSN instrument response. For each phase, the geometrical spreading will be the same for the long and short period arrivals, and we assume the same for the radiation pattern, though this may not be true if the source is very complex.

Amplitude ratios at the two different frequencies of the short and long period data give a frequency domain estimate of  $\bar{t}^*$  using the relation:

$$\bar{t}^* = \frac{d(\ln A)}{df}$$

Nine sets of measurements gave  $\Delta\bar{t}_S^* < 2.5$  seconds for a double pass through the upper mantle.

### Comparison of ScS-ScP Pairs

Following the approach by Burdick (1983), we also looked for ScS-ScP pairs on short period records of deep earthquakes. Several pairs of the observed ScS-ScP pairs are shown in Figure 25. While the paths of the two phases have different reflection points on the core-mantle boundary, they follow nearly the same path in the upper mantle source region where more lateral heterogeneities are expected to exist. Because the first leg of both phases is an S wave, the difference in  $t^*$  between ScS and ScP is simply due to the difference in attenuation between the second legs of the two phases. Thus, this measurement is mostly sensitive to attenuation in the upper mantle in the vicinity of the receiver, and is relatively independent of the nature of the source region.

The differences in period of the ScS and ScP observations were used to estimate  $\bar{t}_S^*$ . For each phase,  $\bar{t}^*$  was estimated from the periods of synthetics, like those in Figure 20 and Table I, generated for a range of source durations and  $t^*$ 's. Assuming all losses in compression,  $t_S^* = 4t_P^*$ . If  $t_S^*$  is the  $t^*$  for an S wave traveling from the core mantle boundary to the surface,  $\bar{t}_S^*(\text{ScS}) = 2\bar{t}_S^*$  and  $\bar{t}_S^*(\text{ScP}) = \bar{t}_S^* + \bar{t}_P^* = (5/4)\bar{t}_S^*$ . Therefore,  $\Delta\bar{t}^* = \bar{t}^*(\text{ScS}) - \bar{t}^*(\text{ScP}) = 2\bar{t}_S^* - (5/4)\bar{t}_S^* = (3/4)\bar{t}_S^*$ . For a single pass through the upper mantle (core to surface),  $\bar{t}_S^* = (4/3)\Delta\bar{t}^*$ , and for a double pass through the upper mantle (say ScS from a surface source),  $\bar{t}_S^* = (8/3)\Delta\bar{t}^*$ .

Measurements from several ScS-ScP pairs give  $\bar{t}_S^* \sim 2.5$  seconds for a double pass through the mantle at around 0.5 Hz. Our measurements are generally smaller than Burdick's result of  $\bar{t}_S^* \sim 4$  to 7 seconds because the differences in the dominant periods of ScS and ScP phases are less than in Burdick's study. Since our observed ScS and

ScP phases tended to be very small, this measurement alone is not sufficient to define  $t^*$  in the mid-period band, though these results are consistent with our other ones for the same frequency range.

### Summary and Conclusions

A variety of different techniques were used to estimate  $t^*$  under the Eurasian shield in the frequency range from 0.3 to 8 Hz. At the highest frequencies, recordings from NORSAR of Soviet nuclear explosions were used. Spectra give  $\bar{t}_P^* \sim 0.15$  seconds. Amplitudes and spectra of the branches of suites of record sections suggest that a low velocity zone is not required in the upper mantle beneath the Eurasian shield, while a slight low Q layer is needed to explain the branch amplitude ratios. The rise times of P waves from nuclear explosions give higher estimates of  $\bar{t}_P^*$ , around 0.5 seconds, but this may be due to scattering of the initial high energy in the P-wave train back into the coda. The periods and rise times of S waves and differential periods of P-PP, S-SS, and ScP-ScS pairs all give  $\bar{t}_S^* \sim 2$  to 3 seconds for frequencies around 0.3 to 1 Hz. And, comparison of short and long period SS/S amplitude ratios gives  $\bar{t}_S^*$  around 2 to 2.5 seconds across the frequency range of 0.07 to 0.5 Hz.

Using the assumption  $t_S^* = 4t_P^*$  to relate the  $t_P^*$  and  $t_S^*$  measurements, it is clear that there is a definite difference in  $t^*$  above 1 Hz and below 1 Hz, although the data cannot resolve the details of the transition between  $t^*$  values. Furthermore, all of the  $t^*$  values estimated from the data in this study are significantly below the whole earth estimates at long periods from free oscillations ( $t_P^* = 1$  second and  $t_S^* = 4$  seconds), so the frequency dependence in  $t^*$  extends to lower frequencies.

### Acknowledgements

We gratefully acknowledge the contributions of our coworkers Jim Burnetti and Thomas W. McElfresh to this research. Dr. Keith McLaughlin has improved the program for computing the synthetic seismograms in this paper.

## References

- Anderson, D.L. and J.W. Given (1982). Absorption band Q model for the earth, *J. Geophys. Res.*, **87**, 3893-3904.
- Bache, T.C. (1984). Q and its effects on short period P waves from explosions in central Asia, *SAI-84/1589*, Science Applications, Inc., La Jolla, CA.
- Bungurn, H. (1983). Power spectral bias sources and quantization levels, in NORSAR Scientific Report No. 2 82/83, Semiannual Technical Summary, 1 October 1982 - 31 March 1983, ed. L.B. Tronrud, 65-71.
- Burdick, L.J. (1983). Estimation of the frequency dependence of Q from ScP and ScS phases, *WCCP-R-83-06*, Woodward-Clyde Consultants, Pasadena, California.
- Chapman, C.H. (1978). A new method for computing synthetic seismograms. *Geophys. J. R. astr. Soc.*, **54**, 481-518.
- Clayton, R.W. and R.P. Comer (1983). A tomographic analysis of mantle heterogeneities from body wave travel times, *EOS*, **64**, 776.
- Der, Z.A. and T.W. McElfresh (1977). The relationship between anelastic attenuation and regional amplitude anomalies of short-period P waves in North America, *Bull. Seism. Soc. Am.*, **67**, 1303-1317.
- Der, Z.A. and A.C. Lees (1984). Methodologies of estimating  $t^*(f)$  from short period body waves and regional variations of  $t^*(f)$  in the United States, submitted to *Geophys. J. R. astr. Soc.*
- Der, Z.A., T.W. McElfresh, and A. O'Donnell (1982). An investigation of the regional variations and frequency dependence of anelastic attenuation in the mantle under the United States in the 0.5-4 Hz band, *Geophys. J. R. Astr. Soc.*, **69**, 67-100.
- Der, Z.A., A.C. Lees, and V.F. Cormier (1985). Frequency dependence of Q in the mantle underlying the shield areas of Eurasia, Part III: the Q model, included in this report.
- Der, Z.A., T. McElfresh, R. Wagner and J. Burnetti (1984). Spectral characteristics of P waves from nuclear explosions and yield estimation, submitted to *Bull. Seism. Soc. Am.*
- Dey-Sarkar, S.K. and C.H. Chapman (1978). A simple method for the computation of body wave seismograms, *Bull. Seism. Soc. Am.*, **68**, 1577-1593.
- Dziewonski, A.M. and D.L. Anderson (1981). Preliminary reference earth model, *Phys. Earth Planet. Int.*, **25**, 297-356.
- Frankel, A. and R.W. Clayton (1984). A finite difference simulation of wave propagation in two-dimensional media, *Bull. Seism. Soc. Am.*, **74**, 2167-2186.
- Given, J.W. and D.V. Helmberger (1980). Upper mantle structure in northwestern Eurasia, *J. Geophys. Res.*, **85**, 7183-7194.



- Helmberger, D.V. and D.M. Hadley (1981). Seismic source functions and attenuation from local and teleseismic observations of the NTS events Jorum and Handley, *Bull. Seism. Soc. Am.*, 71, 52-67.
- King, D.W. and G. Calcagnile (1976). P-wave velocities in the upper mantle beneath Fennoscandia and western Russia, *Geophys. J. R. astr. Soc.*, 46, 407-432.
- Lay, T. and D.V. Helmberger (1981). Body wave amplitude patterns and upper mantle attenuation variations across North America, *Geophys. J. R. astr. Soc.*, 66, 691-726.
- Lay, T., D.V. Helmberger, and D.G. Harkrider (1984). Source models and yield-scaling relationships for underground nuclear explosions across North America, *Bull. Seism. Soc. Am.*, 74, 843-862.
- Lees, A.C., Z.A. Der, V.F. Cormier, M. Marshall and J. Burnetti (1985). Frequency dependence of Q in the mantle underlying the shield areas of Eurasia, Part II: analyses of long period data, included in this report.
- Lundquist, G.M., and V.C. Cormier (1980). Constraints on the absorption band model of Q, *J. Geophys. Res.*, 85, 5244-5265.
- Masse, R.P. and S.S. Alexander (1974). Compressional velocity distribution beneath Scandinavia and western Russia, *Geophys. J. R. astr. Soc.*, 36, 705-716.
- McLaughlin, K.L., and L.M. Anderson (1984). Stochastic dispersion of seismic waveforms due to scattering and multipathing, *Earthquake Notes*, 55.
- McLaughlin, K.L., L.M. Anderson and Z.A. Der (1984). Investigation of seismic waves using 2-D finite difference calculations, submitted to *Geophys. J. R. astr. Soc.*
- Mueller, R.A. and J.R. Murphy (1971). Seismic characteristics of underground nuclear detonations, *Bull. Seism. Soc. Am.*, 61, 1675-1692.
- Nataf, H.-C., I. Nakanishi and D.L. Anderson (1984). Anisotropy and shear-velocity heterogeneities in the upper mantle, *Geophys. Res. Lett.*, 11, 109-112.
- Richards, P.G. and W. Menke (1983). The apparent attenuation of a scattering medium, *Bull. Seism. Soc. Am.*, 73, 1005-1021.
- Shore, M.J. (1983). Short period P-wave attenuation in the middle and lower mantle of the earth, *VSC-TR-83-7*, VELA Seismological Center, Alexandria, Virginia.
- Stewart, R.C. (1984). Q and the rise and fall of a seismic pulse, *Geophys. J. R. Astr. Soc.*, 76, 793-805.
- Stump, B.W. and L.R. Johnson (1984). Near-field source characterization of contained nuclear explosions in tuff, *Bull. Seism. Soc. Am.*, 74, 1-26.
- Tanimoto, T. and H. Kanamori (1984). The upper mantle velocity structure by the Backus-Gilbert method and its comparison to other models, *EOS*, 65, 1003.
- von Seggern, D.H., and R.R. Blandford (1972). Source time functions and spectra from underground nuclear explosions, *Geophys. J. R. Astr. Soc.*, 31, 83-97.
- Woodhouse, J.H. and A.M. Dziewonski (1984). Mapping the upper mantle: three-dimensional modeling of earth structure by inversion of seismic waveforms, *J. Geophys. Res.*, 89, 5953-5986.

Table I

Periods of Synthetic Waveforms,  
in seconds, for Various Source Durations and  $t^*$ 's

$t^*$ (seconds)	Source Duration			
	0 seconds (impulse)	1 second triangle	2 second triangle	3 second triangle
0.5	0.7	1.1	1.8	2.2
1.0	1.1	1.4	2.2	2.6
1.5	1.4	1.7	2.3	3.0
2.0	1.8	2.1	2.5	3.3
2.5	2.1	2.6	3.0	3.8
3.0	2.6	2.9	3.3	4.0
3.5	3.2	3.3	3.8	4.3
4.0	3.6	3.8	4.2	4.7
5.0	4.4	4.6	4.8	5.3

Table II

Rise Times of Synthetic Waveforms,  
in seconds, for Various Source Durations and  $t^*$ 's

$t^*$ (seconds)	Source Duration			
	0 seconds (impulse)	1 second triangle	2 second triangle	3 second triangle
0.5	0.2	0.3	0.4	
1.0	0.3	0.4	0.5	0.6
1.5	0.4	0.5	0.6	0.7
2.0	0.5	0.6	0.7	0.9
2.5	0.6	0.7	0.8	1.0
3.0	0.7	0.8	0.9	1.1
3.5	0.8	0.9	1.0	1.2
4.0	0.9	1.1	1.1	1.3
5.0	1.0	1.3	1.5	1.7

## Figure Captions

**Figure 1.** Representative P-wave spectra at NORSAR from Soviet peaceful nuclear explosions.

**Figure 2.** Locations of Soviet peaceful nuclear explosions used in this study. Each PNE is labeled with the value of  $t_P^*$  for the path to NORSAR, assuming a von Seggern and Blandford source model.

**Figure 3.** Array averaged power spectra at NORSAR of (a) a Soviet peaceful nuclear explosion on 24 November 1972 and (b) a Kazakh explosion on 10 July 1973. The bounds are 95% confidence limits. Theoretical spectra derived using a von Seggern and Blandford (1972) source model and the  $t^*$  noted next to each figure.

**Figure 4.** Seismic profiles from Soviet PNE's at NORSAR. The travel time triplications from the model of King and Calcagnile (1976) are superposed.

**Figure 5.** Seismic profiles from Soviet PNE's at NORSAR, filtered into the 0.5-1.5 Hz frequency band. The travel time triplications from the model of King and Calcagnile (1976) are superposed.

**Figure 6.** Seismic profiles from Soviet PNE's at NORSAR, filtered into the 2.0-4.0 Hz frequency band. The travel time triplications from the model of King and Calcagnile (1976) are superposed.

**Figure 7.** Seismic profiles from Soviet PNE's at NORSAR, filtered into the 5.0-8.0 Hz frequency band. The travel time triplications from the model of King and Calcagnile (1976) are superposed.

**Figure 8.** Detailed section of profiles from Soviet PNE's recorded at NORSAR at around  $16^\circ$ .

**Figure 9.** Detailed section of profiles from Soviet PNE's recorded at NORSAR at around  $28^\circ$ .

**Figure 10.** Detailed section of profiles from Soviet PNE's recorded at NORSAR at around  $30^\circ$ .

**Figure 11.** Velocity versus depth for the KCA (King and Calcagnile, 1976) and K8 (Given and Helmberger, 1980) P-wave velocity models for Northwestern Eurasia.

**Figure 12.** Suite of synthetic P-wave seismograms for the KCA velocity model (King and Calcagnile, 1976), with no attenuation. A von Seggern and Blandford (1972) explosion source has been convolved with the impulse response.

**Figure 13.** Suite of synthetic P-wave seismograms for the K8 velocity model (Given and Helmberger, 1980), with no attenuation. A von Seggern and Blandford (1972) explosion source has been convolved with the impulse response.

**Figure 14.** Spectral ratios of the CD/AB branches at  $16^\circ$  and the AB/EF branches at  $30^\circ$  for synthetic record sections generated using the KCA model (King and Calcagnile, 1976) and an elastic earth.

**Figure 15.** Representative spectral ratios of (a) the CD/AB branches at  $16^\circ$  and (b) the AB/EF branches at  $30^\circ$  for Soviet PNE's recorded at NORSAR. These spectral ratios give estimates of  $t_S^*$  of a) -0.07 and b) 0.07 seconds.

**Figure 16.** Model of Q versus depth that satisfies the spectral characteristics of the P wave profiles (dashed line) as compared to a model of the western United States (Der and McElfresh, 1977).

**Figure 17.** P-wave travel time curve for the KCA model (King and Calcagnile, 1976) with  $t_P$  values labeled for various points on the travel time curve. The Q model in Figure 16 was used in a raytracing program to calculate the  $t_P$  values.

**Figure 18.** Estimation of  $\overline{t_P^*}$  from the rise times of Soviet PNE's as observed at NORSAR. The lines are theoretical curves of rise time versus  $t_P^*$  for different yields, derived from measured rise times of synthetic waveforms, assuming a von Seggern and Blandford (1972) granite source model, the minimum scale depth, a range of  $t^*$ , a surface reflection coefficient of unity, and an uphole velocity of 5.5 km/sec.

**Figure 19.** Representative short period S and ScS waveforms recorded across Fennoscandia from events in the Far East and the Hindu Kush.

**Figure 20.** Synthetic waveforms for a range of source models and values of  $t^*$ . A short period WWSSN instrument response is convolved with the waveforms and the amplitudes are normalized.

**Figure 21.** Estimation of  $\overline{t_S^*}$  from the dominant periods of short period S waves like those in Figure 19. The periods of synthetic waveforms are plotted on the graph for a range of source durations and  $t^*$  values. The observed periods are marked with arrows on the right-hand side of the graph, and correspond to  $t_S^* \sim 1$ -2 seconds for source durations between 1 and 3 seconds.

**Figure 22.** Estimation of  $\bar{t}_S^*$  from rise times of short period S waves like those in Figure 19. The rise times of synthetic waveforms are plotted on the graph for a range of source durations and  $t^*$  values. The observed rise times are marked with arrows on the right-hand side of the graph, and correspond to  $\bar{t}_S^* \sim 1-3$  seconds.

**Figure 23.** Tracings of short period P and PP arrivals from Far Eastern events.

**Figure 24.** Tracings of short and long period S and SS arrivals from Far Eastern events.

**Figure 25.** Tracings of ScP and ScS arrivals from Far Eastern events.

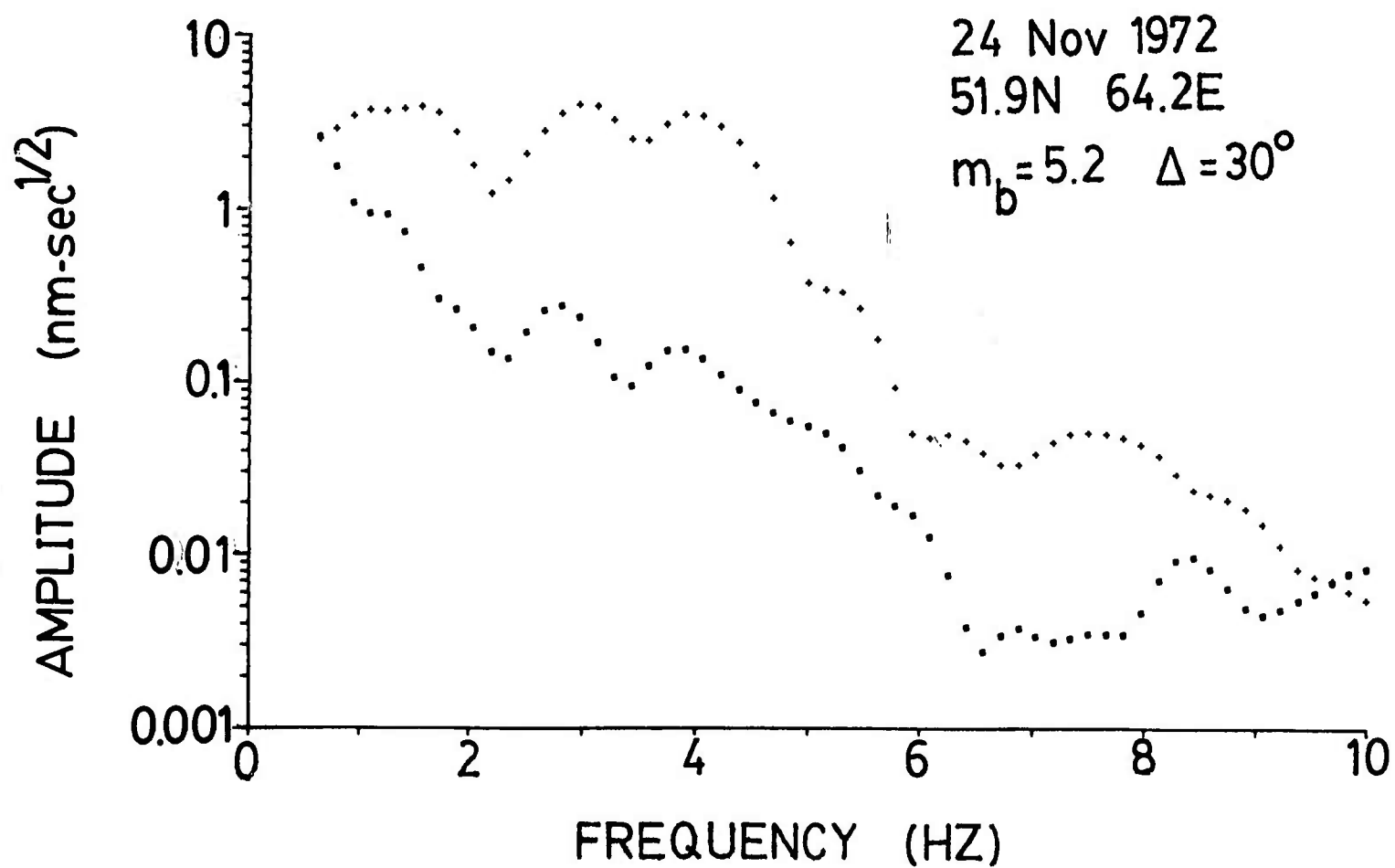
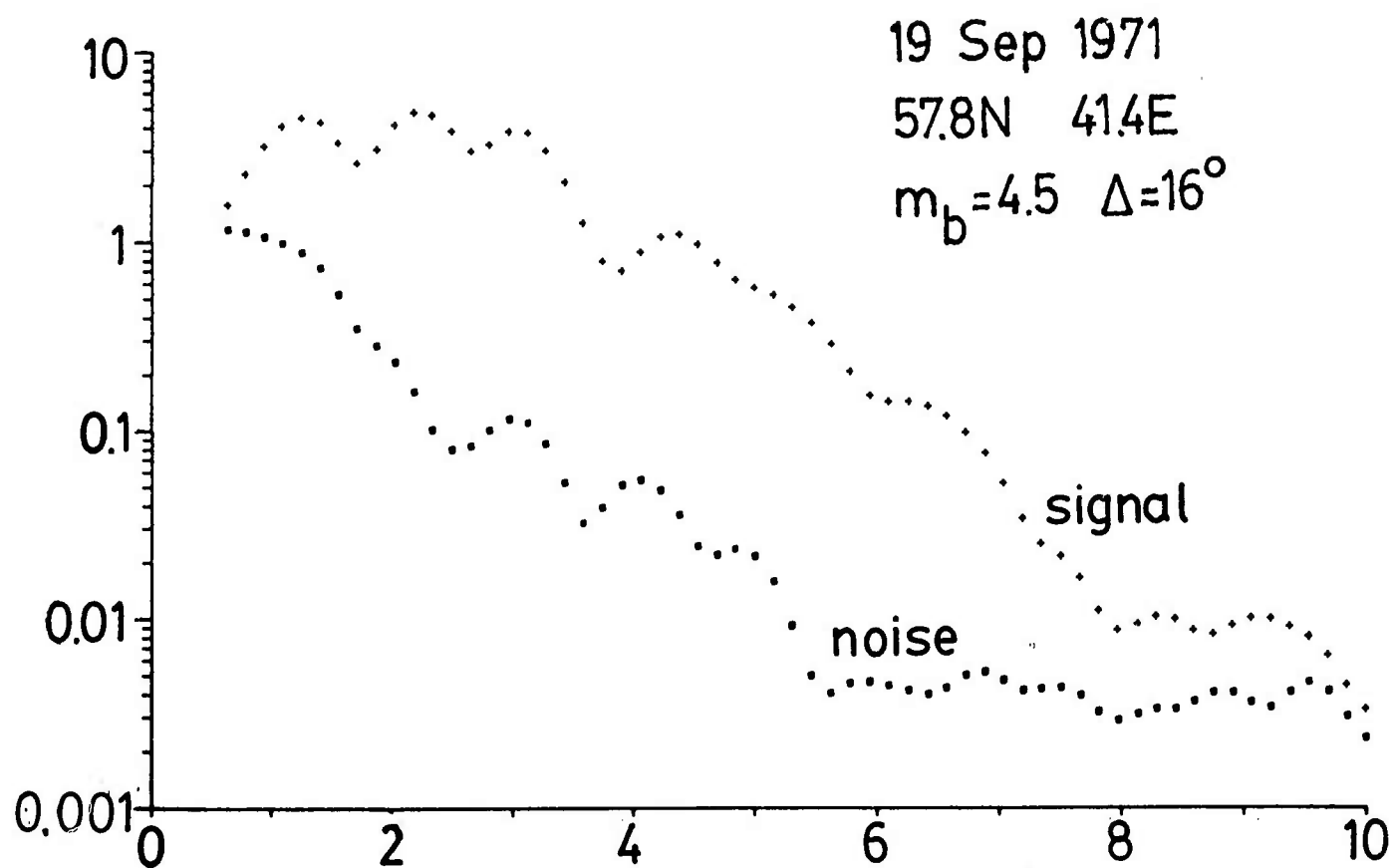


Figure 1

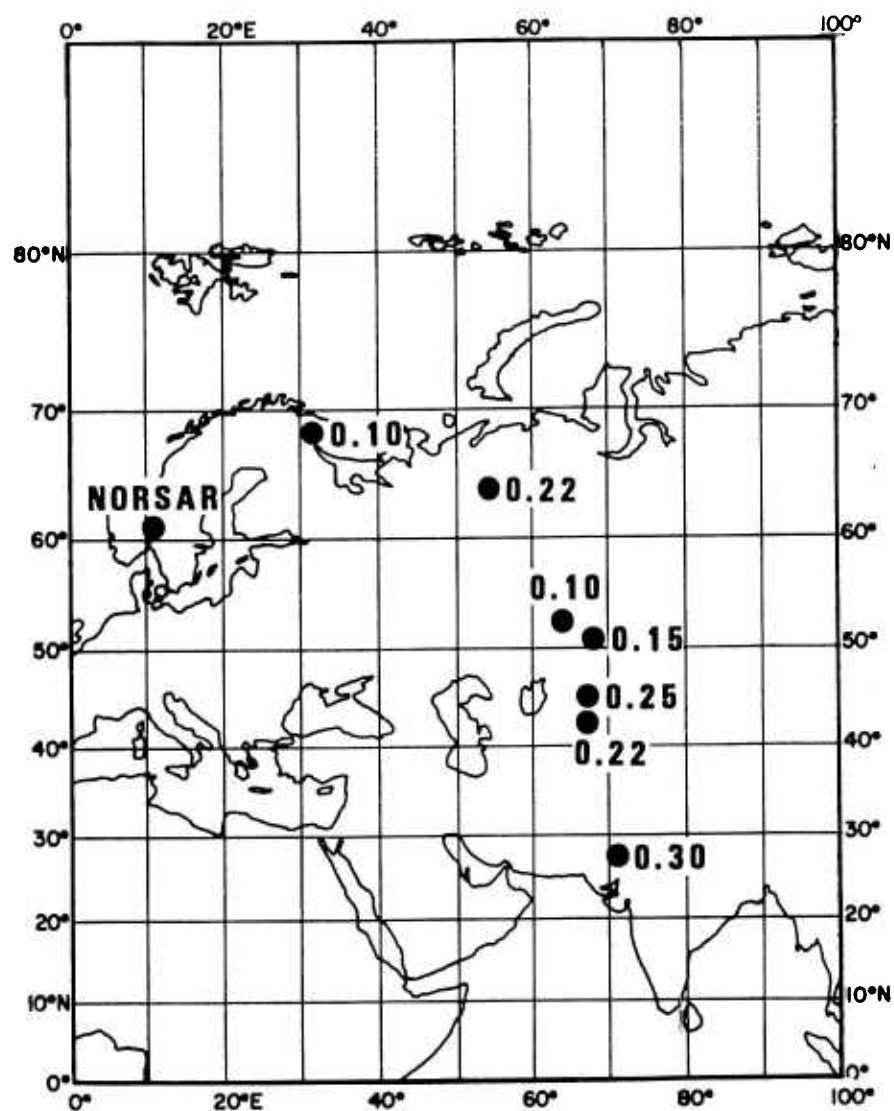
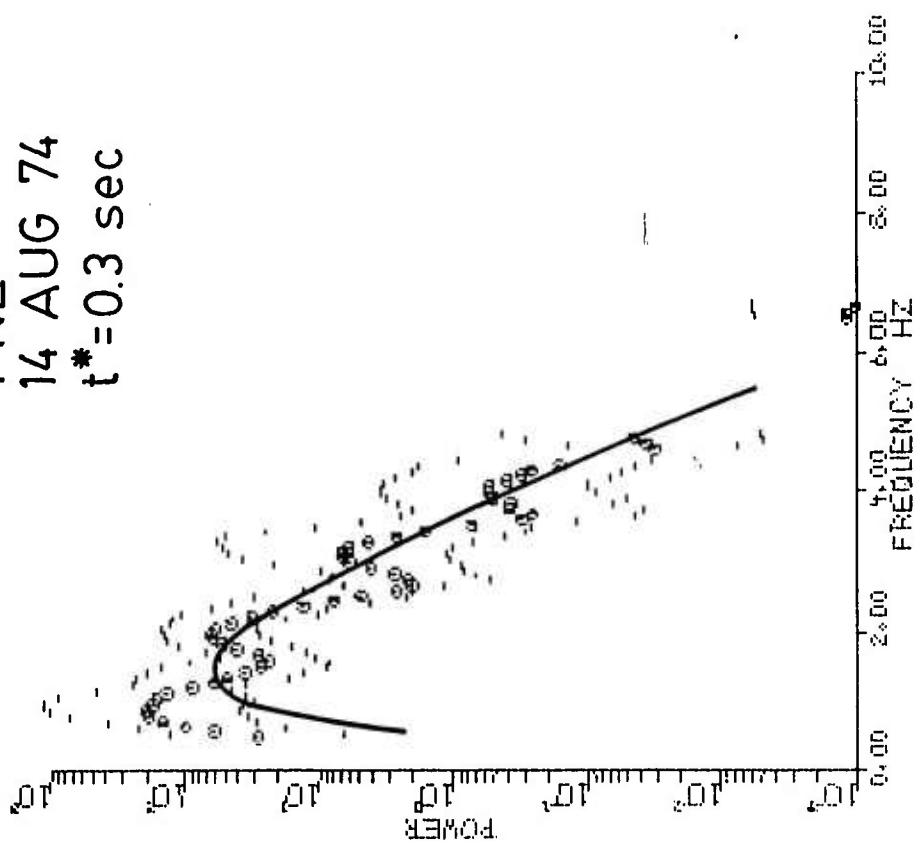


Figure 2



(a)

PNE  
14 AUG 74  
 $t^* = 0.3$  sec



(b)

KAZAKH  
10 JUL 73  
 $t^* = 0.1$  sec

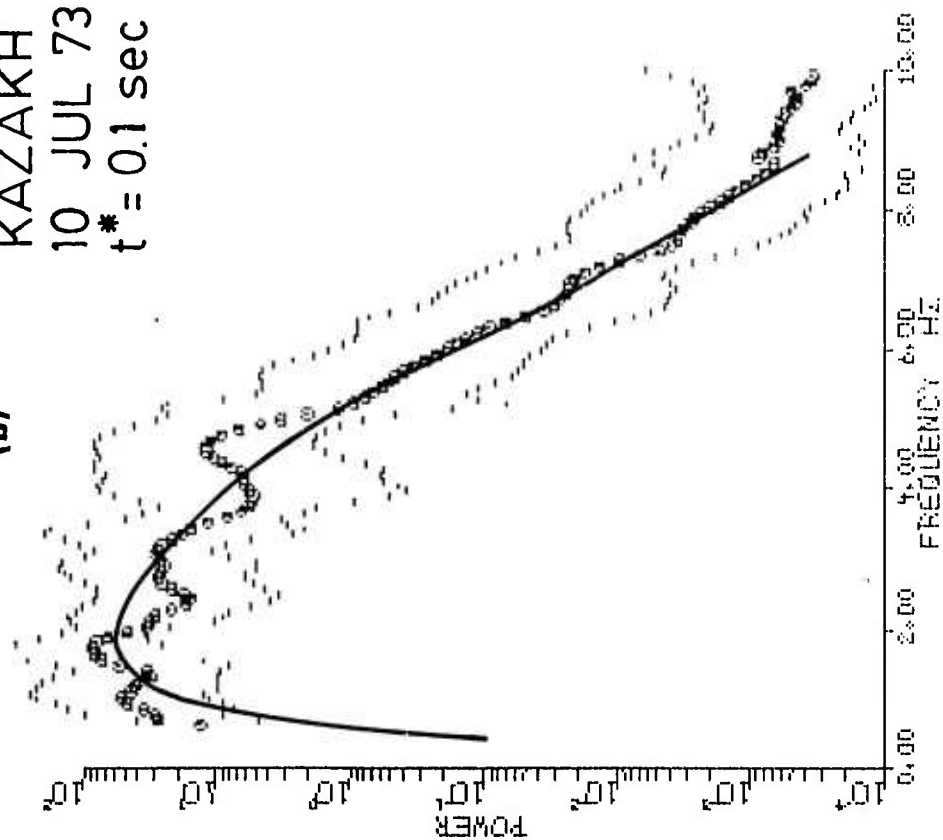


Figure 3

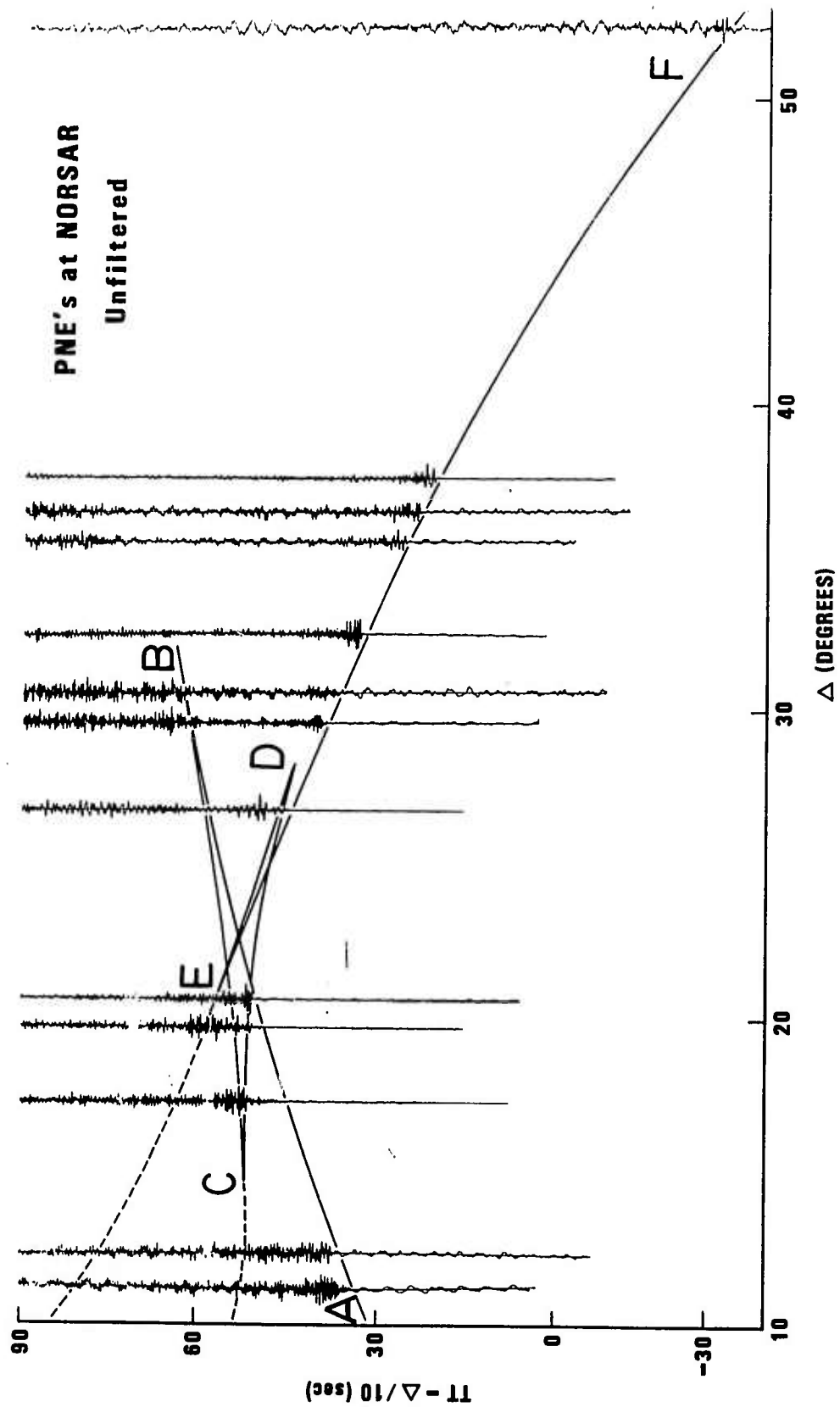


Figure 4

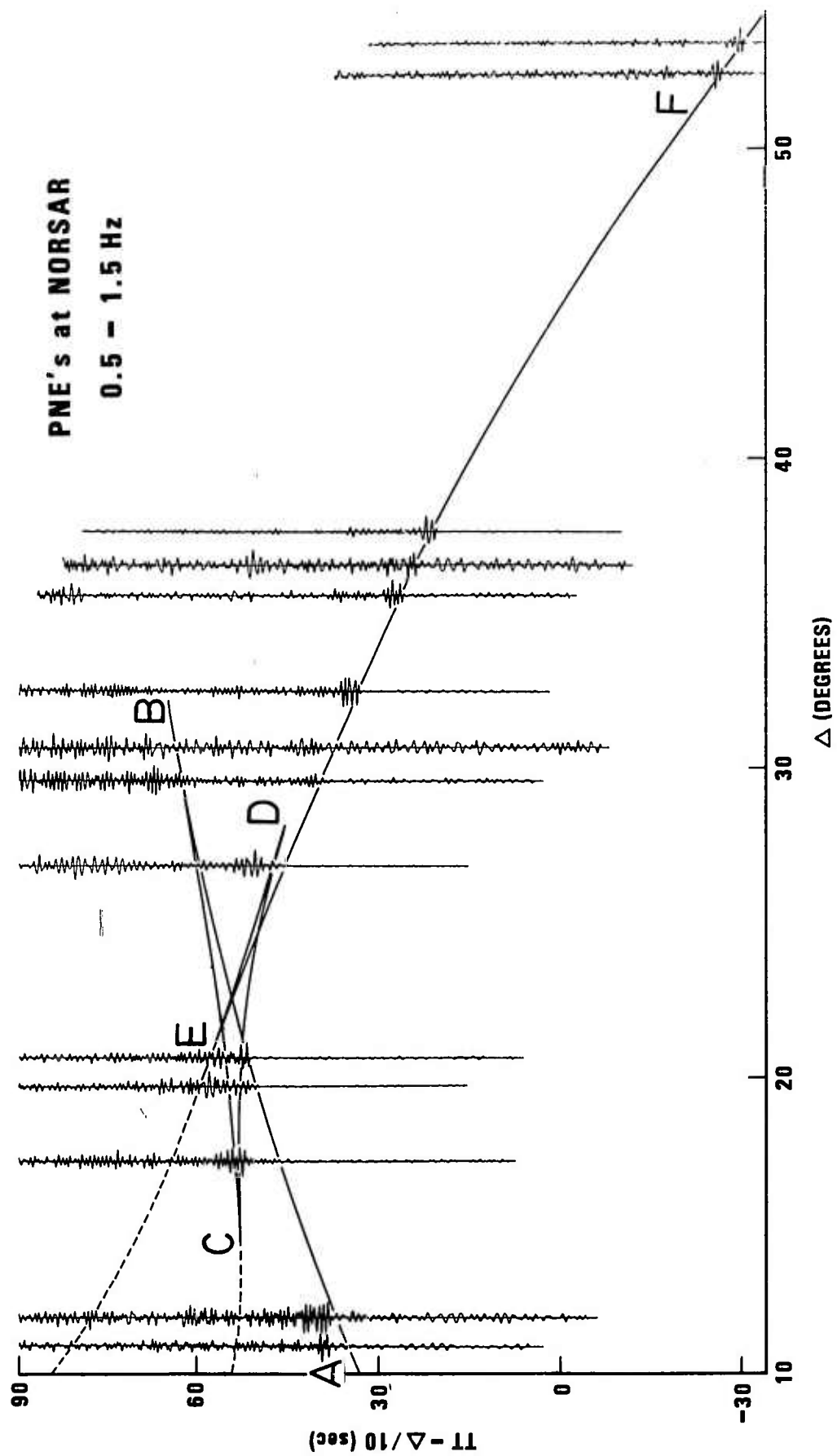


Figure 5

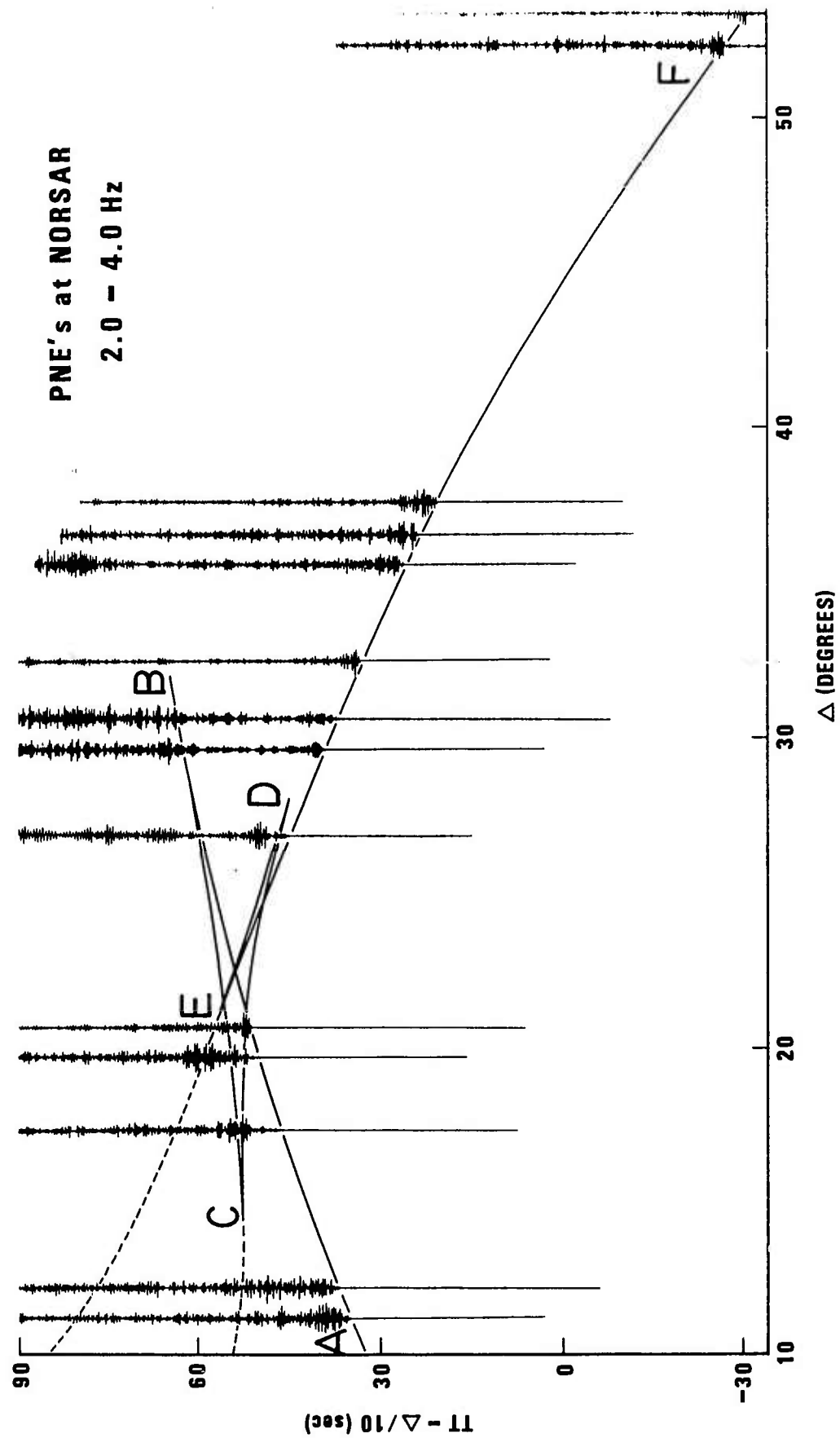


Figure 6

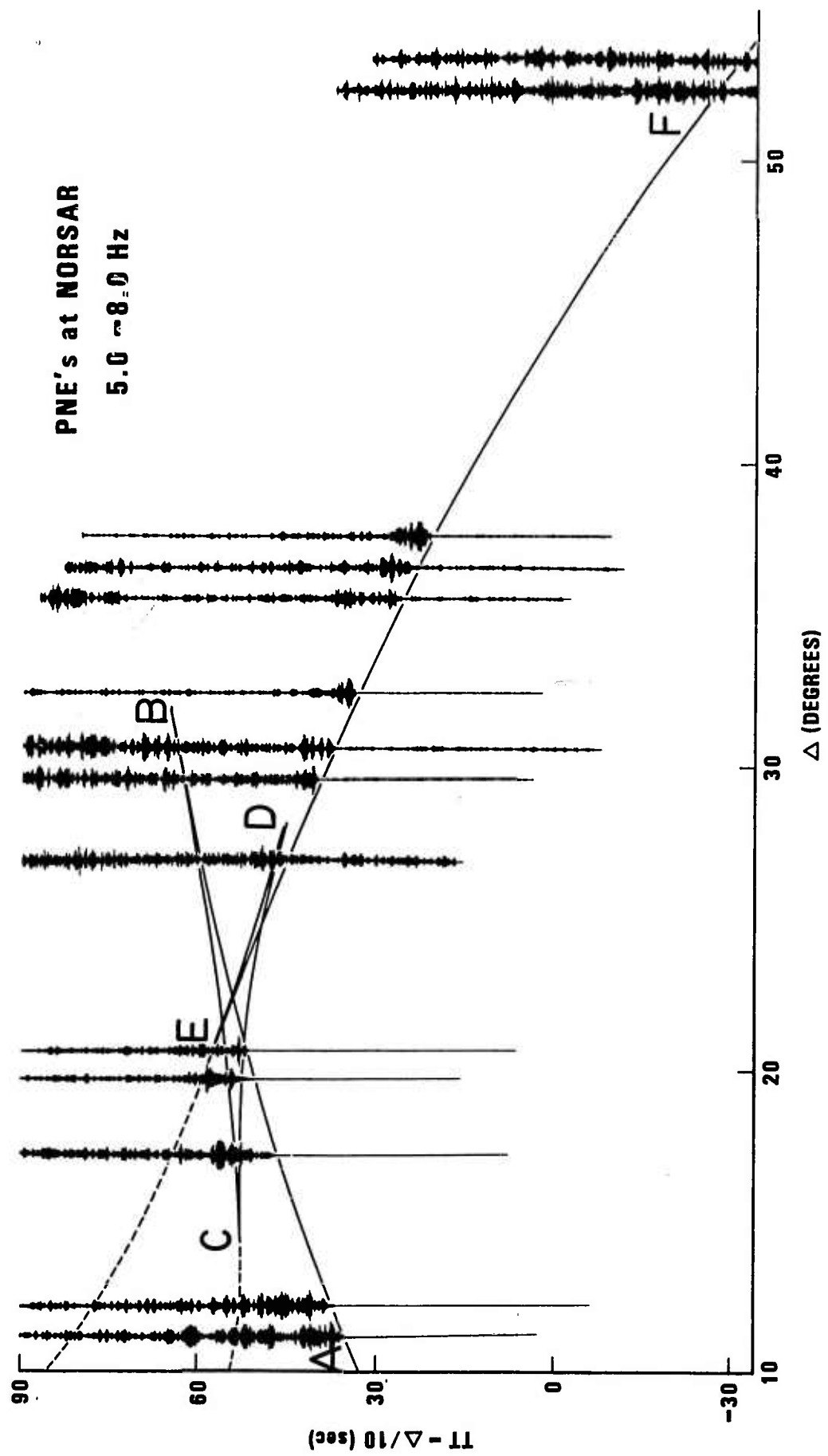


Figure 7

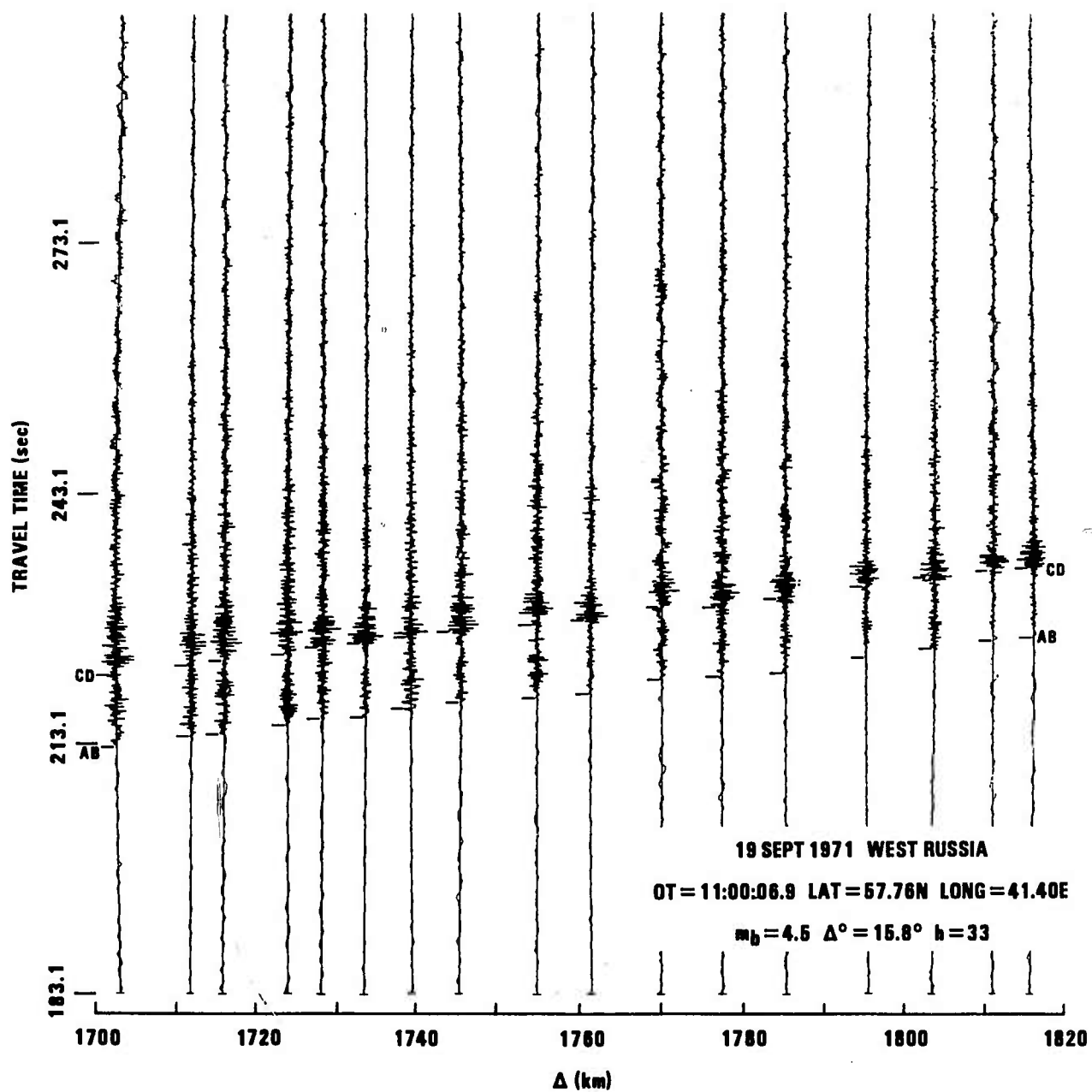


Figure 8

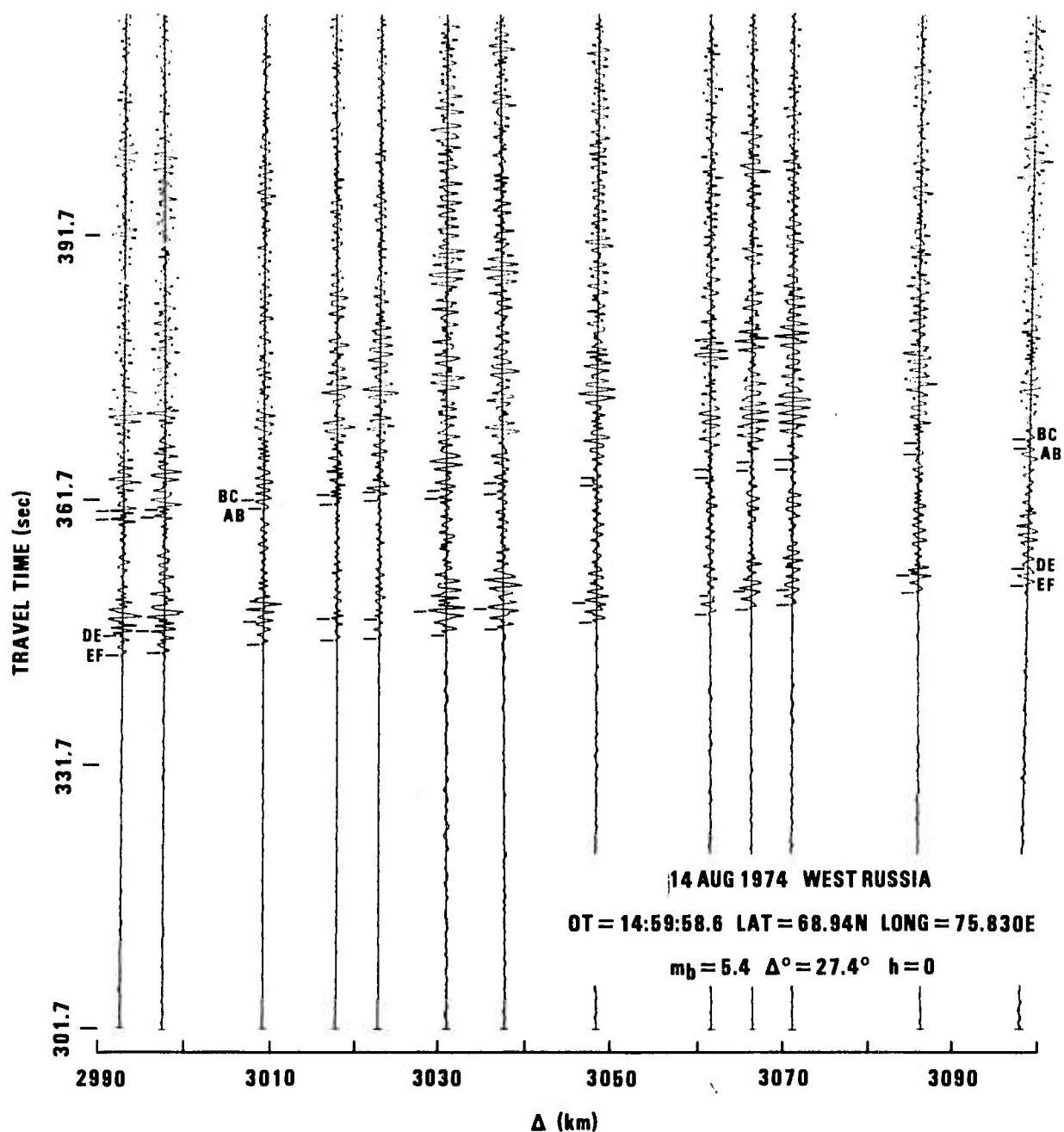


Figure 9

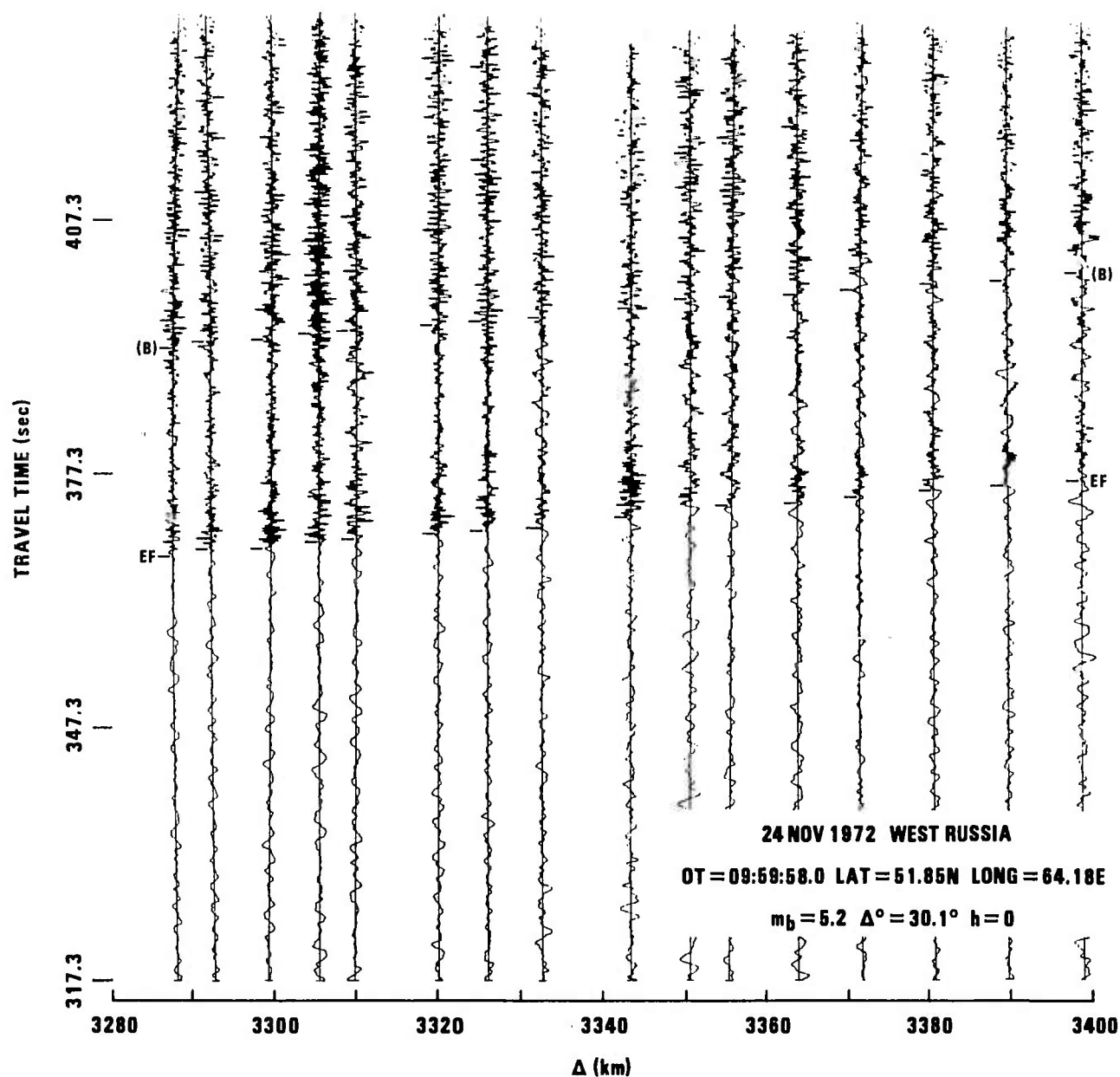


Figure 10



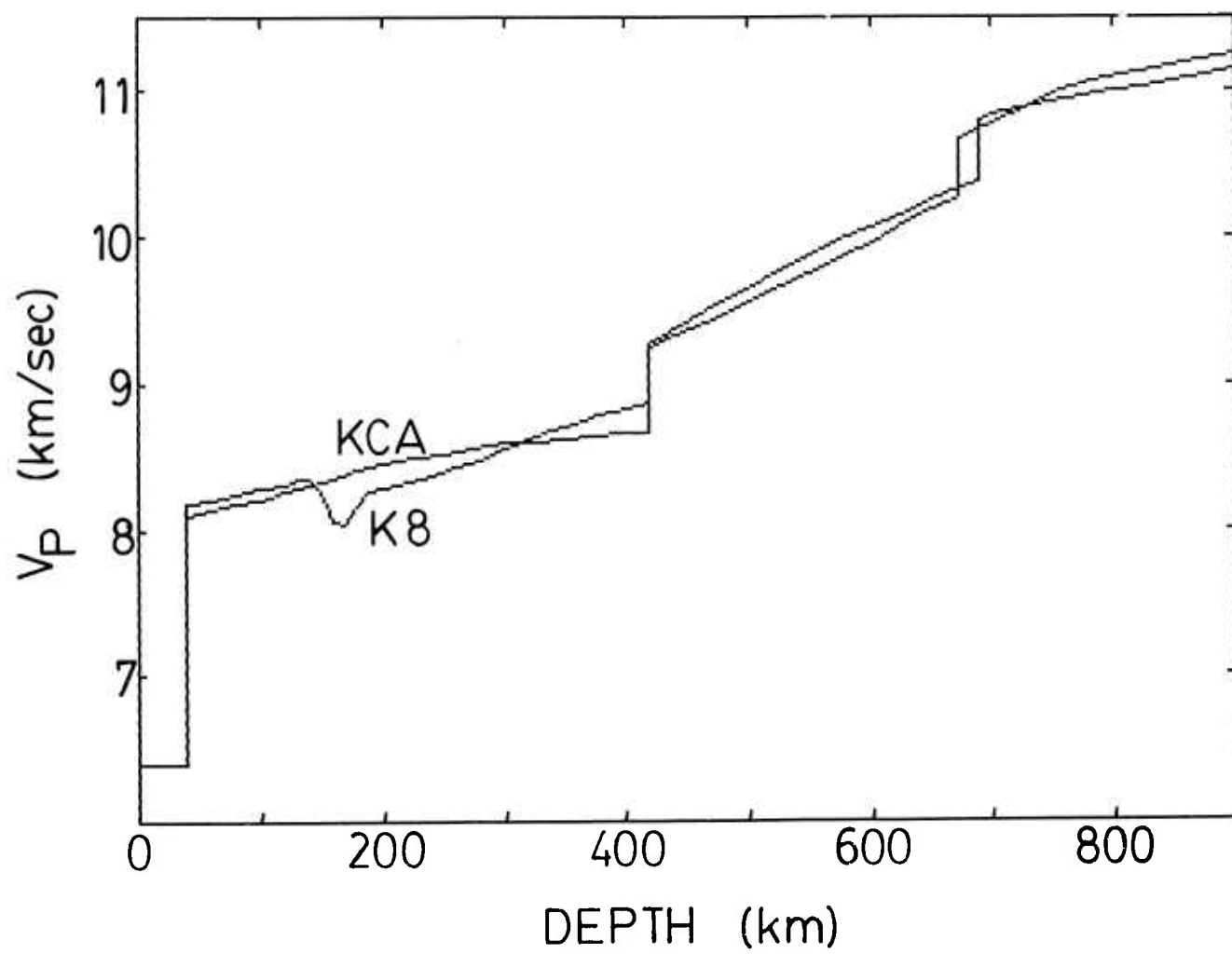


Figure 11

KCA

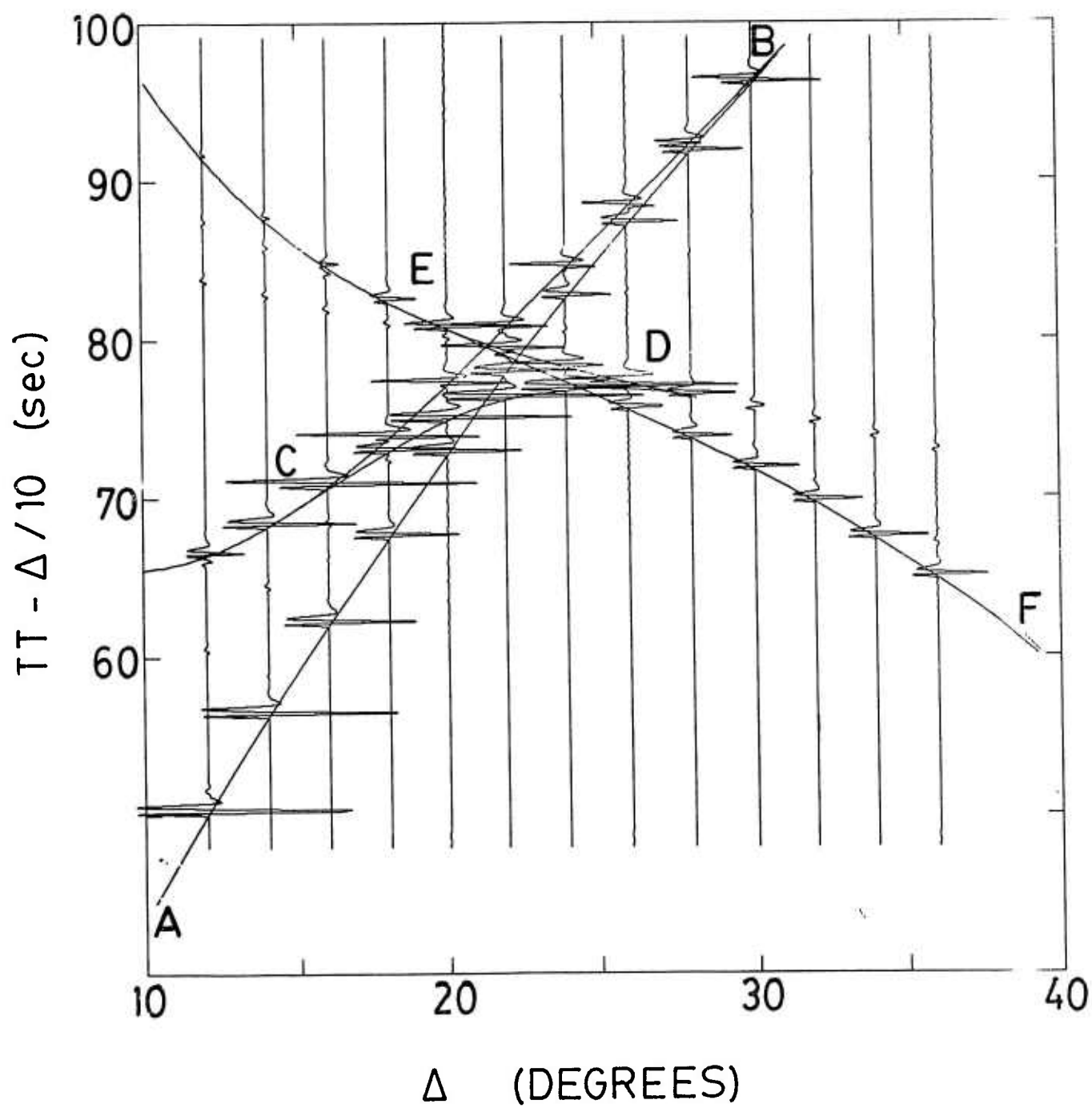


Figure 12

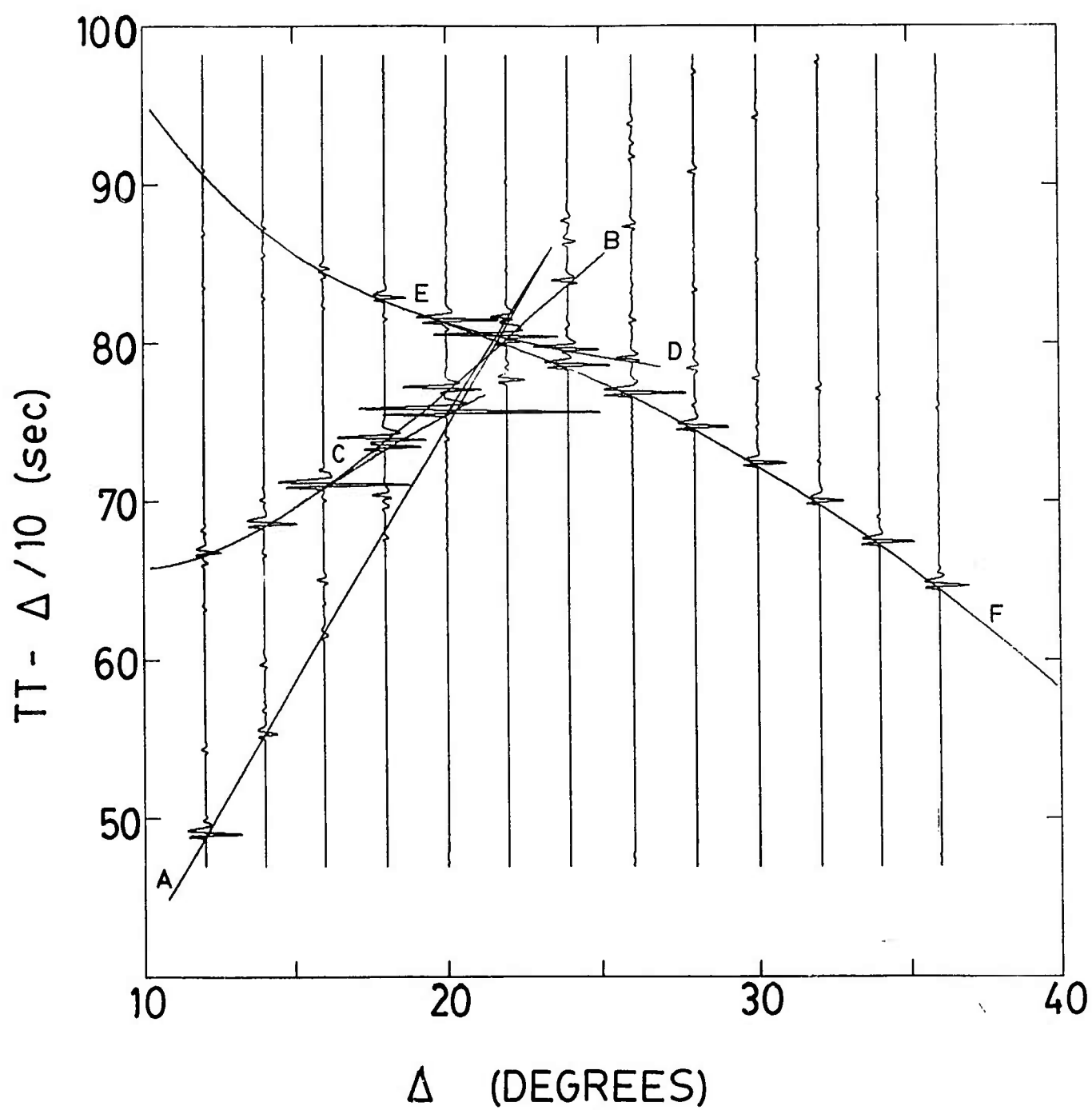


Figure 13

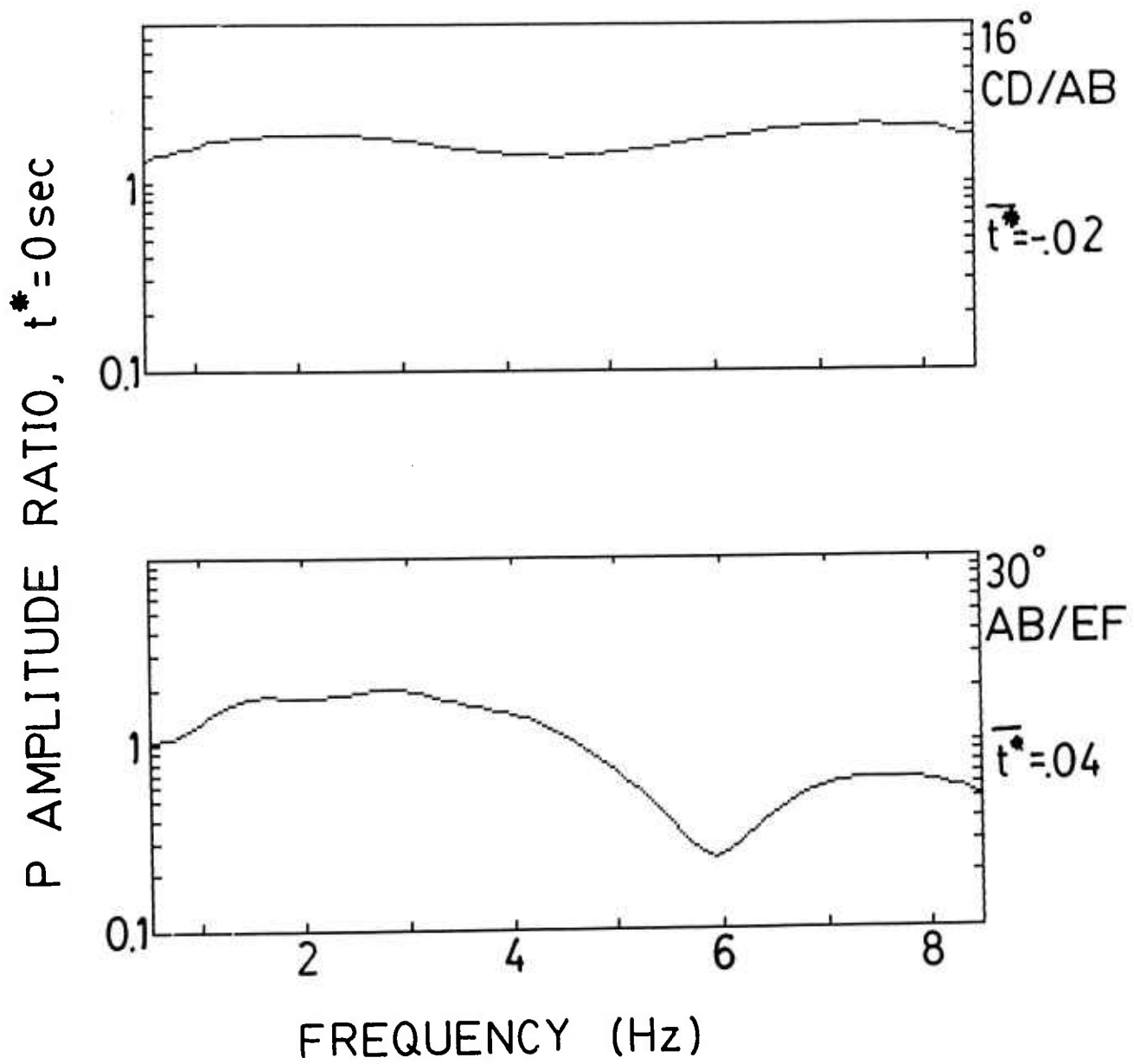


Figure 14

19 SEPT 1971 WEST RUSSIA

OT = 11:00:06.9 LAT = 57.76N LONG = 41.40E

$m_b = 4.5$   $\Delta^\circ = 15.8^\circ$   $h = 0$

SPECTRAL RATIO BRANCHES  $\frac{CD}{AB}$

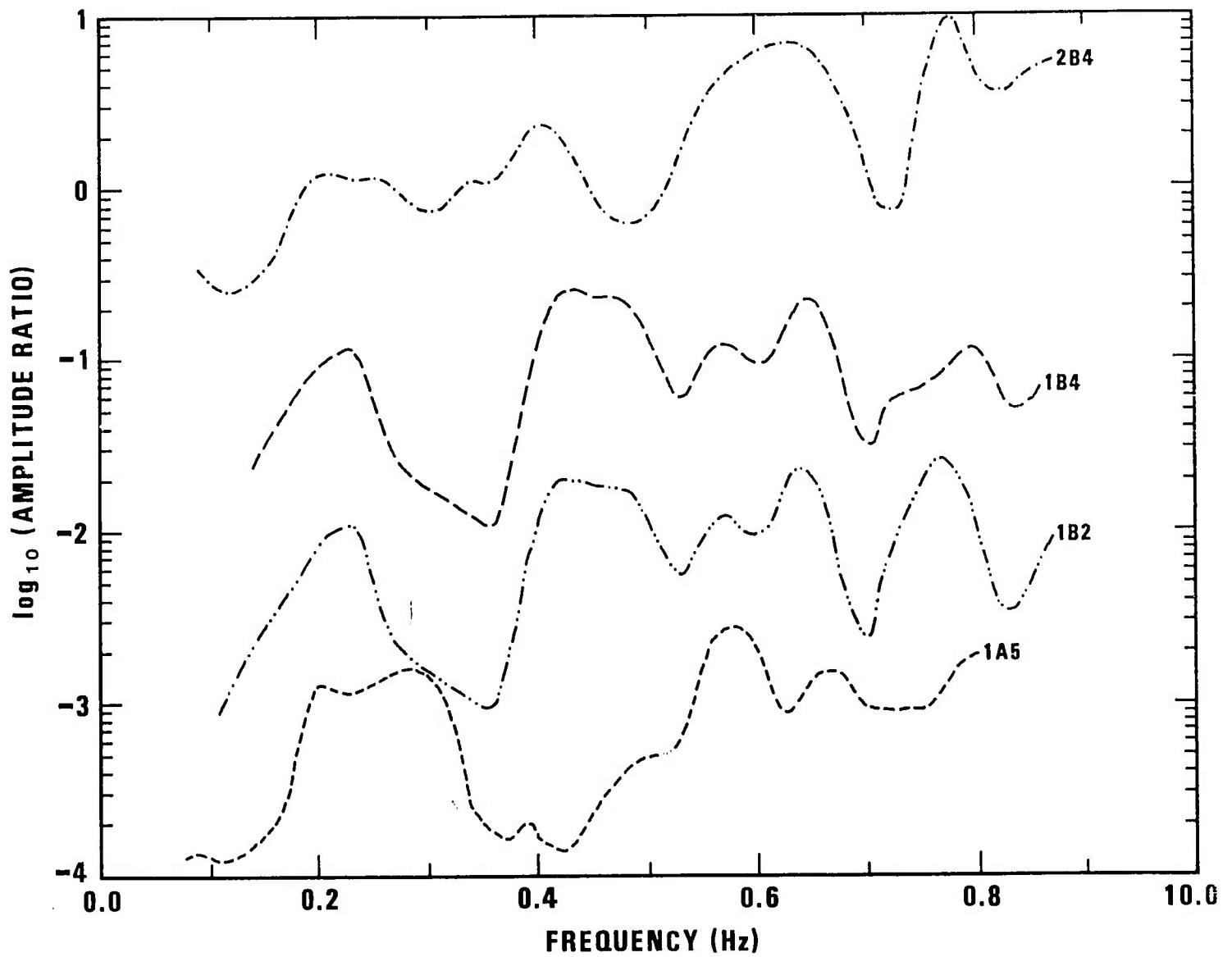


Figure 15a

24 NOV 1972 WEST RUSSIA

OT = 09:59:58.0 LAT = 51.85N LONG = 64.18E

$m_b = 5.2$   $\Delta^\circ = 30.1^\circ$   $h = 0$

SPECTRAL RATIO BRANCHES  $\frac{(B)}{EF}$

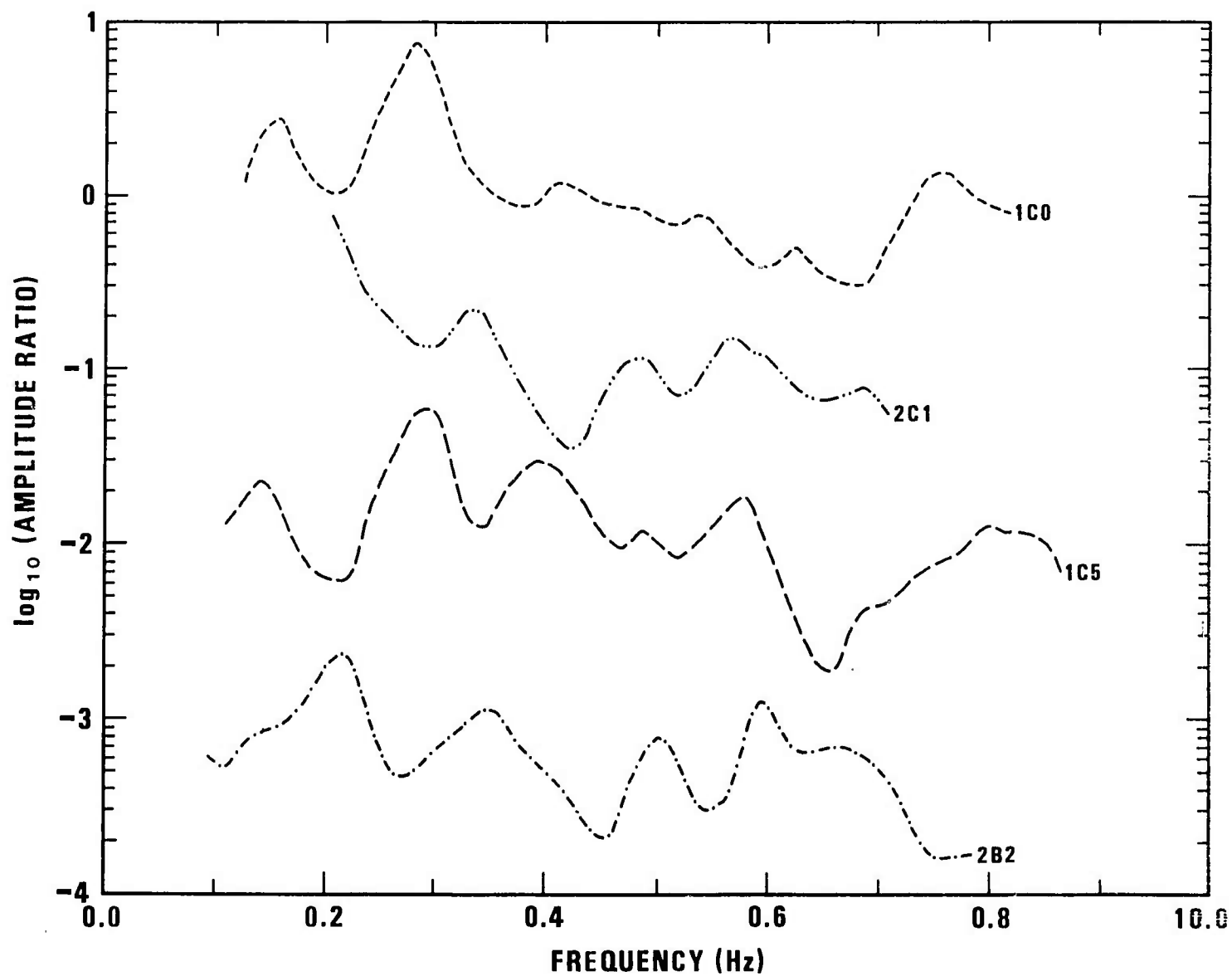


Figure 15b

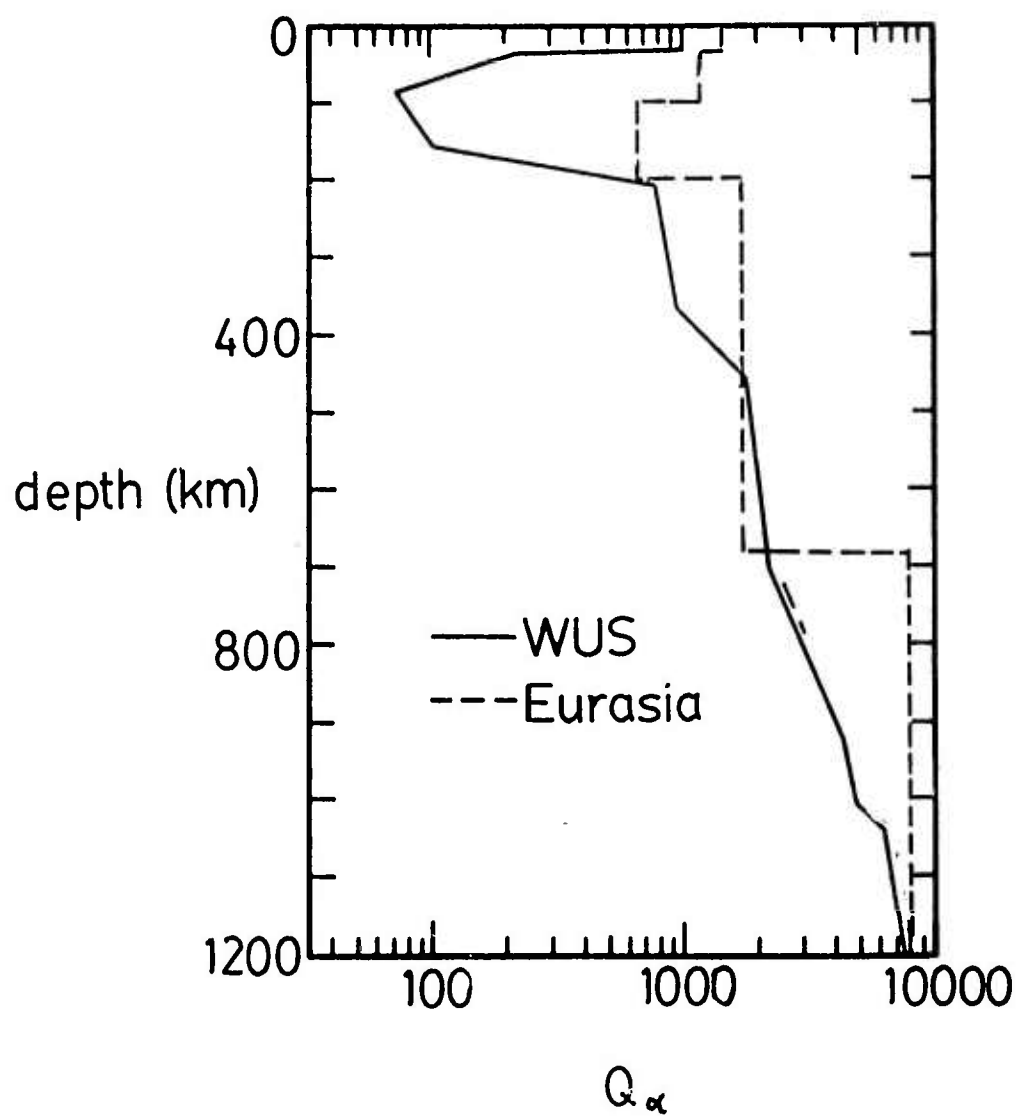


Figure 16

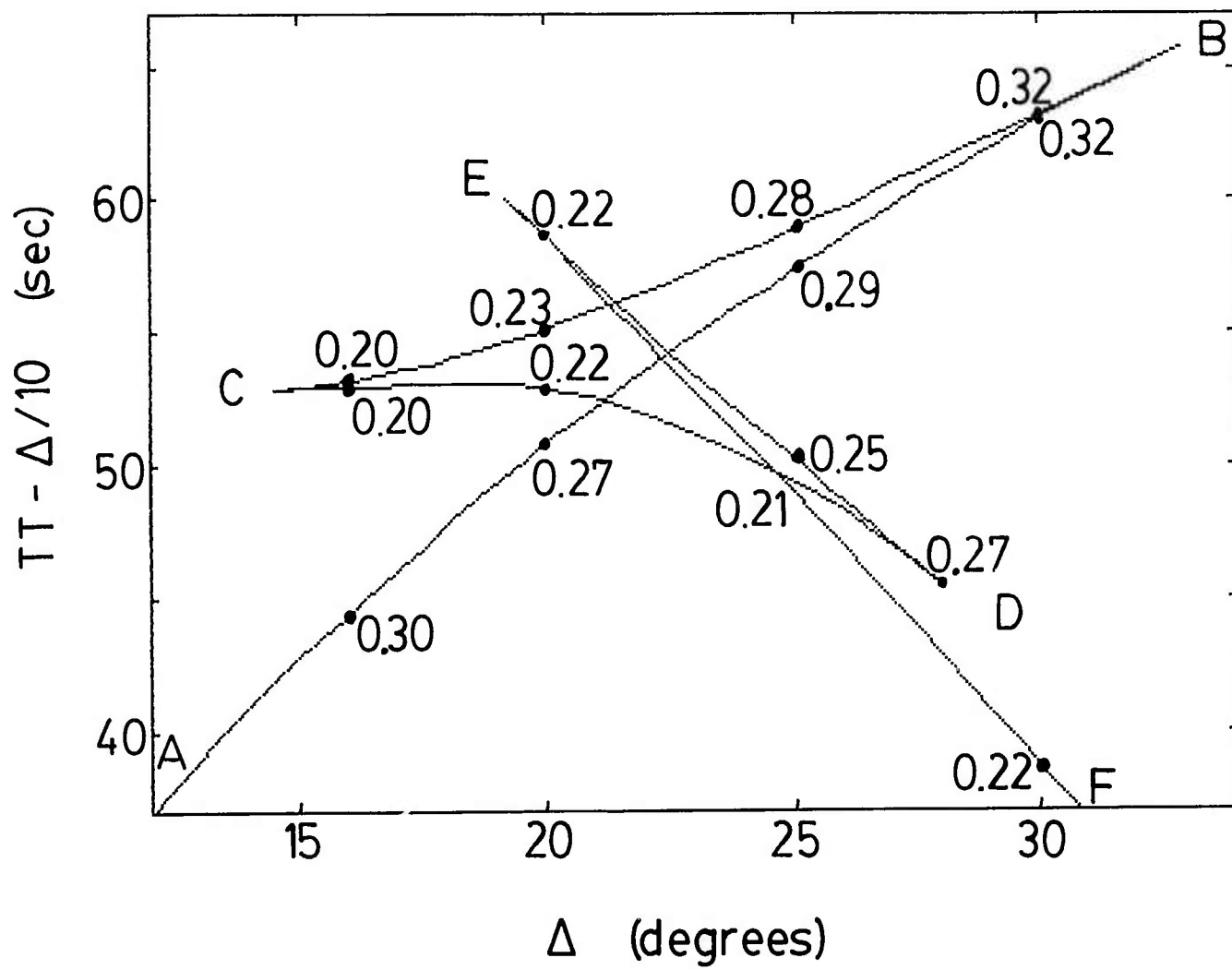
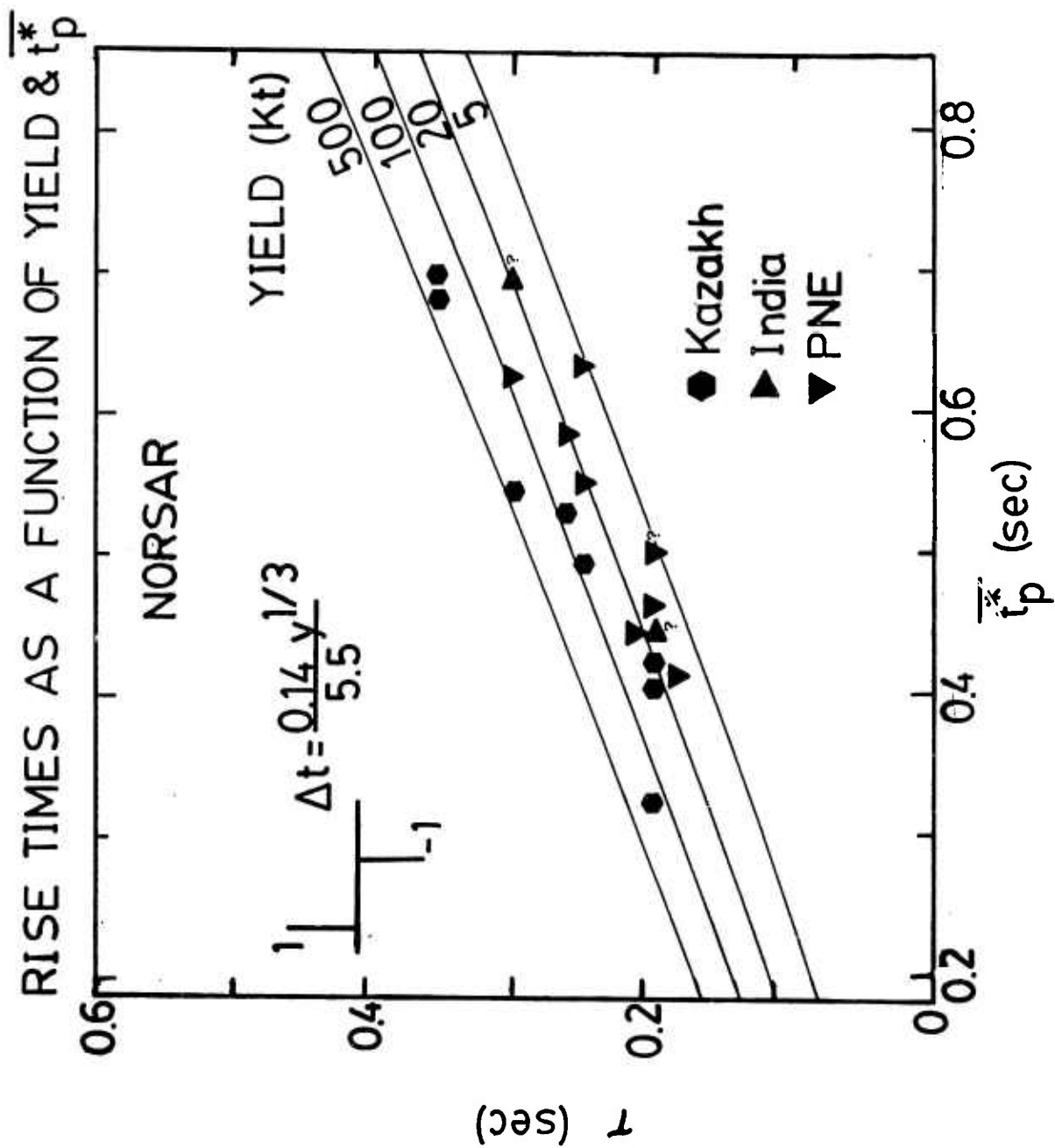


Figure 17





# SHORT PERIOD S & ScS

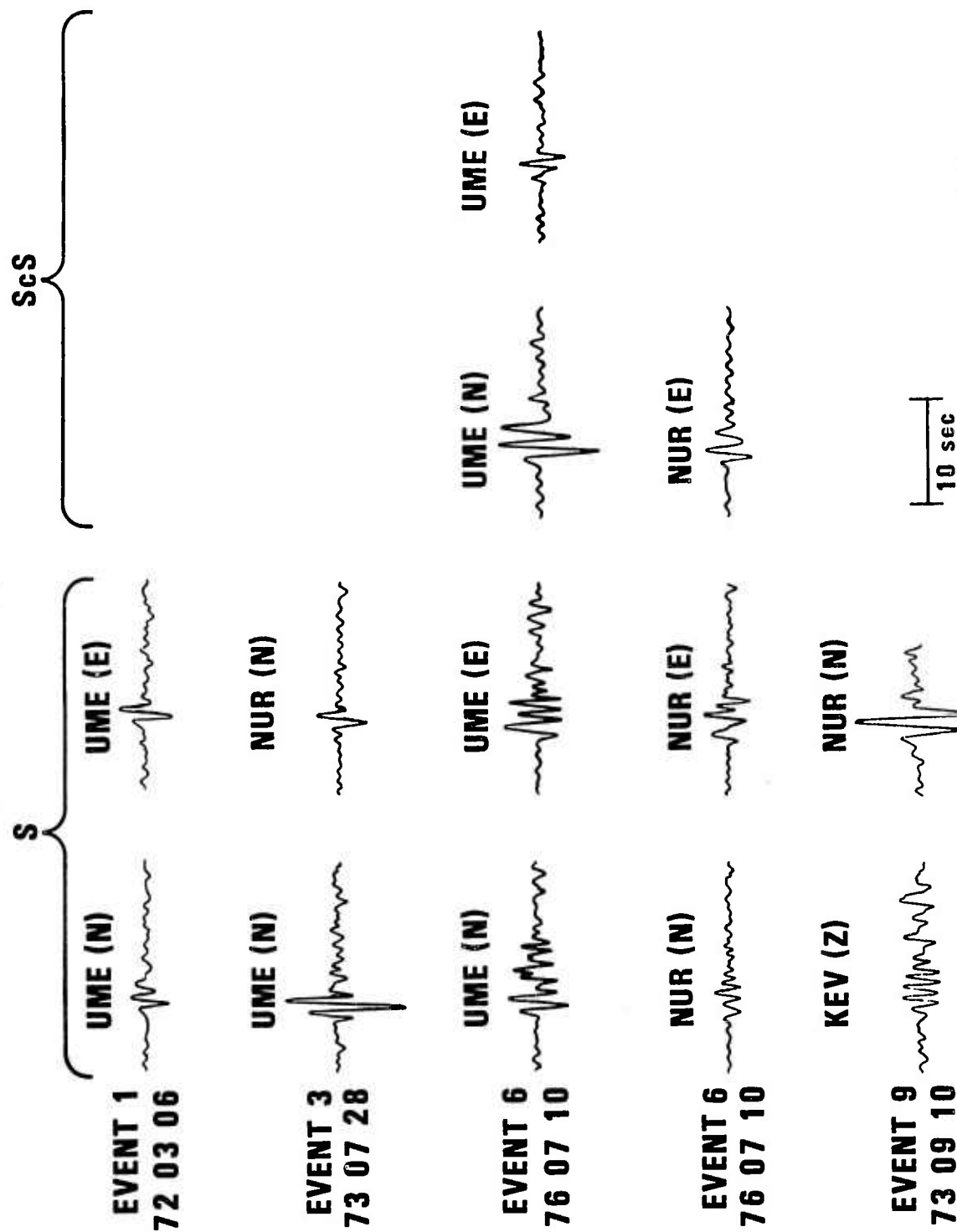
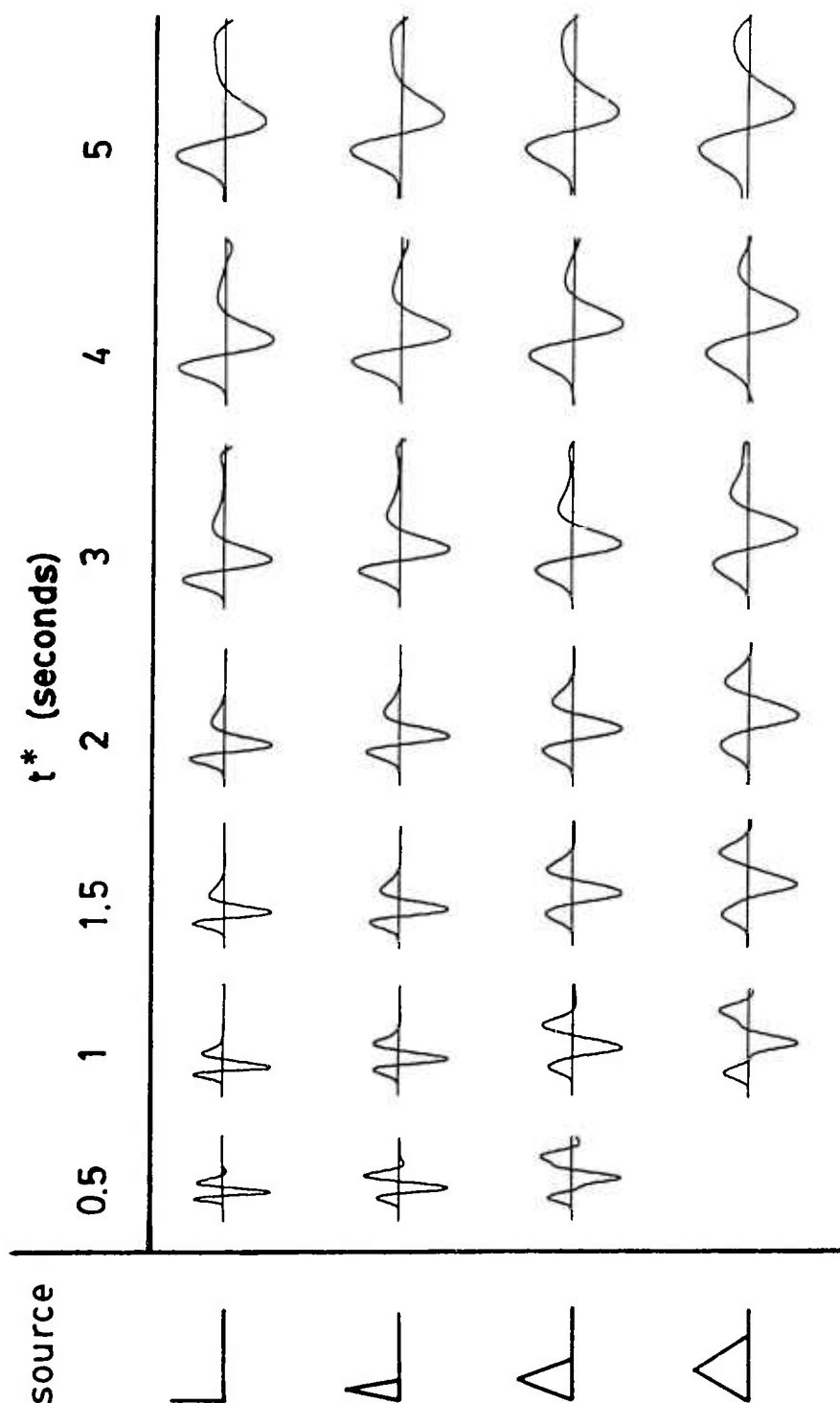


Figure 19



5 sec

Figure 20

# S-WAVE PERIODS

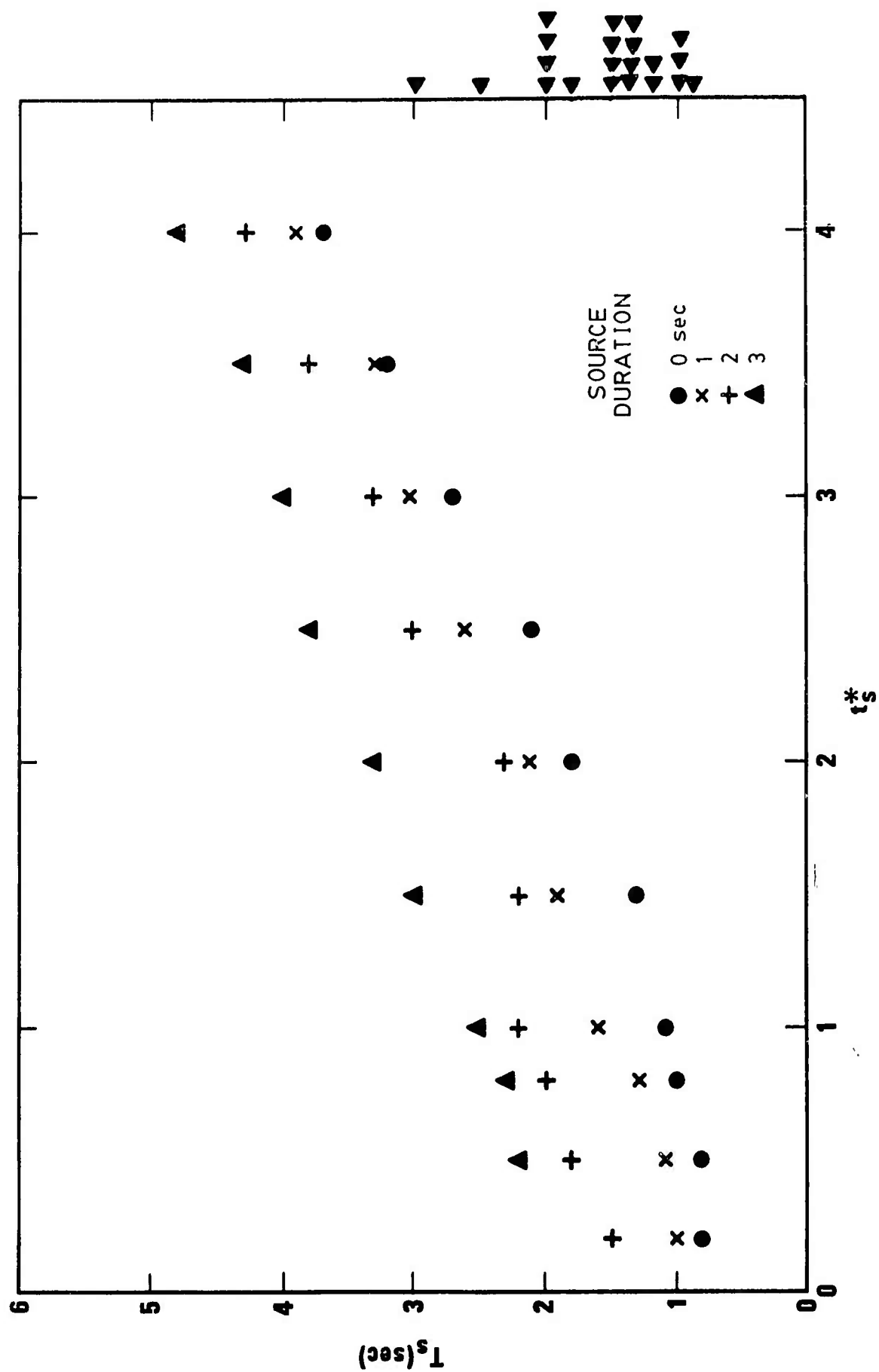


Figure 21

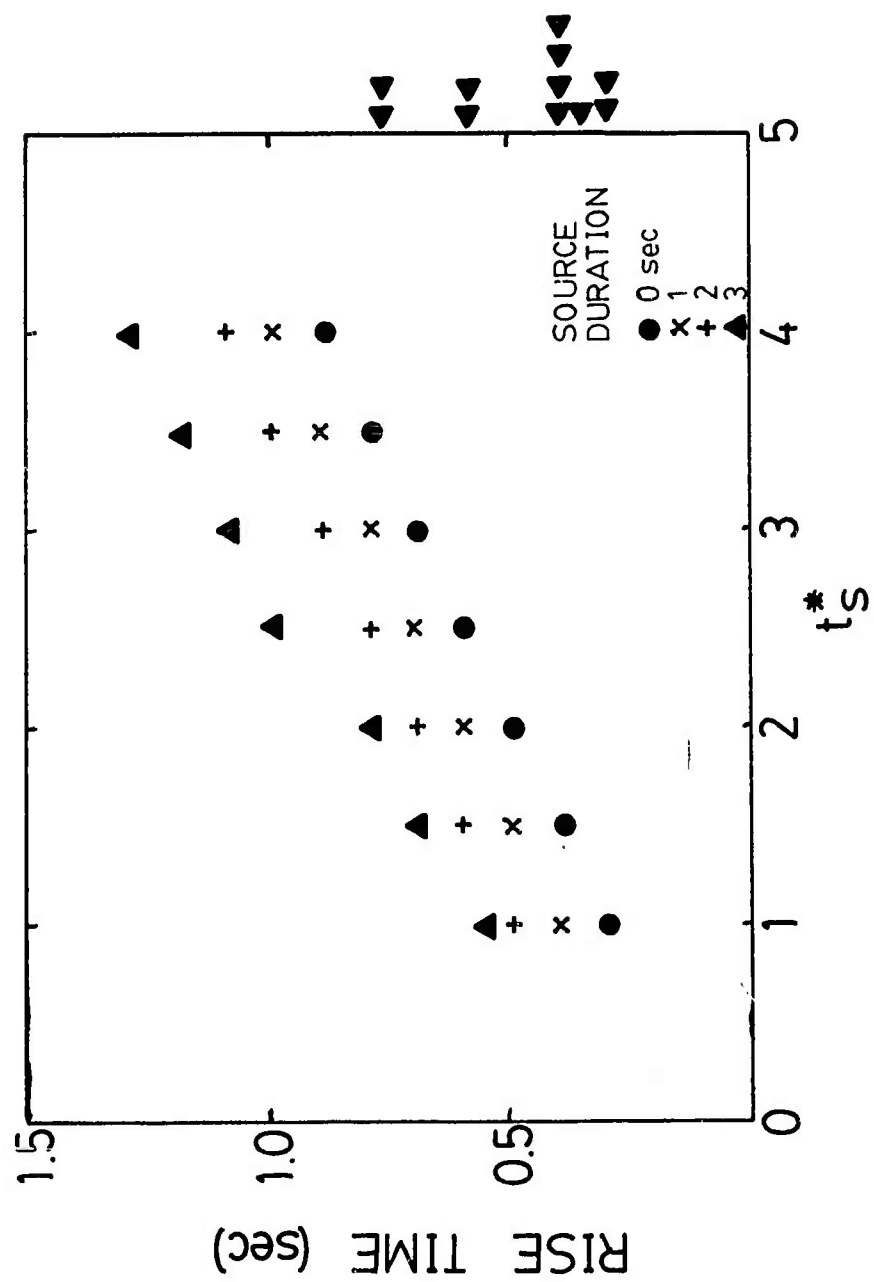


Figure 22

780306  
NUR Z  
 $\Delta = 73^{\circ}$



PP



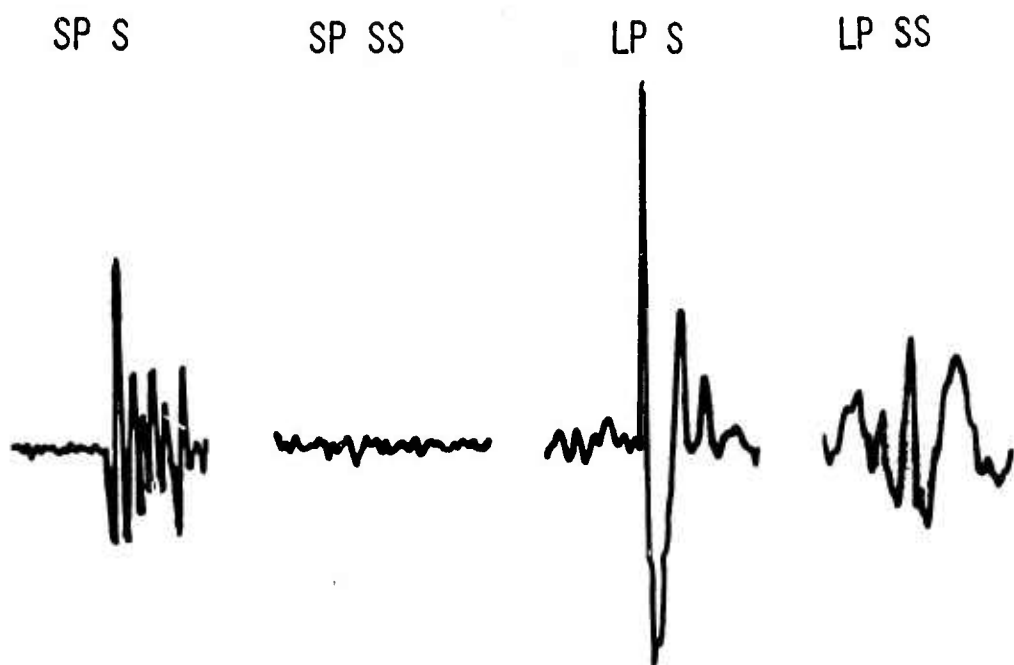
770602  
KEV Z  
 $\Delta = 41^{\circ}$



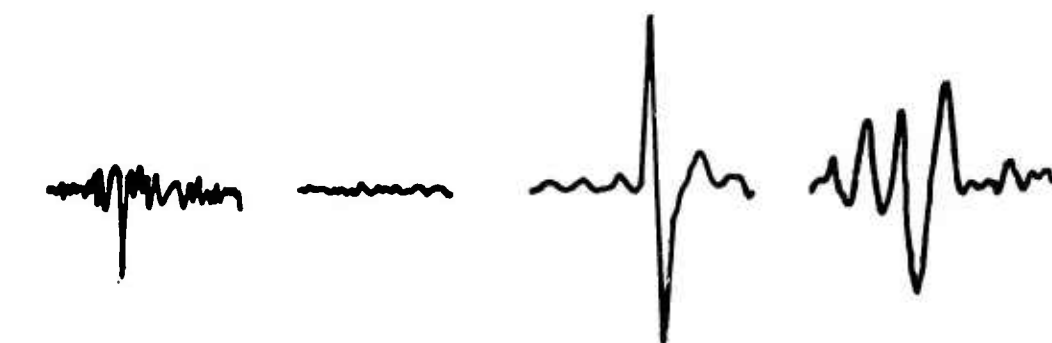
10.0 SEC

Figure 23

761212  
 UME EW  
 $\Delta = 77^\circ$



790816  
 KEV NS  
 $\Delta = 56^\circ$



770602  
 KEV NS  
 $\Delta = 41^\circ$



10.0 SEC

1 MIN

Figure 24

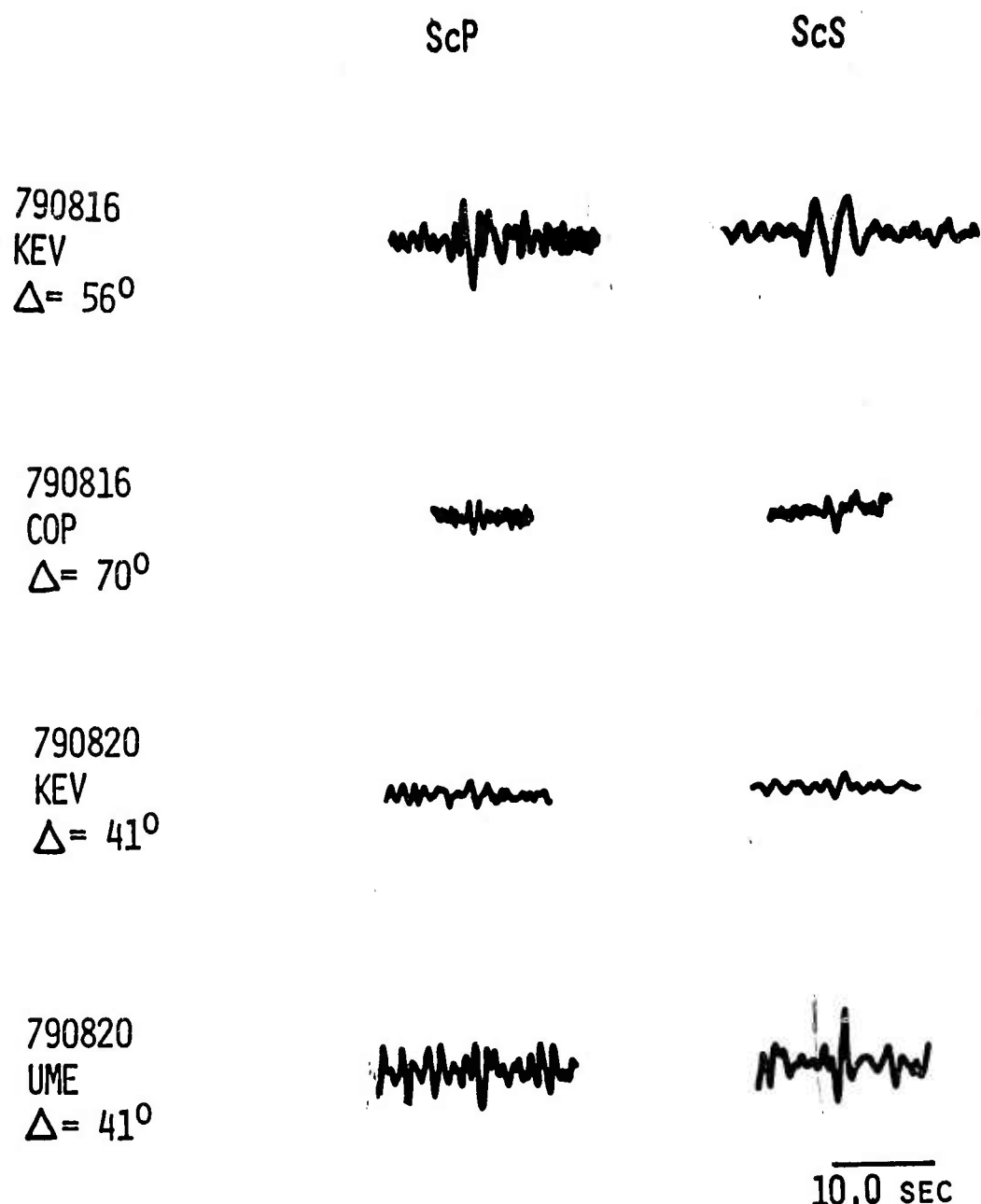


Figure 25



**Frequency Dependence of Q in the Mantle  
Underlying the Shield Areas of Eurasia,  
Part II: Analyses of Long Period Data**

by  
Alison Lees  
Zoltan Der  
Vernon Cormier\*  
Margaret Marshall  
and  
James Burnetti

Teledyne-Geotech  
314 Montgomery Street  
Alexandria, Virginia 22314

\* Earth Resources Laboratory  
Massachusetts Institute of Technology  
Cambridge, Massachusetts 02412

11 January 1985

## Abstract

Long period multiple S and ScS phases observed in northern Europe were analyzed to determine mantle attenuation in the 0.02 to 0.2 Hz range under the Eurasian shield. Two groups of events are used: deep Far-Eastern earthquakes and large earthquakes near the edges of the shield areas of Eurasia. The Q of the upper mantle under the Eurasian shield region was estimated in the time domain by taking amplitude ratios and in the frequency domain by taking spectral amplitude ratios among various arrivals and matching waveforms of synthetic seismograms and observed data. Under shield regions, SS/S amplitude ratios give  $t_S^* \sim 2.5-3$  seconds and multiple ScS amplitude ratios give  $t_S^* \sim 4.2$  seconds. Under tectonic regions, multiple S amplitude ratios suggest  $t_S^* \sim 5$  seconds. The results show that the upper mantle Q under this shield area is larger than the global average, but less than the Q values inferred from our studies of short period data in the same area. Preliminary results also suggest that at frequencies around 0.02 to 0.2 Hz, there is a  $\Delta t_S^*$  differential of around 2 seconds between shield and tectonic regions.

## Introduction

While it is easy to estimate attenuation in the short period band due to the sensitivity of wave amplitudes and spectra to  $Q$ , at low frequencies the direct P and S wave amplitudes and waveforms show little change even for relatively large variations in mantle  $Q$ . Therefore, the measurement of attenuation within a given region in the long period band is much more difficult because of the sensitivity of the wave properties to factors unrelated to mantle  $Q$  such as structural effects, source directivity and the complex superpositions of various wave arrivals.

There have been relatively few studies of attenuation in the long period band specifically in shield regions, although it has been noticed that  $Q$  measurements in continental areas which included shield regions tended to yield higher values than the worldwide averages (Kovach and Anderson, 1964; Sato and Espinosa, 1967; Mills, 1978; Sipkin and Jordan, 1980). Tectonically active continental areas have been found to be characterized by low  $Q$  in the underlying upper mantle within the long period seismic band (Solomon and Toksoz, 1970; Lee and Solomon, 1975, 1979; Sipkin and Jordan, 1980; Lay and Helmberger, 1981). The mantle  $Q$  values under tectonic areas were found to be similar or lower than the worldwide averages.

The seismic arrivals most suitable for the study of mantle  $Q$  at low frequencies are the multiple S and ScS phases with surface reflection points within the geographical region to be studied, in this case the shield area of northern Eurasia. Because of the relatively weak sensitivity of long period waves to attenuation, it is important to use a robust methodology for the measurement of mantle  $Q$  that minimizes the effects of the unrelated factors mentioned above. Since large events must be used for observing multiple S and ScS wave amplitudes and spectra, the additional complicating factor introduced by the possibility of directionality of large earthquake sources is minimized by the fact that the takeoff angles of such phases of various multiplicity are similar. To minimize the variety of difficulties mentioned above, we have averaged the  $t^*$  from

many events. We have verified that the fault plane orientations of the events analyzed were varied enough to eliminate any significant bias due to similar radiation patterns, even though a part of the assumed source mechanisms may be in error. We find that our approach is preferable to only doing detailed modeling of a few selected events with the inevitable tradeoffs between mantle  $Q$  and source directivity. In order to minimize structural effects we have considered a variety of plausible upper mantle velocity structures. Ideally both the sources and receivers should be located in shield areas, but since practically all natural earthquakes occur in tectonic areas we had to pay careful attention to the locations of surface reflection points for all multiple S phases. We have also found that because of the complex nature of long period S wave arrivals due to upper mantle triplications and scattered background noise, the spectral and waveform methods for estimating  $Q$  are much less stable than in the short period band. Multiple P arrivals in the long period band, although prominent on the seismograms, are not useful because of their relative insensitivity to  $Q_\beta$  and the P-SV conversions at reflections which add the complication of estimating conversion coefficients. To simplify our analyses and reduce structural effects we have also restricted our studies to the SH component of all shear wave arrivals. An increase in  $t_S^*$  of 4 seconds should result in a change of S wave amplitudes by roughly a factor of 2 at the dominant periods of long period S waves on the WWSSN records, around 20-25 seconds.

In the initial part of our work we have utilized northern European recordings of Far-Eastern deep earthquakes which contained many well-separated multiple S and ScS arrivals. The amplitudes of the multiple S arrivals were compared with full wave theory synthetic seismograms to estimate  $t^*$ . After having gained some experience with the problems associated with estimating mantle  $Q$  in the long period band, we decided to analyze a larger data set of central Asian earthquakes, mostly not deep, in order to increase the statistical stability of our results and decrease the number of tectonic-shield mixed paths. The use of the relatively uncomplicated SS/S amplitude ratios for these events tends to minimize the effects of structural variations.

We find  $t_S^* \sim 2.5$  to 3 seconds for S waves and 4.2 seconds for ScS under shield regions. Preliminary results suggest that  $t_S^*$  under tectonic regions is  $\sim 5$  seconds for S. These values of  $t^*$  are substantially higher than those we found in the previous paper for high frequency ( $f > 1$  Hz) waves under the same region (Der et al, 1985a, hereafter referred to as Paper I). In the third paper of this series (Der et al, 1985b, hereafter referred to as Paper II), we develop a  $Q(f)$  model which is consistent with both the short and long period results for  $t^*$ .

### Analyses of Data from Far-Eastern Deep Earthquakes

Multiple S and ScS arrivals from several deep earthquakes in the Far East were obtained from digital recordings at northern European and Scandinavian stations. To simplify the analysis, the records were rotated, and only the SH components were used, which for the case of radial symmetry do not have conversions to P waves or coupling to PL, resulting in simpler seismograms and total reflection at the core mantle boundary. The events are listed in Table I, and the source and receiver locations are plotted in Figure 1. Figure 1 also shows the surface reflection points under the Eurasian continent of SS and SSS. The SS surface reflection points are clearly under the Eurasian shield, while the higher order multiple S bounce points are often under tectonically active regions of China.

Long period SH seismograms have been synthesized using full wave theory for comparison with selected rotated records. In full wave theory, the synthetics are produced by numerical integration along the raypath in the complex plane; this allows for the proper treatment of such non-ray theory effects such as tunneling, head waves, diffracted phases, and caustics (Richards, 1973; Choy, 1977; Cormier and Richards, 1977). We have modeled some of the main S phases of the best four records from three Far Eastern events including all major arrivals due to triplications from reflections off of the two major upper mantle discontinuities.

Figure 2 shows four of the observed seismograms with the corresponding synthetic seismograms. The synthetic seismograms were computed assuming a perfectly elastic earth and using the SNA shear velocity upper mantle model of Grand and Helmberger (1984) merged with PREM model (Dziewonski and Anderson, 1981) in the lower mantle. The seismograms include the best fitting double-couple radiation pattern for the events but assume no directional variations in the shapes of the source time functions, which, for these synthetic records were assumed to be delta functions. Note that the arrival times of phases on the synthetics are close to those seen on the records for S, ScS, and SS but the later phases are delayed and their periods increase on the observed records relative to the synthetics. This can be explained by the observation that the multiple S and ScS arrivals of higher order cross the upper mantle in tectonic areas with lower velocities (Grand and Helmberger, 1984) and lower Q, while the synthetic records were derived from a high velocity mantle model for shields. The synthetics also show the complexity of the SSS waveform in this distance range due to multiple travel paths in the upper mantle.

The differences in peak to peak amplitudes and pulse shapes of the synthetic pulses as compared with the corresponding observed phases should thus provide opportunities to estimate  $t^*$ . Before the observed and synthetic phases can be compared, an appropriate source time function must be convolved with the synthetic pulses. The source time function was modeled by constructing a transfer function between the observed and synthetic S or S+ScS, depending on the distance range, and convolving the other synthetic waveforms with the appropriate transfer function. In Figure 3, some examples of the observed SS and SSS waveforms are shown, matched with corresponding synthetic seismograms which include the source transfer function and have been convolved with attenuation operators corresponding to various values of  $t^*$ . Comparing the amplitudes of the synthetic and observed phases gives estimates of  $\Delta t_S^* \sim 1.4$  seconds from SS, but much higher values,  $2\Delta t_S^* \sim 10$  seconds or  $\Delta t_S^* \sim 5$  seconds from SSS. Thus, it is clear that the SSS waves are being attenuated much

more than the SS waves, as was noted when the synthetic records were compared with the observed seismograms. One reason for this is that the SSS have their first surface reflection point under tectonic regions in Southeast Asia, while the SS reflection point is under a shield region as seen in Figure 1. Also, at this distance range the SSS is a more complex waveform due to multiple travel paths in the upper mantle. Care must be taken to avoid cases where there is interference from sSS.

To complement the results from amplitude studies, spectral ratios between multiple S or multiple ScS pairs can be used to estimate  $\bar{t}^*$  for the same set of arrivals. In order to more accurately estimate the intrinsic attenuation, any effect of the earth structure on the spectra must also be taken into account. This is especially important with the SSS and higher order multiple S phases since they interact strongly with the upper mantle discontinuities around 400 and 670 km and with the low velocity zone.

The structural effect on the spectra was estimated by taking the SSS/SS spectral ratios of synthetic pulses for an elastic earth. In this case, any curvature in the spectral ratio would be due to structural effects. The synthetic phases were treated the same way as the data; time domain phases were tapered with a 20% cosine window and Fourier transformed. Three SSS/SS spectral amplitude ratios from synthetic seismograms generated with  $t^*=0$  seconds are shown in Figure 4. Within the range of significant instrument response (about 0 to 1.5 Hz), the resultant spectral ratios are quite flat, suggesting that the mantle structure makes no significant contribution to  $t_S^*$  in the long period band.

Spectral ratios were taken of both the long period multiple S and ScS phases from several events. The range of good signal-to-noise ratio varied, but generally included 0.3-0.6 Hz. The multiple S ratios gave a range of  $t^*$ 's, with  $t_S^*$  averaging around 4 seconds for rays passing through tectonic-region upper mantle. The ScS spectral ratios were very variable, averaging around -2 seconds. Representative spectral ratios are shown in Figure 5. Waveform matching studies for multiple S and ScS phases have

also been used to estimate  $t_S^*$ ; examples of these fits are shown in Figure 6. Because of the many factors involved in correcting the amplitudes, such as geometrical spreading, instrument response, and radiation pattern, only the periods were compared in the waveform matching. At least for short periods, frequency content tends to be a more robust measurement than amplitude anyway (e.g., Der and Lees, 1984). The waveform matching suggests  $\Delta \bar{t}^*$  values for both S and ScS that are low,  $\bar{t}^* \sim 1-3$  seconds, especially given that the ratios mostly apply to tectonic paths.

The somewhat conflicting results between the various approaches used for Q estimation above need some discussion. The amplitude studies of SS which reflect under the shield give  $t_S^* \sim 1.5$  seconds, while SSS which have a reflection point under a tectonic region give  $2t_S^* \sim 10$  seconds or  $t_S^* \sim 5$  seconds. These results are not surprising as one might expect a difference in  $t^*$  between paths through shield and tectonic regions. However, while the spectral estimates of multiple S phases for these same paths give  $\bar{t}^* \sim 4$  seconds for tectonic paths, the spectral estimates for the ScS phases give  $\bar{t}^* \sim -2$  seconds. Also, for the S phases, spectral ratios of synthetic waveforms for the anelastic case ( $t^* = 0$  seconds) with observed phases give  $\bar{t}^* \sim 0.5$  seconds. Clearly, some of the very low  $t_S^*$  estimates from spectral ratio measurements and waveform matches are suspect. It is likely that these phases are either so complex or too contaminated by the scattered background that they cannot be isolated well enough by windowing to yield stable, meaningful spectral ratios. This is suggested by the fairly narrow frequency ranges over which there was good signal-to-noise ratio for most of the arrivals. Also, the long period instruments are narrowly peaked around 0.05 Hz, so small changes in period are not very discernible. The ScS phases seem especially effected, as both the periods and amplitudes show a great deal of scatter; Sipkin and Jordan (1979,1980) have also observed that the quality of the multiple ScS arrivals is generally not very good, perhaps due to surface scattering or contamination by surface wave modes.



Given these limitations on the data, it appeared at this point of the investigation that we needed a more robust approach to define  $Q$  in the long period band under shields.

### **Analyses of WWSSN Seismograms for Central Asian Earthquakes**

To complement the above results from detailed comparison of four records with the corresponding synthetics, a more statistically oriented analysis was performed by comparing the SS/S amplitude ratios from about 80 records with the amplitude ratios predicted for the elastic case. There are several reasons for doing this additional study. First, long period S waves are not attenuated much in a high  $Q$  environment, so measuring the amount of attenuation is difficult, and performing many measurements allows a more quantitative determination of statistical bounds on  $t^*$  as opposed to the more qualitative results we were forced to draw from the Far-Eastern data above. Also, it is difficult to accurately model the wavetrain of the large events needed to produce visible multiple S phases by a simple double-couple mechanism. By using many events, hopefully these variations will be averaged out and will not have too significant an effect on the attenuation estimate. Finally, this is a fairly simple way to estimate the attenuation and using this data set it is easier to restrict the area of investigation to the shield areas proper.

The locations of the Central Asian events and European recording stations used are shown in the map in Figure 7. The surface reflection points for the SS phases are also shown in Figure 7; they are located in the central portions of the Russian shield. The source parameters including the fault plane solutions are given in Table II. Whenever possible, the solutions were taken from the literature (references with Table II). For the events for which there are no published solutions, we have derived our own solutions using P wave first motions from the bulletins of the International Seismic Centre. Most events have a pair of complementary focal solutions. In each case, we com-

puted the radiation pattern correction for each focal solution, and in nearly all cases, both solutions gave similar absolute amplitude ratios. We did not use the data in cases where there was a large difference.

Station-event pairs were chosen so that one component of the receiver was within  $10^\circ$  of transverse so as to eliminate most P-SV contamination and provide simpler records. Station-event pairs were eliminated if the receiver was close to a node in the radiation pattern for either S or SS.

The double-couple corrected amplitude ratios of SS/S are plotted as functions of epicentral distance in Figure 8. The theoretical predictions using the SNA model of Grand and Helmberger (1984) are also shown for comparison. These curves are the results of ray tracing calculations assuming a lossless medium and smoothed over  $3^\circ$  intervals. Geometrical spreading has been taken into account in the ray tracing calculations. To verify the validity of these results we have also computed synthetic seismograms using full wave theory (Cormier and Richards, 1977) and WKBJ synthetics (Chapman, 1978; Dey-Sarkar and Chapman, 1978) (Figure 9) for several distances covering the same range and found a good agreement between the results of the three methods. At distances where there are multiple arrivals, the arrival of largest amplitude was read off of the records and the largest amplitude arrival was used from the ray tracing calculations or synthetic seismograms. Small perturbations of the SNA model did not change the overall trend of these curves, although in limited distance ranges the amplitude ratios varied considerably. Therefore, we have concluded that our deductions will not be very model-dependent as long as we use a high velocity, shield type upper mantle.

Although there is a considerable scatter in the observed amplitude ratios in Figure 8, the mean trend of the data points is clearly below the theoretical curve for  $t^*=0$  seconds, thus indicating anelastic losses in the mantle for SS relative to S. The  $\bar{t}_S^*$  which fits the data points with the least rms error is around 2.5 to 3 seconds. These

values are comparable, given the uncertainties associated with such measurements, to the values used by Burdick et al (1982) to match the observed amplitude ratios of SS relative to S in synthetic seismograms for the same area. Due to the averaging over many events it is unlikely that these results are biased by source directivity or a few wrong fault plane solutions. Given this many events, the results do not change even when isotropic source radiation is assumed.

In the 35 to 65° distance range, SS has multiple arrivals due to interactions with the 420 and 670 km discontinuities. For this study, we took the maximum SS amplitude observed on each record in determining the SS/S amplitude ratio. In most cases, the maximum observed amplitude is on the same branch of the SS triplication as the maximum SS amplitude on the synthetic seismograms calculated for an anelastic earth ( $t^* = 0$  seconds). However, the branch with maximum amplitude changes over the 45° to 80° range as seen in the WKBJ synthetics in Figure 9. We are now in the process of recalculating SS/S amplitude ratios individually for the different branches, and this should allow further refinement of our  $t^*$  models.

We have also attempted to estimate  $t^*$  from the decay rates of amplitudes of successive multiple ScS phases from Hindu-Kush and Far Eastern events where the surface reflection points are all under shield areas. The event parameters are listed in Table III and the surface reflection points are shown in Figure 10. Individual amplitudes are corrected for geometrical spreading and radiation pattern. On some of the long period records ScS comes in close behind S, so the amplitude ratios were taken with respect to  $ScS_2$ . The amplitude of the ratio, (amplitude  $ScS_N$  / amplitude  $ScS_2$ ), can be written as  $A \sim \exp [-\pi f(N-2)t^*]$ , where  $t^*$  is the  $t^*$  for one leg of the path (a single ScS). Then,  $\ln A \sim -\pi f(N-2)t^*$ , and  $t^*$  can be estimated from the slope of a plot of  $\ln A$  vs  $(N-2)f$ , as in Figure 11. The  $t_S^*$  value for a single passage through the mantle is  $\sim 4.2$  seconds. This gives an average  $Q$  of 230 over the path of a single ScS, remarkably similar to the value estimated by Sipkin and Jordan (1980) for  $Q_{ScS}$  for continental regions. These results

must be interpreted with caution as we were only able to use eleven pairs of amplitude ratios for the shield region, and because, as noted previously, SeS data with good signal to noise ratio is scarce in continental areas where these phases are buried in the high amplitude surface wave codas. We are in the process of enlarging our data set so as to better be able to resolve the differences in attenuation between the two areas.

### Summary and Conclusions

Analyses of waveforms, amplitude ratios, and spectra of multiple S from Eurasian earthquakes give  $t_S^*$  estimates for a double passage of S waves through the mantle under shields around 2 to 3 seconds, while ScS give  $t_{ScS}^*$  around 4 seconds. Similar, though less extensive analyses of S passing through the tectonic regions of China and southern Asia give  $t_S^*$  around 5 seconds. This is significantly higher than for paths under shield regions alone.

The above estimates of  $t_S^*$  for shields from long period S and SS measurements are lower than the global averages for this parameter but significantly higher than the  $\bar{t}_S^*$  values derived from short to intermediate period (0.3 to 8 Hz) S waves in Paper I. The corresponding  $\bar{t}_P^*$  values are 0.6-0.75 seconds, much higher than the allowable *upper limits* for  $\bar{t}_P^*$  values in the 1-8 Hz range (Paper I). These results are quite important because, as we shall show in Paper II, they indicate that simple frequency independent Q models cannot be used to explain both these results and those presented in Paper I. Moreover, since the upper mantle regions sampled are the same as those studied in Paper I the possibility of differences in areal sampling does not exist here, unlike in some global arguments used for the frequency dependence of Q. It is interesting that the long period multiple ScS arrivals give a higher  $t_S^*$  than the S and SS arrivals (4.2 seconds as opposed to 2.5 or 3 seconds). The simplest explanation is that there is a low Q layer in the mantle just above the core mantle boundary. Even if this layer is several hundred km thick, S waves arriving at epicentral distances less than 80° do not bottom

deeply enough to sample such a layer. It is also of interest that higher values of  $t_S^*$  were found for paths crossing the upper mantle under the tectonic areas of Eurasia, than under the shield areas of Eurasia. This suggests a  $t_S^*$  differential of around 2 seconds for long period S waves for shield versus tectonic paths, corresponding to a  $t_P^*$  differential of  $>0.5$  seconds. Such a  $t_P^*$  differential is larger than the similar differential proposed for short period waves, implying  $t^*$  versus frequency curves for shield and tectonic regions which are separated over the 0.01 to 10 Hz band and divergent at low frequencies.

### Acknowledgements

Tom McElfresh has written several of the computer programs utilized in the data analyses. We have benefited from discussions with Drs. Keith McLaughlin and Robert R. Blandford. Special thanks are due to Professor P.G. Richards who has made his programs available for the generation of the synthetic seismograms shown in this paper.

## References

- Berberian, M. (1982). Aftershock tectonics of the 1978 Tabas-e-Golshan (Iran) earthquake sequence: a documented active "thin- and thick-skinned" tectonic case, *Geophys. J. R. astr. Soc.*, **68**, 499-530.
- Burdick, L.J., S. Grand, D.V. Helmberger, T. Lay and J. Rial (1982). Remote sensing of attenuation bias using SS, *WCCP-R-83-01*, Woodward-Clyde Consultants, Pasadena, California 91109.
- Chapman, C.H. (1978). A new method for computing synthetic seismograms, *Geophys. J. R. astr. Soc.*, **54**, 481-518.
- Choy, G.L. (1977). Theoretical seismograms of core phases calculated by a frequency-dependent full wave theory, and their interpretation, *Geophys. J. R. astr. Soc.*, **51**, 275-311.
- Cormier, V.F. and P.G. Richards (1977). Full wave theory applied to a discontinuous velocity increase: the inner core boundary, *J. Geophys.*, **43**, 3-31.
- Der, Z.A. and A.C. Lees (1984). Methodologies of estimating  $t^*(f)$  from short period body waves and regional variations of  $t^*(f)$  in the United States, submitted to *Geophys. J. R. astr. Soc.*
- Der, Z.A., A.C. Lees and V.C. Cormier (1985a). Frequency dependence of Q in the mantle underlying the shield areas of Eurasia, Part III: the Q model, included in this report.
- Der, Z.A., A.C. Lees, V.C. Cormier and L. Anderson (1985b). Frequency dependence of Q in the mantle underlying the shield areas of Eurasia, Part I: analyses of short and intermediate period data, included in this report.
- Dey-Sarkar, S.K. and C.H. Chapman (1978). A simple method for the computation of body-wave seismograms, *Bull. Seismol. Soc. Am.*, **68**, 1577-1593.
- Dziewonski, A.M. and D.L. Anderson (1981). Preliminary reference earth model, *Phys. Earth Planet. Inter.*, **25**, 297-356.
- Dziewonski, A.M. and J.H. Woodhouse (1983). An experiment in systematic study of global seismicity: centroid-moment tensor solutions for 201 moderate and large earthquakes of 1981, *J. Geophys. Res.*, **88**, 3247-3271.
- Dziewonski, A.M., A. Friedman, D. Giardini and J.H. Woodhouse (1983). Global seismicity of 1982: centroid-moment tensor solutions for 308 earthquakes, *Phys. Earth Planet. Inter.*, **33**, 76-90.
- Grand, S. and D.V. Helmberger (1984). Upper mantle structure of North America, *Geophys. J. R. astr. Soc.*, **76**, 399-438.
- Giardini, D. (1984). Systematic analysis of deep seismicity: 200 centroid-moment tensor solutions for earthquakes between 1977 and 1980, *Geophys. J. R. astr. Soc.*, **77**, 883-914.
- Jackson J. and D. McKenzie (1984). Active tectonics of the Alpine-Himalayan belt between western Turkey and Pakistan. *Geophys. J. R. astr. Soc.*, **77**, 185-264.

- Kovach, R.L. and D.L. Anderson (1964). Attenuation of shear waves in the upper and lower mantle, *Bull. Seismol. Soc. Am.*, *54*, 1855-1865.
- Lay, T. and D.V. Helmberger (1981). Body wave amplitude patterns and upper mantle attenuation variations across North America, *Geophys. J. R. Astr. Soc.*, *66*, 691-726.
- Lee, W.B. and S.C. Solomon (1975). Inversion schemes for surface wave attenuation and  $Q$  in the crust and mantle, *Geophys. J. R. astr. Soc.*, *43*, 47-71.
- Lee, W.B. and S.C. Solomon (1979). Simultaneous inversion of surface wave phase velocity and attenuation, Rayleigh and Love waves over continental and oceanic paths, *Bull. Seismol. Soc. Am.*, *69*, 65-96.
- Mills, J.M. (1978). Great circle Rayleigh wave attenuation and group velocity, Part IV, regionalization and pure-path models for shear velocity and attenuation, *Phys. Earth Planet. Inter.*, *17*, 323-352.
- Molnar, P. and W-P. Chen (1983). Focal depths and fault plane solutions of earthquakes under the Tibetan Plateau. *J. Geophys. Res.*, *88*, 1180-1196.
- Richards, P.G. (1973). Calculation of body waves for caustics and tunneling in core phases, *Geophys. J. R. astr. Soc.*, *35*, 243-264.
- Roecker, S.W., O.V. Soboleva, I.L. Nerseov, kA.A. Lukk, D. Hatzfeld, J.L. Chatelain and P. Molnar (1980). Seismicity and fault plane solutions of intermediate depth earthquakes in the Pamir-Hindu Kush region, *J. Geophys. Res.*, *85*, 1358-1364.
- Sato, R. and A.F. Epsinosa (1967). Dissipation in the Earth's mantle and rigidity and viscosity in the Earth's core determined from waves multiply reflected from the mantle-core boundary, *Bull. Seismol. Soc. Am.*, *57*, 829-856.
- Sipkin, S.A., and T.H. Jordan (1979). Frequency dependence of  $Q_{ScS}$ , *Bull. Seismol. Soc. Am.*, *69*, 1055-1079.
- Sipkin, S.A., and T.H. Jordan (1980). Regional variations of  $Q_{ScS}$ , *Bull. Seismol. Soc. Am.*, *70*, 1071-1102.
- Solomon, S.C. and M.N. Toksoz (1970). Lateral variation of attenuation of P and S waves beneath the United States, *Bull. Seism. Soc. Am.*, *60*, 819-838.
- Tapponnier, P. and P. Molnar (1977). Active faulting and tectonics in China, *J. Geophys. Res.*, *82*, 2905-2930.

Table I

Event Parameters for Deep Far-Eastern Earthquakes

date	latitude (degrees)	longitude (degrees)	depth (km)	origin time	$m_b$	focal mechanism 1			focal mechanism 2		
						strike	dip	rake	strike	dip	rake
780307	31.99	137.61	441.0	02 46 47.6	6.5	153.0	76.0	77.0	18.0	19.0	133.0
790816	41.81	130.19	588.0	21 31 26.3	6.1	56.0	24.0	133.0	190.0	73.0	73.0
800422	32.10	137.60	394.0	05 34 13.8	5.7	84.0	22.0	189.0	346.0	87.0	292.0

These focal mechanisms are from Giardini (1984).



Table II

## Event Parameters

date	latitude (degrees)	longitude (degrees)	depth (km)	origin time	$m_b$	focal mechanism 1			focal mechanism 2			ref
						strike	dip	rake	strike	dip	rake	
700104	24.14	102.50	31.0	17 00 40.2	5.9	121.	64.	184.	31.	90.	356.	7
700224	30.58	103.03	33.0	02 07 36.6	5.9	256.	50.	124.	30.	50.	57.	7
700729	26.02	95.40	59.0	10 16 19.3	6.5	170.	65.	339.	270.	66.	205.	
700730	37.62	55.66	19.0	00 52 19.0	5.7	197.	42.	55.	313.	68.	35.	5
710324	35.46	98.17	13.0	13 54 17.7	5.6	262.	16.	323.	2.	65.	231.	7
710403	32.32	95.44	33.0	04 50 45.6	5.6	170.	79.	160.	80.	90.	347.	7
710510	42.76	71.36	33.0	14 51 46.6	5.6	122.	25.	90.	302.	65.	90.	
710526	35.51	56.22	26.0	02 41 46.0	5.4	57.	42.	20.	309.	75.	130.	5
711028	41.66	72.37	22.0	13 30 57.1	5.5	145.	54.	90.	315.	36.	90.	
730206	31.40	100.58	33.0	10 37 10.1	6.1	6.0	66.0	10.	276.0	60.0	176.	
730531	24.26	93.55	30.0	23 39 56.7	5.9	180.	65.	355	270.	66.	184	
730714	35.16	86.46	33.0	04 51 21.0	6.0	190.	60.	215.	81.	60.	325.	6
730714	35.26	66.60	33.0	13 39 30.0	5.9	37.	68.	304.	156.	40.	216.	6
740510	26.24	104.01	11.0	19 25 15.0	6.2	0.	10.	90.	180.	80.	90.	
740704	45.14	94.03	33.0	19 30 42.1	6.1	69.	66.	175.	179.	66.	4.	
740611	39.47	73.65	9.0	20 05 30.1	5.6	45.	40.	90.	225.	50.	90.	
740927	26.60	65.50	70.0	05 26 39.4	5.6	90.	74.	349.	160.	76.	200.	
750426	35.62	79.92	7.0	11 06 43.5	5.8	169.	62.	211.	63.	63.	326.	6
750505	33.09	92.92	33.0	05 16 49.3	5.6	250.	78.	346.	343.	96.	192.	6
750530	26.64	97.03	70.0	17 45 00.6	5.6	105.	75.	90.	285.	15.	90.	
751003	30.41	66.35	33.0	17 31 36.0	5.7	28.	86.	2.	—	—	—	5
760529	24.54	96.60	33.0	14 00 19.0	5.7	85.	85.	166.	175.	78.	5.	
760531	24.37	96.62	24.5	05 06 30.5	5.5	28.	75.	270.	208.	15.	270.	
760721	24.76	98.68	33.0	15 10 45.1	5.7	46.	90.	162.	326.	68.	0.	
760726	39.71	116.37	37.1	10 45 37.2	6.1	0.	30.	90.	180.	60.	90.	
760812	26.07	97.04	31.4	23 26 47.1	6.2	12.	80.	90.	192.	10.	90.	
760816	32.76	104.09	6.9	14 06 45.1	6.1	70.	72.	334.	170.	64.	193.	
760621	32.59	104.24	14.6	21 49 51.6	6.0	140.	76.	90.	320.	12.	90.	
760623	32.49	104.16	17.5	03 30 05.5	6.2	20.	60.	343.	116.	75.	210.	
761106	27.66	101.04	5.4	18 04 05.5	5.7	270.	60.	192.	160.	76.	350.	
761115	39.50	117.73	27.1	13 53 02.6	6.0	58.	75.	270.	236.	15.	270.	
770101	36.19	90.96	33.0	21 39 43.9	5.6	285.	15.	90.	105.	75.	90.	
770119	37.02	95.73	33.0	00 46 15.8	5.6	2.	60.	345.	100.	75.	210.	
770714	40.35	63.71	33.0	05 49 08.3	5.5	5.	40.	90.	185.	50.	90.	
771118	32.65	66.39	33.0	05 20 10.3	5.7	335.	65.	0.	60.	90.	5.	
780307	31.99	137.61	441.0	02 46 47.6	6.5	153.0	76.0	77.0	16.0	19.0	133.0	4
780421	36.63	71.26	229.6	15 22 57.9	5.6	340.	80.	90.	160.	10.	90.	
781008	39.40	74.76	49.7	14 20 04.2	5.6	5.	50.	90.	185.	40.	90.	
781104	37.67	46.90	34.0	15 22 19.0	6.1	0.0	160.	270.	0.0	70.	90.	5
780116	33.90	59.47	33.0	09 50 10.0	5.9	125.	64.	47.	168.	146.	47.	5
790329	41.95	83.36	33.0	02 01 32.1	5.8	85.	60.	90.	265.	30.	90.	
790520	29.93	80.27	33.0	22 59 11.6	5.7	68.	67.	90.	246.	23.	90.	
790816	41.81	130.19	566.0	21 31 26.3	6.1	56.0	24.0	133.0	190.0	73.0	73.0	4
790624	41.15	108.13	33.0	16 59 28.9	5.7	28.	82.	270.	208.	6.	270.	
791114	33.92	59.74	33.0	02 21 22.0	6.0	75.	90.	160.	165.	60.	0.	5
800112	33.49	57.19	33.0	15 31 42.0	5.4	172.	148.	40.	—	—	—	1
800222	30.55	68.64	14.2	03 02 44.8	5.7	102.	90.	270.	192.	0.	0.	
800331	35.49	135.52	362.0	07 32 31.8	5.7	210.	41.	207.	99.	73.	308.	2
800422	32.10	137.60	394.0	05 34 13.8	5.7	84.0	22.0	169.0	346.0	87.0	292.0	4
800504	36.05	46.99	46.0	18 35 20.0	5.4	0.0	90.	90.	0.0	0.	270.	5
800729	29.63	81.09	33.0	14 56 42.0	6.1	105.	75.	90.	285.	15.	90.	
801119	27.39	68.75	17.0	19 00 46.9	6.0	63.	62.	335.	166.	67.	207.	

810123	30.93	101.10	33.0	21 14 02.6	5.7	230.0	80.0	186.	139.0	84.0	350.	2
810508	42.66	139.13	200.0	23 34 44.9	6.0	158.0	47.0	336.0	205.0	72.0	226.0	2
810531	44.60	137.30	295.0	08 42 17.7	5.1	146.	61.	2.	55.	88.	151.	2
810728	30.01	57.78	33.0	17 22 54.0	5.5	173.0	28.0	152.	--	--	--	2
810812	35.69	73.59	33.0	07 15 57.4	6.2	120.0	36.0	101.	286.0	55.0	82.	2
820123	31.70	82.25	33.0	17 37 30.3	6.0	184.0	37.0	262.	15.0	53.0	276.	
820506	40.07	71.54	33.0	17 37 44.8	6.0	112.0	37.	116.	267.0	57.	72.	3

For cases where only one focal solution is given, the author of the cited reference constrained the solution from surface tectonics. Focal mechanisms without a reference were done by the authors using first motions from the ISC Bulletin.

References: 1, Berberian (1982); 2, Dziewonski and Woodhouse (1983); 3, Dziewonski et al (1983); 4, Giardini (1984); 5, Jackson and McKenzie (1984); 6, Molnar and Chen (1983); 7, Tapponnier and Molnar (1977).

Table III

Event Parameters for Deep Events Used in Determining  $t_{ScS}^*$  Under Shields

date	latitude (degrees)	longitude (degrees)	depth (km)	origin time	$m_b$	focal mechanism 1			focal mechanism 2			ref
						strike	dip	rake	strike	dip	rake	
660606	36.4	71.1	221.0	07 46 16.1	6.2	286.8	29.1	115.6	78.0	64.1	76.6	3
731017	36.4	71.2	221.0	03 16 18.6	5.5	72.0	70.0	270.0	252.0	20.0	270.0	
740730	36.4	70.8	211.0	05 12 40.6	6.5	80.0	75.0	270.0	260.0	15.0	270.0	
770603	36.4	70.8	207.0	02 31 04.4	5.4	314.0	25.0	270.0	128.0	65.0	270.0	
790816	41.81	130.19	588.0	21 31 26.3	6.1	56.0	24.0	133.0	190.0	73.0	73.0	2
790820	36.5	70.2	231.0	19 04 27.4	4.5	90.0	75.0	270.0	270.0	15.0	270.0	
810502	36.8	70.99	229.0	16 05 2.2	5.9	277.0	41.0	110.0	72.0	52.0	73.0	1

Focal mechanisms without a reference were done by the authors.

References: 1, Dziewonski and Woodhouse (1983); 2, Giardini (1984); 3, Roecker et al (1980).

## Figure Captions

**Figure 1.** Event locations, recording stations, and surface reflection points of multiple S phases for several deep earthquakes in the Far East.

**Figure 2.** SH traces from deep Far Eastern earthquakes, recorded at digital European stations, aligned with the corresponding synthetics generated using full wave theory. The synthetics are for an elastic earth with the SNA velocity structure (Grand and Helmberger, 1984) with the appropriate radiation pattern taken into account; a source time function is not included in these synthetics. Some of the event parameters are noted with each record, and a fuller description is in Table I.

**Figure 3.** Waveform matching to estimate  $t^*$  of SS and SSS phases. In each suite of waveforms, the first waveform is the observed phase. The succeeding waveforms are synthetics which include a source transfer function, radiation pattern, and attenuation per the value of  $t^*$  listed next to the waveform. The  $t^*$ 's estimated by comparing amplitudes of the unattenuated synthetics with the observed waveforms are a) 1 second, b) 1.8 seconds, and c) 8 seconds.

**Figure 4.** SSS/SS spectral amplitude ratios for synthetic waveforms generated for an anelastic earth. The spectral ratios are quite flat, consistent with the possibility that mantle structure makes no significant contribution to  $t^*$  in the long period band.

**Figure 5.** Representative spectral ratios of long period multiple S and ScS waves.

**Figure 6.** Examples of waveform matching for a) SS-SSS and b) ScS-ScS<sub>2</sub>. In both cases, the top trace is the original waveform, and the bottom trace is another arrival from the same record. In (a), a hilbert transform has been applied to SS in the second trace to account for the phase shift between SS and SSS. Various values of  $t^*$  have been applied to the original waveform in the intermediary traces, to find the value of  $t^*$  which best describes the broadening between the two phases.

**Figure 7.** Event locations, receivers, and surface reflection points for SS phases from central Asian events.

**Figure 8.** Plot of SS/S amplitude ratios versus epicentral distance. The amplitude ratios have been corrected for radiation pattern. The theoretical predictions of the SNA model (Grand and Helmberger, 1984) for a number of  $t^*$  values are also shown for comparison.

**Figure 9.** Long period S and SS WKBJ synthetics for distances between 45° and 80°, generated for the SNA velocity model and an anelastic earth. The ratios of the maximum SS amplitude to the S amplitude are in good agreement with the SS/S amplitude ratios from raytracing in Figure 10.

**Figure 10.** Event locations, recording stations, and surface reflection points of multiple ScS phases with surface reflection points under the Eurasian shield.

**Figure 11.** Plot of  $\ln (A_N/A_2)$  versus  $(N-2)f$  for ScS phases where  $\text{ScS}_2$  and  $\text{ScS}_N$  have surface reflection points under a shield region. The slope of a least squares fit through the points gives  $t_S^* \sim 4.2$  seconds.



- ⊗ source
- ▲ WWSSN station
- bounce points
- \* SS
- X SSS

Figure 1

790816  
KONO  
z=588 km  
 $\Delta=67^\circ$

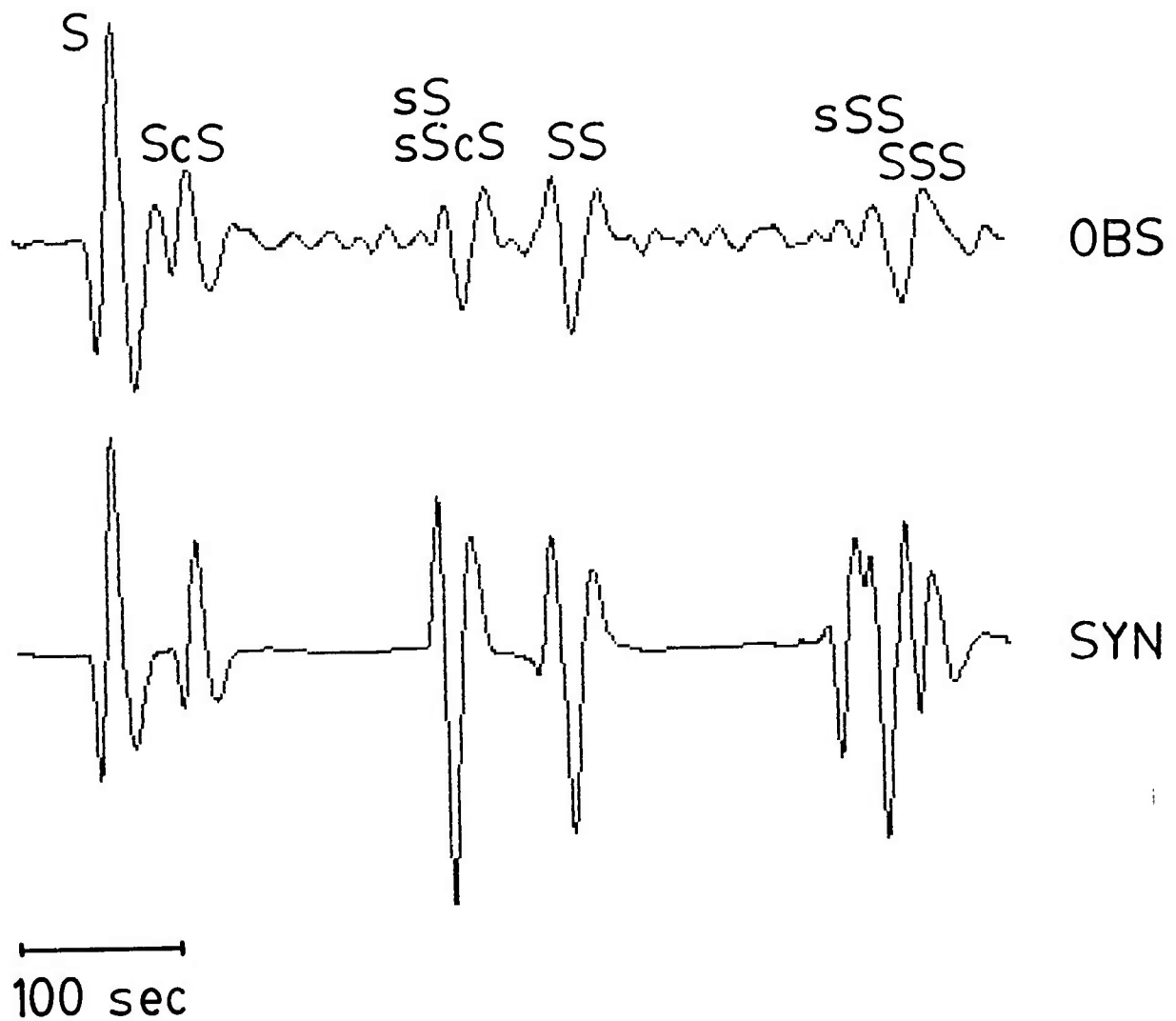


Figure 2a

780307  
NA0  
z=441 km  
 $\Delta = 77^\circ$

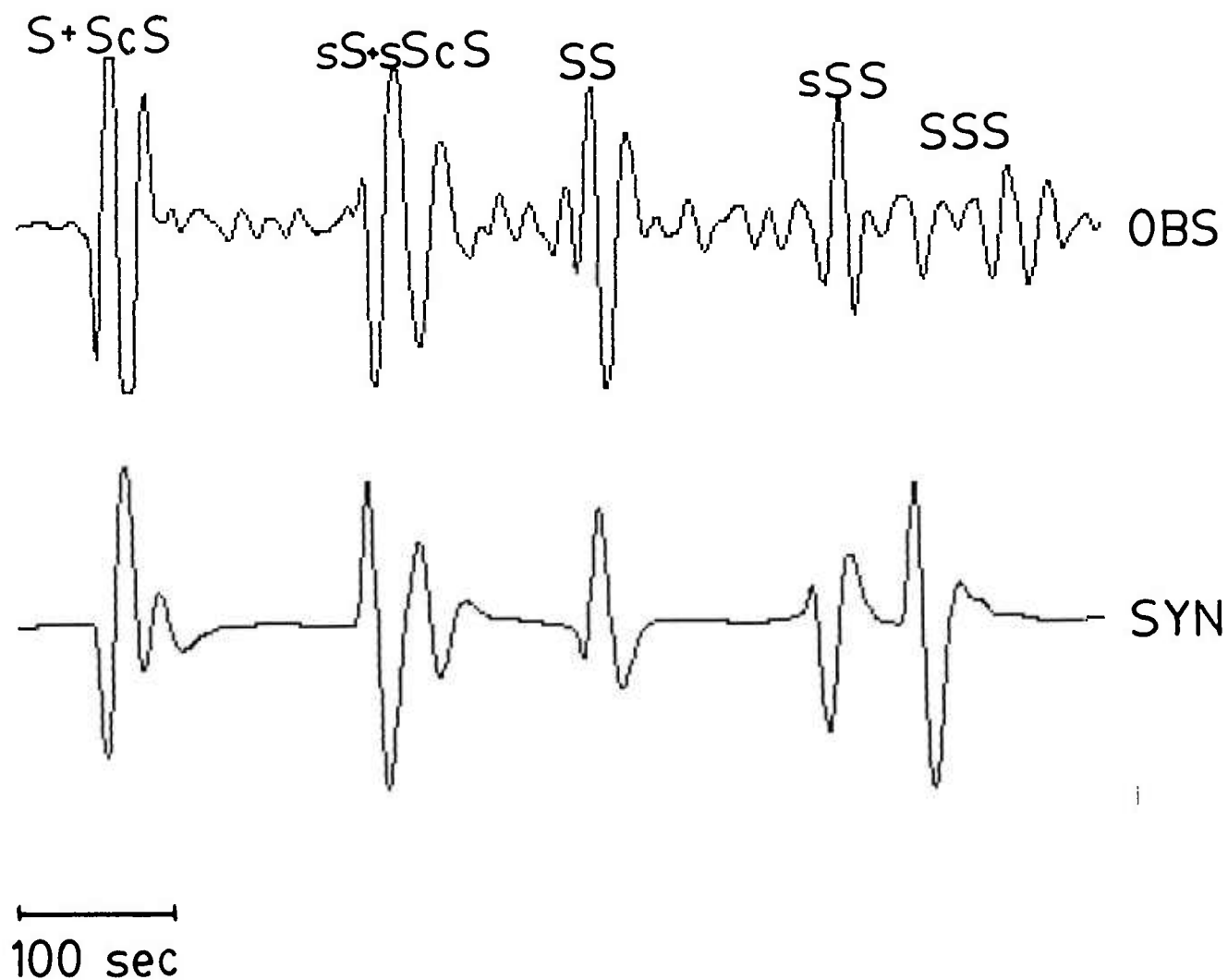


Figure 2b



800422  
KONO  
z=394 km  
 $\Delta=78^\circ$



100 sec

Figure 2c

780307  
NAO  
z=441 km  
 $\Delta = 77^\circ$



100 sec

Figure 2b

800422  
KONO  
z=394 km  
 $\Delta=78^\circ$



100 sec

Figure 2c

800422  
GRFO  
z=394 km  
 $\Delta = 85^\circ$

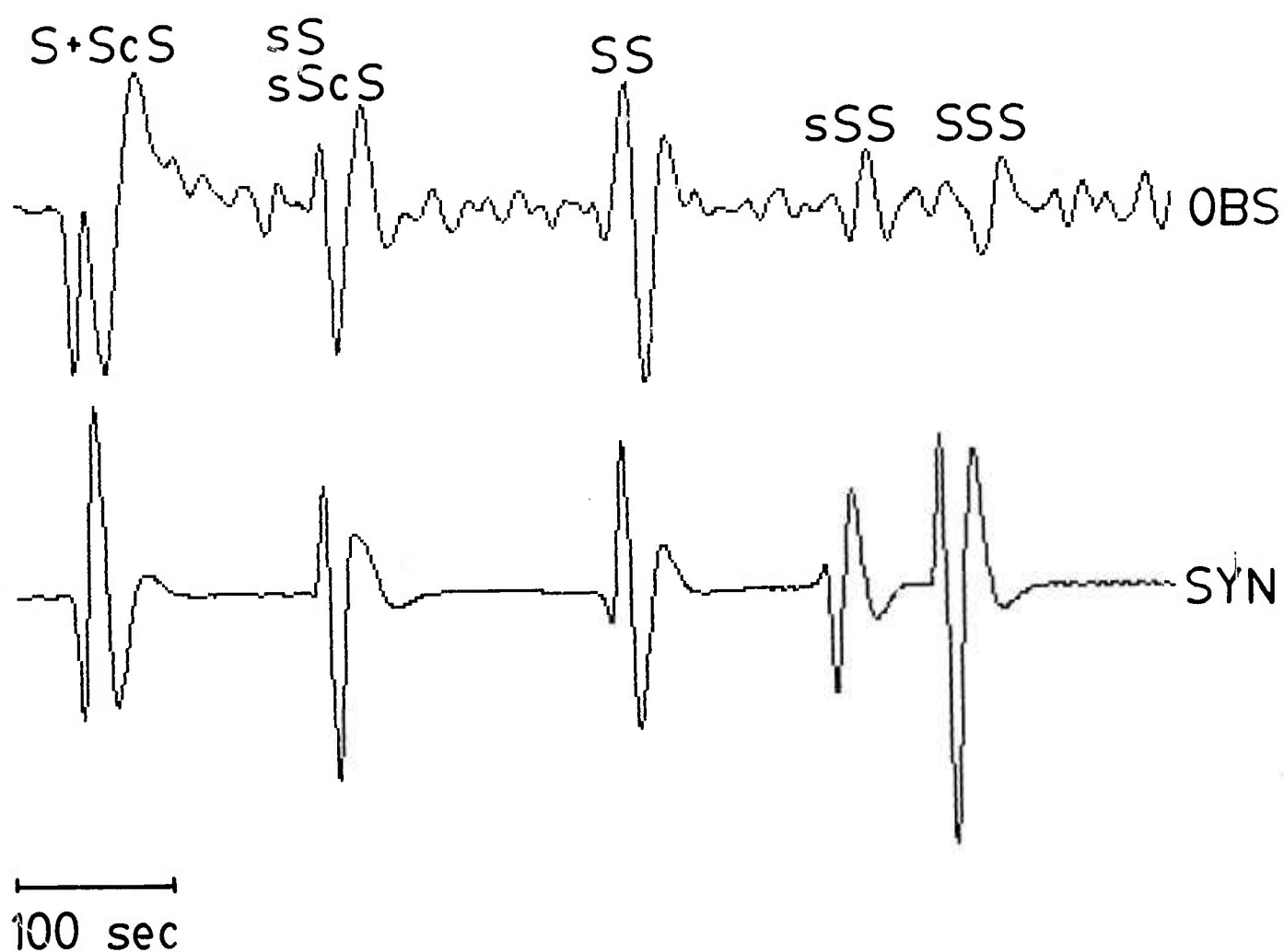
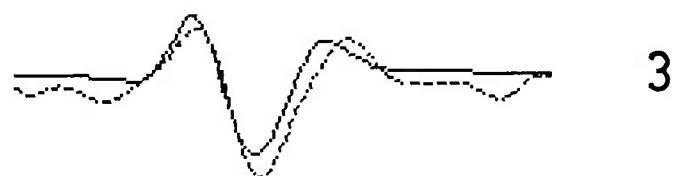
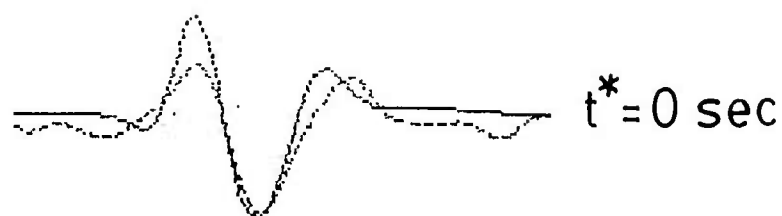


Figure 2d

SS

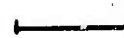


—  
20 sec

Figure 3a

SS

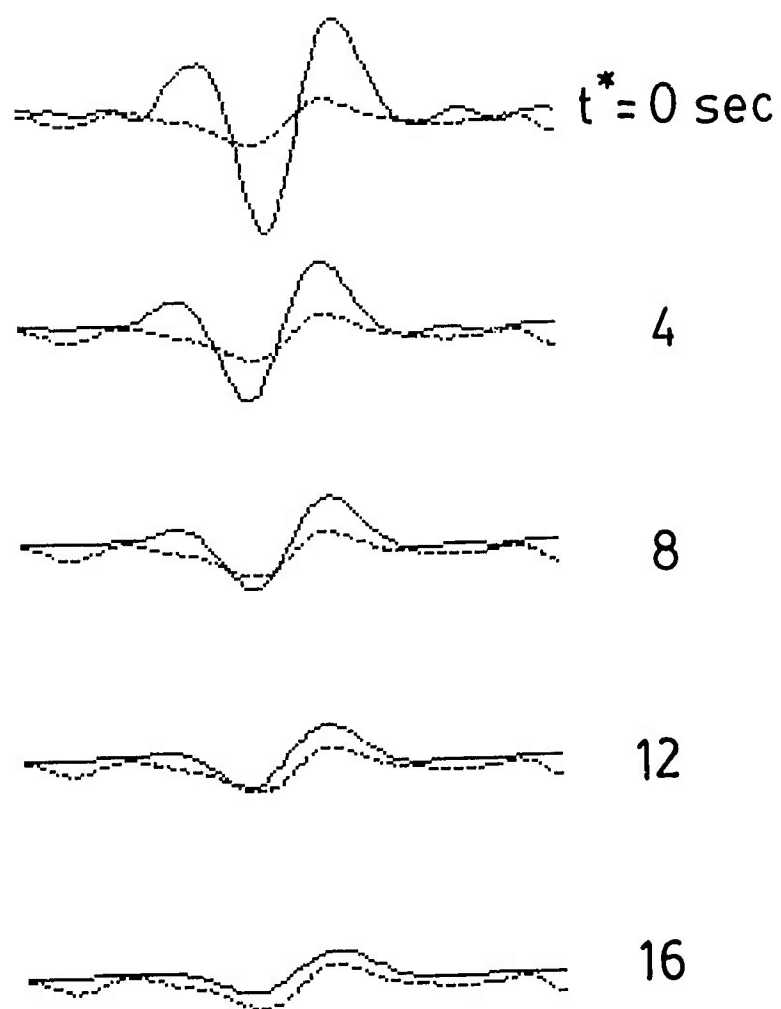


  
20 sec

A horizontal scale bar is shown above the text "20 sec", indicating the time duration represented by the length of the bar.

Figure 3b

SSS



—  
20 sec

Figure 3c

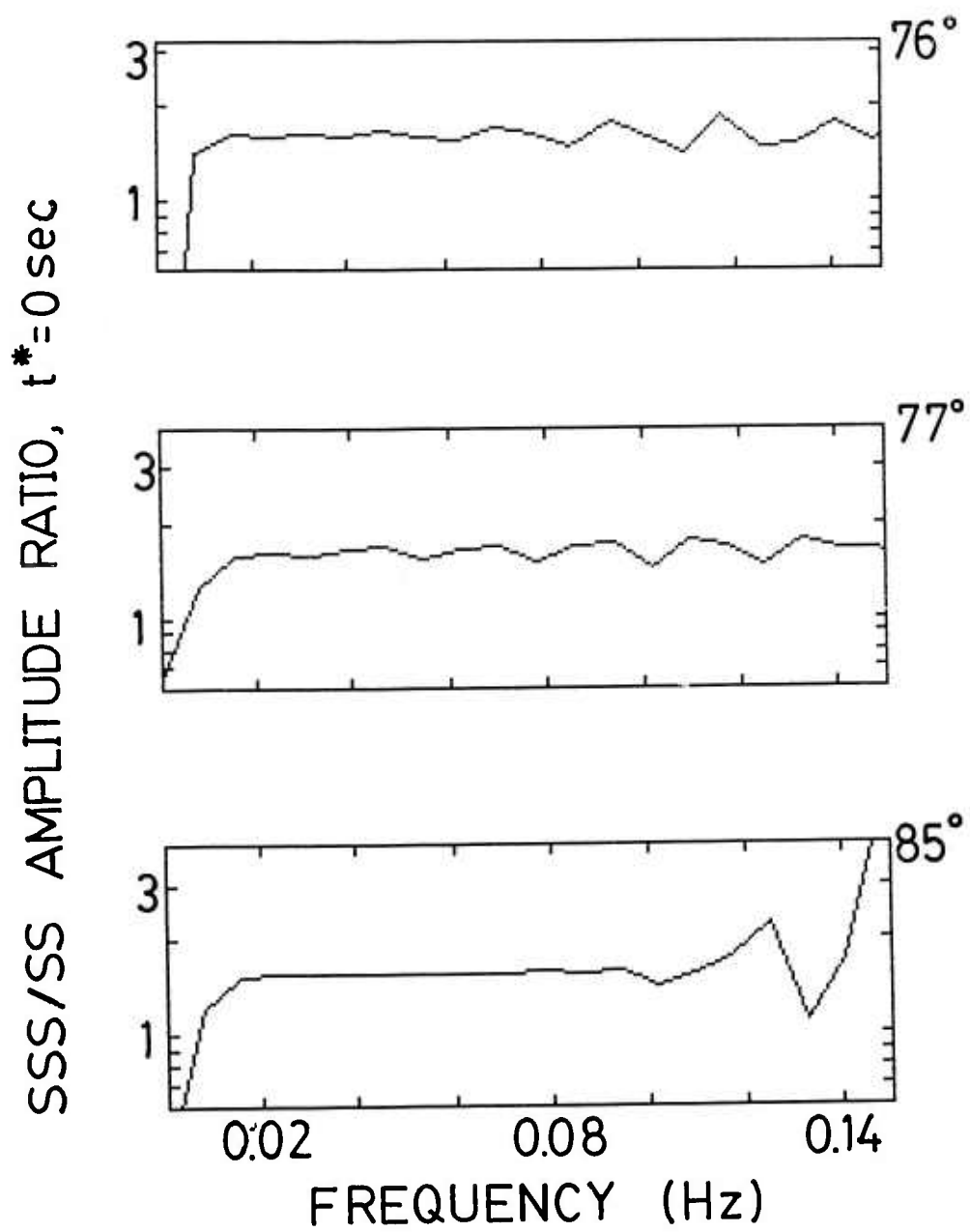


Figure 4



721014  
NORSAR  
 $m_b = 5.5$

## SPECTRAL RATIOS

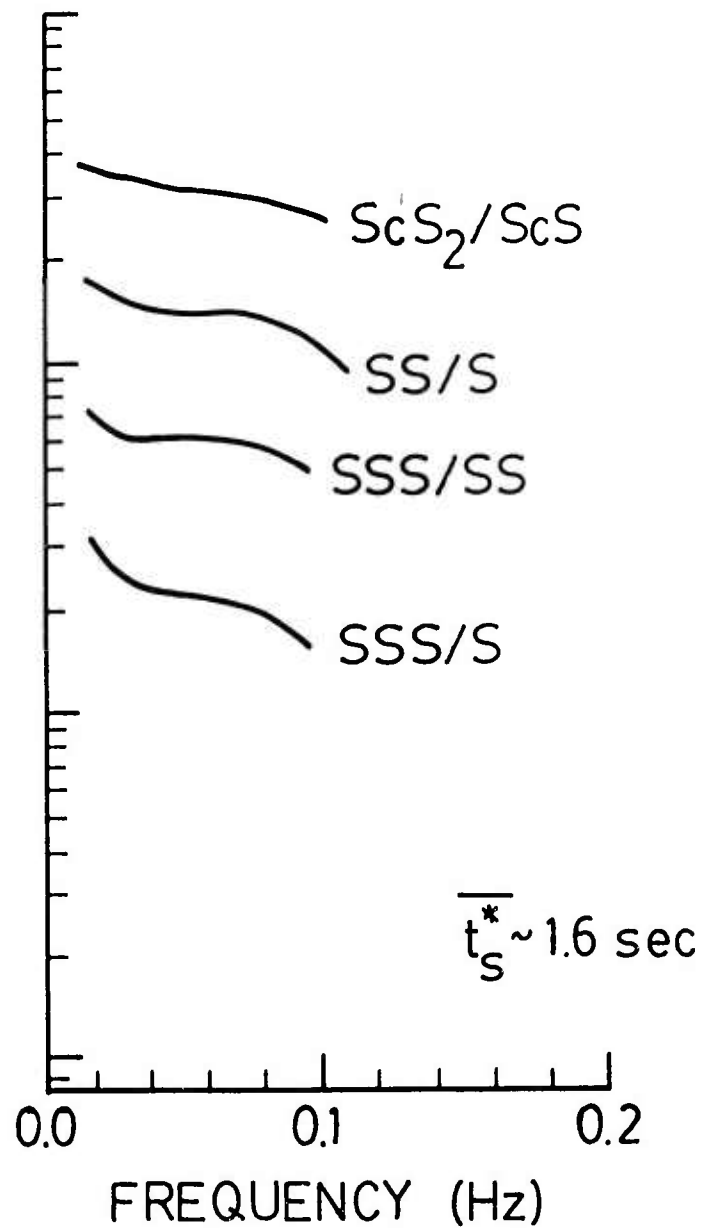


Figure 5

WAVEFORM MODELING OF  
LONG PERIOD SS-SSS PAIR

KONO  
790816  
588 KM DEPTH  
 $\Delta = 67.4^\circ$

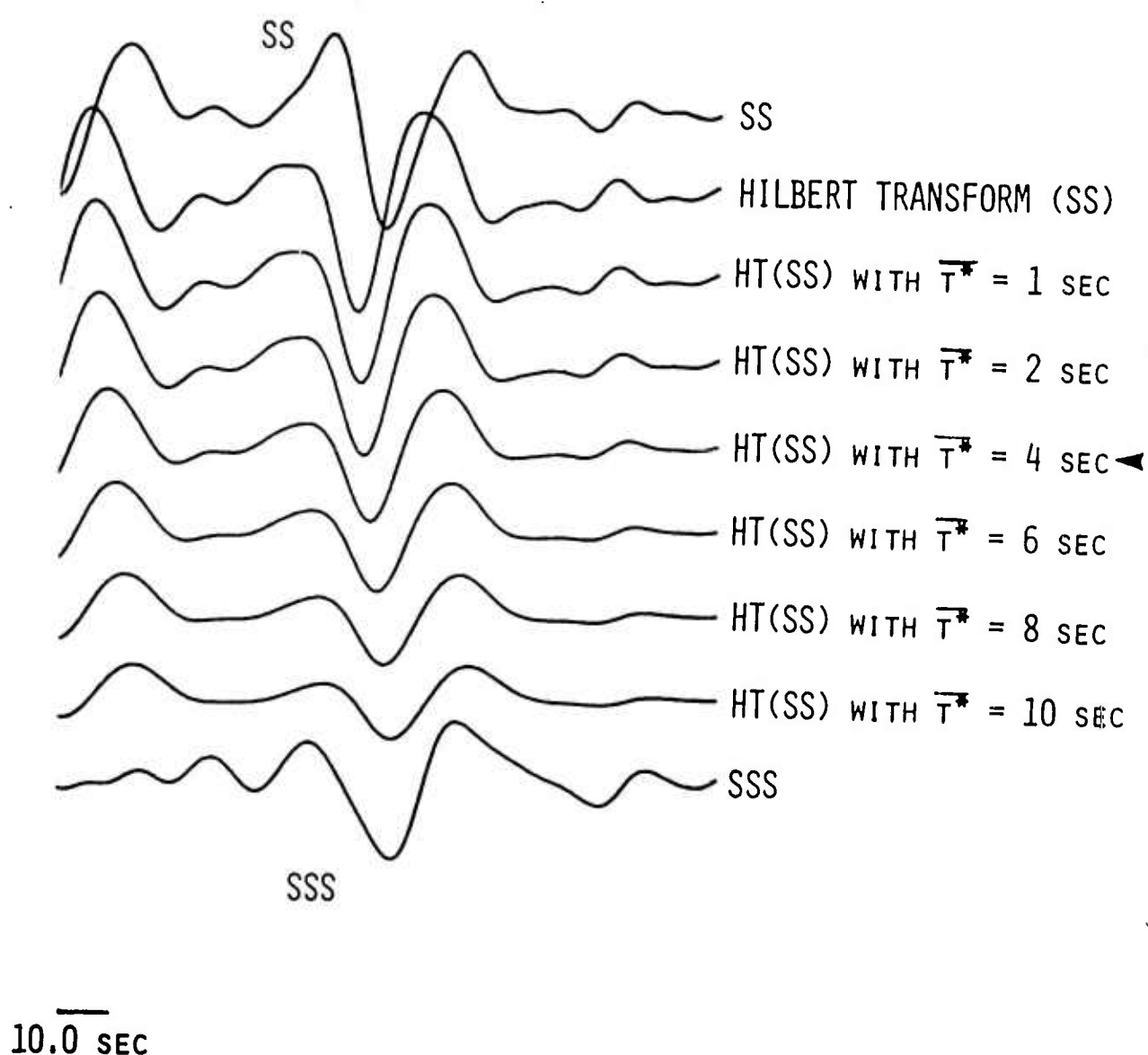


Figure 6a

# WAVEFORM MODELING OF LONG PERIOD $ScS_2$ - $ScS$ PAIR

KONO  
790816  
588 KM DEPTH  
 $\Delta = 67.4^\circ$

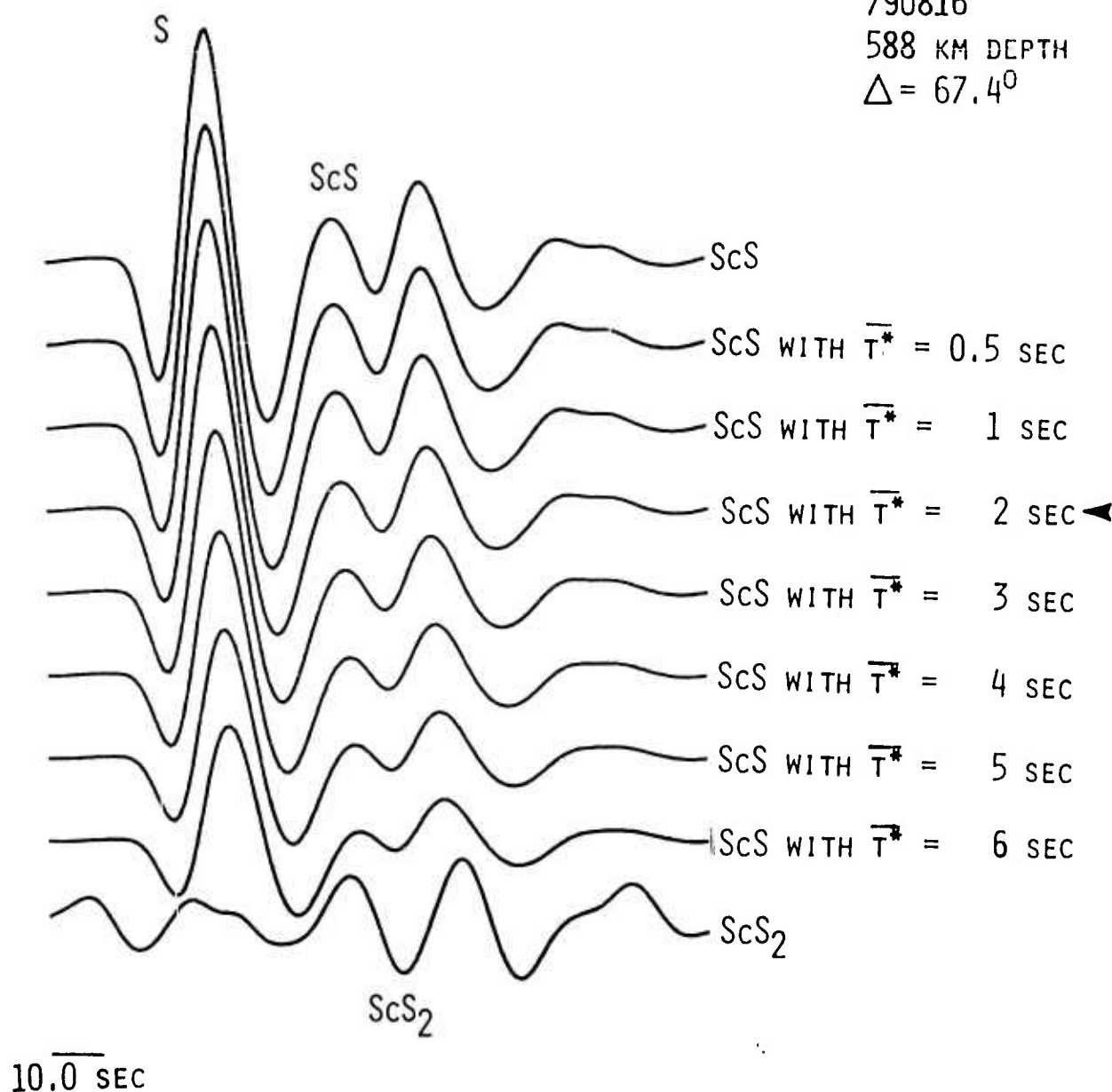


Figure 6b

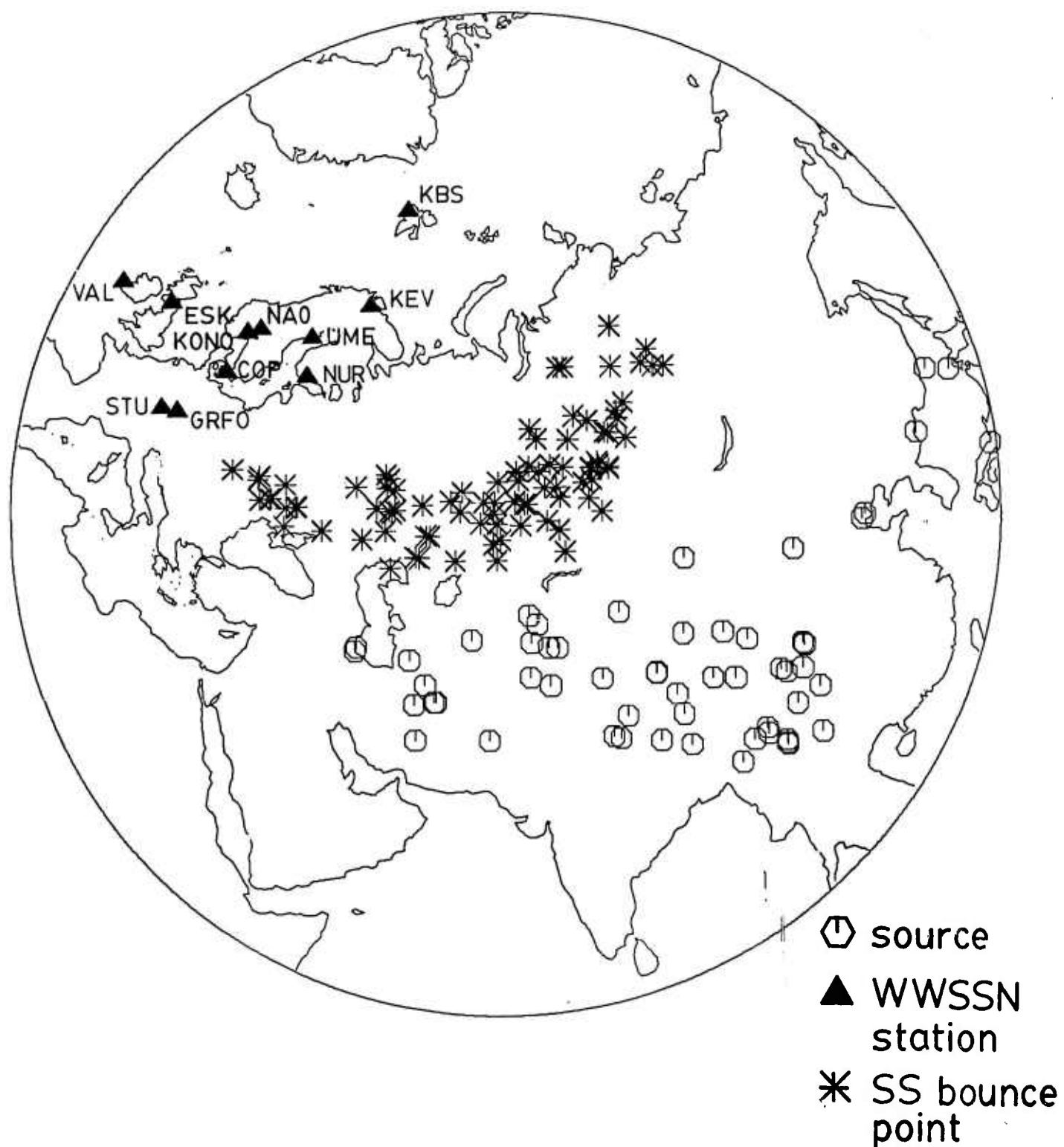


Figure 7

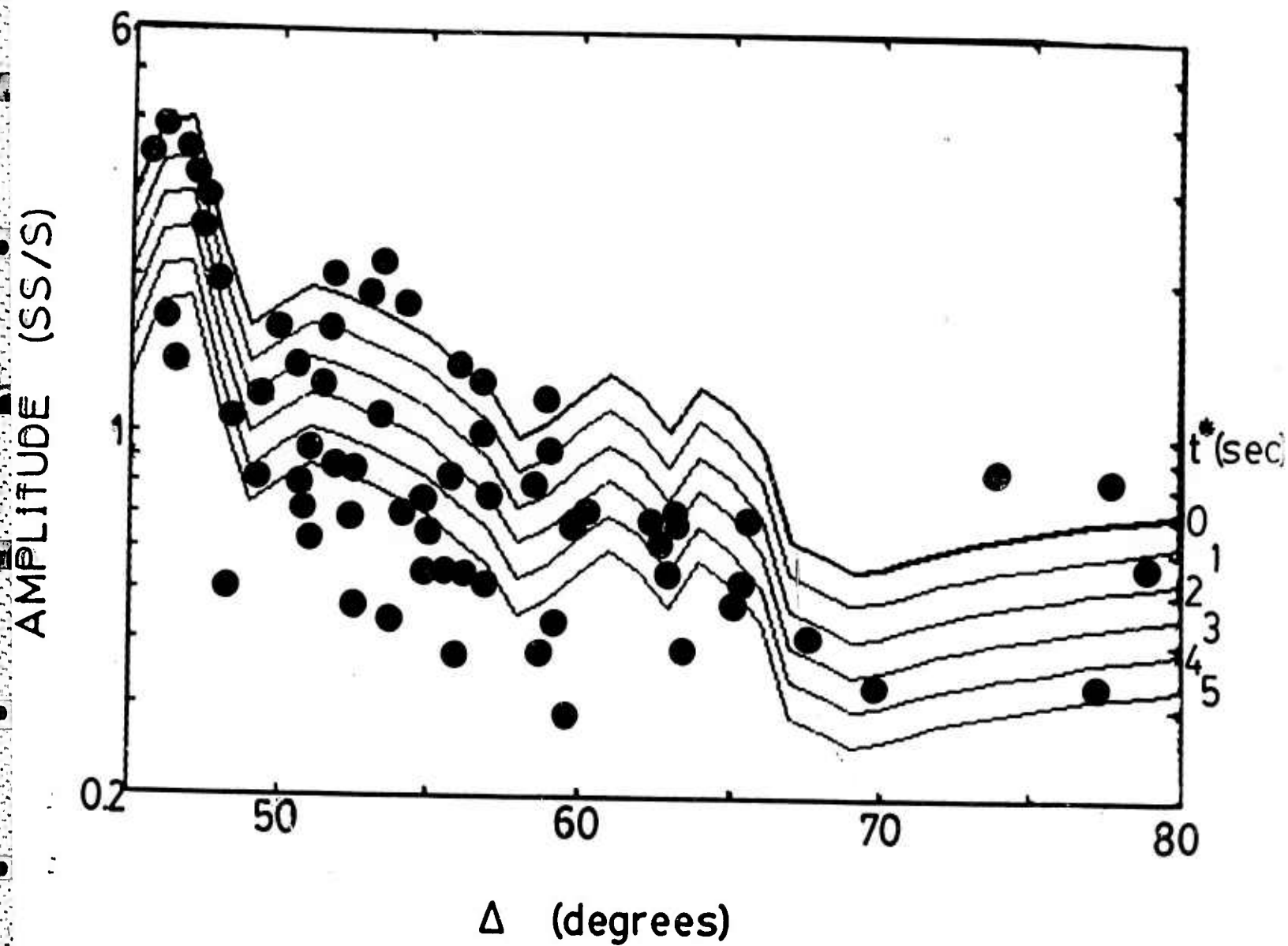


Figure 8

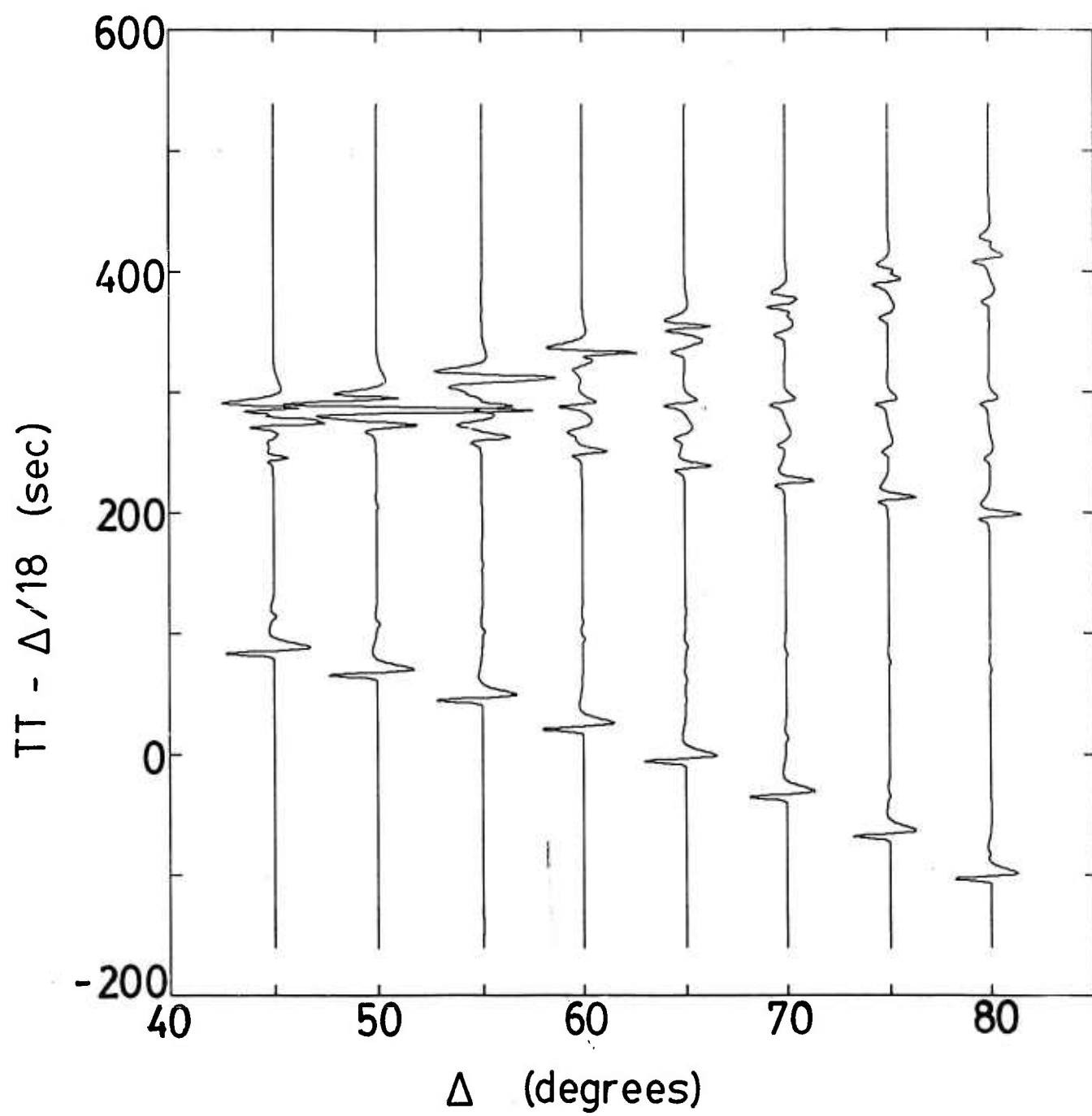


Figure 9

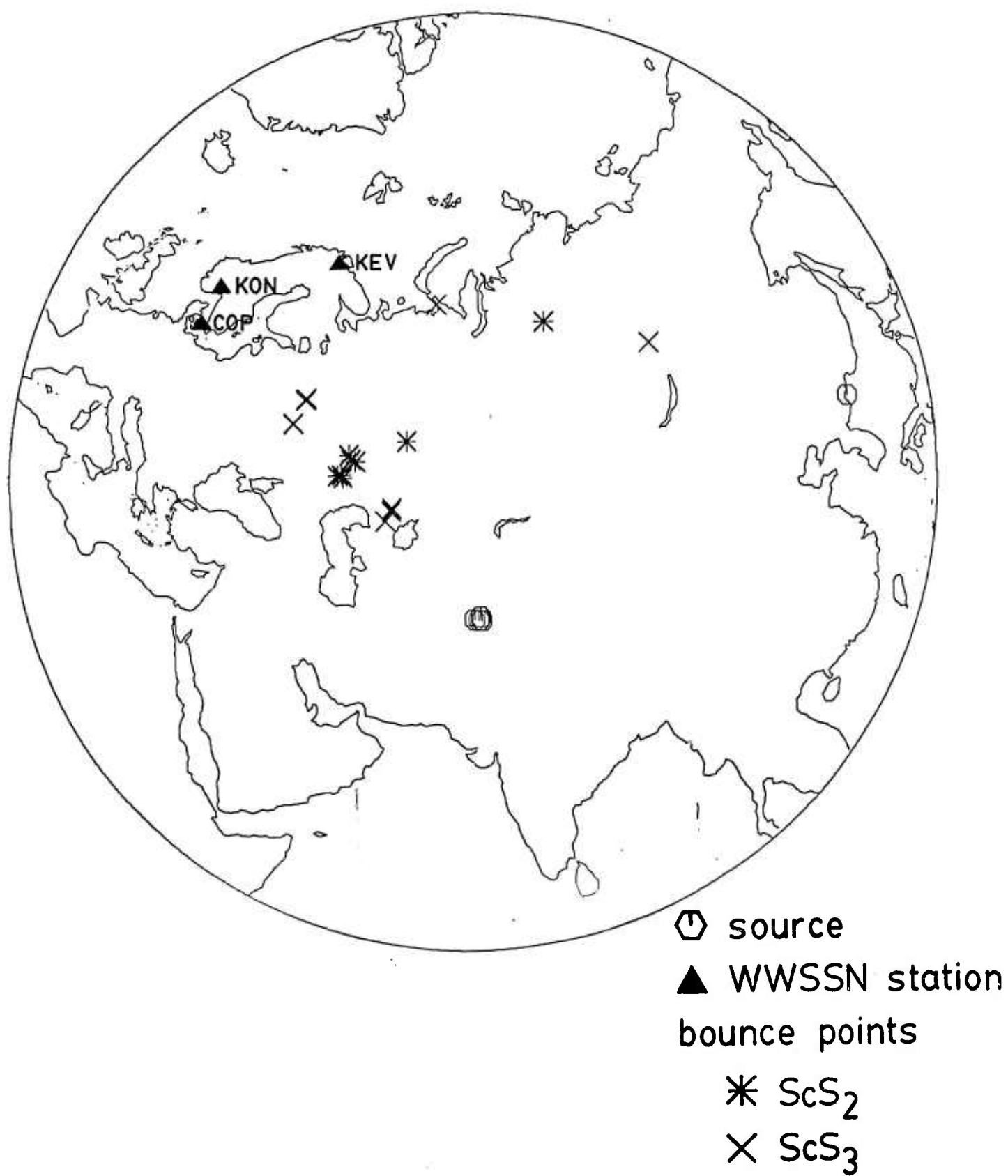


Figure 10

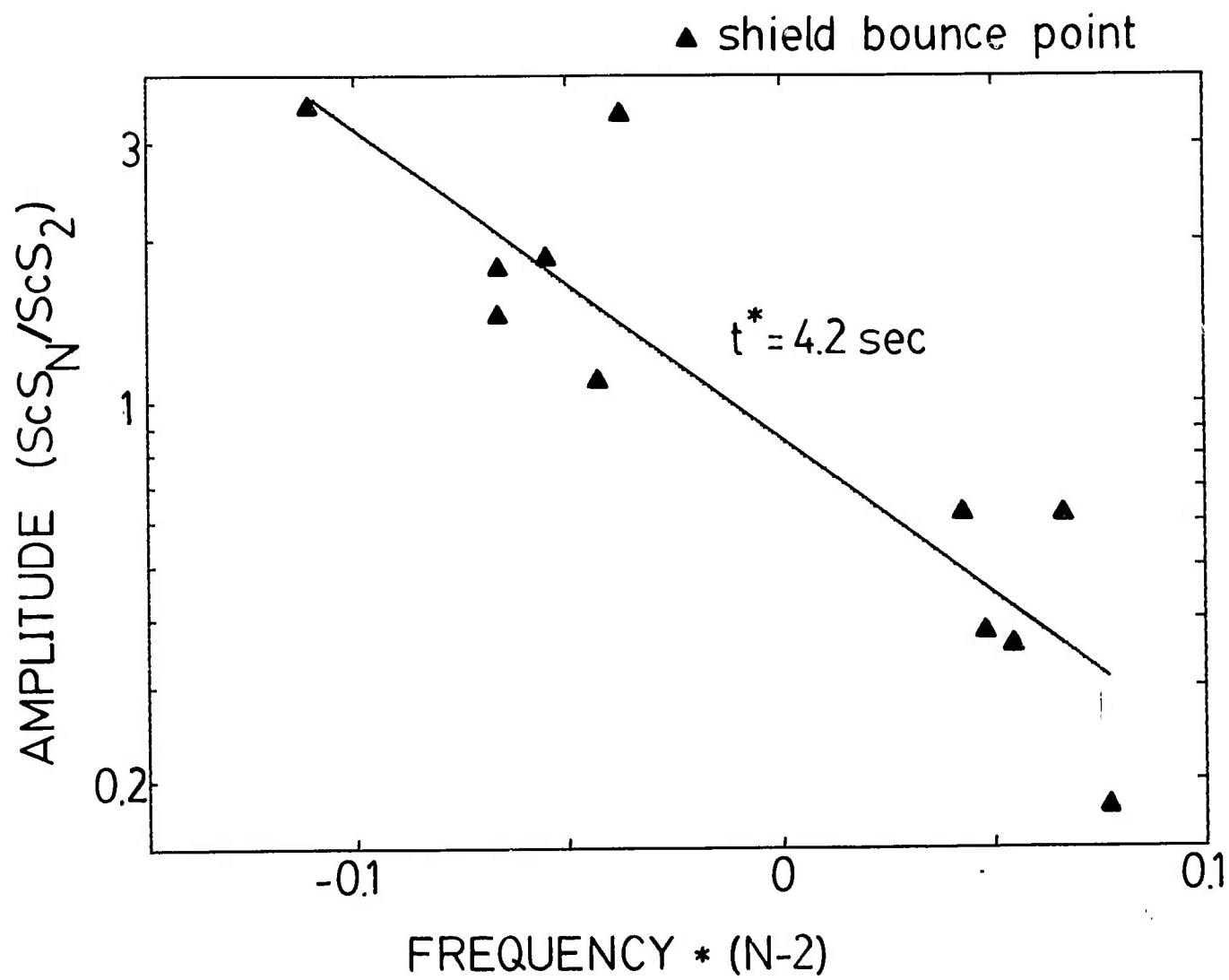


Figure 11



Frequency Dependence of  $Q$  in the Mantle  
Underlying the Shield Areas of Eurasia,  
Part III: The  $Q$  Model

by  
Zoltan Der  
Alison Lees  
and  
Vernon Cormier\*

Teledyne-Geotech  
314 Montgomery Street  
Alexandria, Virginia 22314

\* Earth Resources Laboratory  
Massachusetts Institute of Technology  
Cambridge, Massachusetts 02412

11 January 1985

## Abstract

A large set of broad band data was analyzed to determine the frequency and depth dependence of  $Q$  for P and S waves under the northern shield areas of Eurasia. A wide range of techniques utilizing spectra, amplitude ratios and waveform modeling were used to derive apparent and absolute  $t^*$  estimates for P and S waves covering the seismic band between 0.01 to 10 Hz. A  $Q$  model of the Eurasian shield was constructed on the basis of these results. The data require a model in which  $Q$  increases with frequency and which is characterized by  $Q$  values in the upper mantle that are generally higher than those of global average models. The model with the best fit includes a minimum in  $Q$  between about 100 and 200 km depth and high  $Q$  values of the order of thousands throughout the bulk of the mantle. The long period multiple ScS may require a low  $Q$  zone near the core-mantle boundary. Preliminary results suggest that  $t^*$  versus frequency in tectonic regions is higher and roughly parallel, or slightly divergent towards low frequencies, when compared to  $t^*$  versus frequency in shield regions, with a  $t_P^*$  differential of about 0.2 seconds.

## Introduction

Average  $Q$  values for the Earth are well defined from free oscillation measurements (Anderson and Hart, 1978) in the long period band. Translating these measurements into  $t_p^*$  and  $t_s^*$  estimates for an average spherically symmetric Earth, these are close to 1 and 4 seconds respectively. With the advent of digital recording of seismic signals over a broad dynamic range, it became apparent that the  $t^*$  values derived from long period, free oscillation observations cannot be applied to short period signals. It was found that teleseismic short period P waves often contain significant energy in the frequency range of 4-8 Hz and that high frequency S waves from deep earthquakes may contain 2 Hz energy above the noise (Der et al, 1982a,b). If frequency-independent  $Q$  is assumed in the Earth, the high frequencies observed with short period data would be undetectable in practically all cases if we apply the values of  $Q$  derived from long period data.

An explanation proposed for these apparent discrepancies is that  $Q$  is frequency dependent in the Earth (Solomon, 1972; Der and McElfresh, 1977; Lundquist and Cormier, 1980). Physical arguments also support this idea since many plausible attenuation mechanisms in the Earth are inherently frequency dependent (Jackson and Anderson, 1970; Lundquist and Cormier, 1980; Minster and Anderson, 1981).

Unfortunately, global arguments do not prove the frequency dependence of  $Q$ ;  $Q$  values from free oscillation measurements are global averages, while those from body waves are pertinent to specific paths. It is quite plausible that most of the attenuation of the free oscillations (traveling surface waves) takes place in some low  $Q$  regions of the upper mantle which are very limited in volume, such as mid-ocean ridges and back-arc basins. Thus the radially symmetric, averaged  $Q$  models of the Earth derived from free oscillation data may not be representative for any particular region and the actual  $Q$  values may be considerably different in most parts of the upper mantle. To eliminate any biases associated with differences in sampling the Earth it is desirable,

therefore, in any study of frequency dependence of  $Q$ , to restrict the investigation to a chosen, limited area, as far as this is possible, in all frequency bands. This was attempted in our study.

Clearly, the specific forms of this frequency dependence for various parts of the Earth's mantle could provide valuable information about the physical processes occurring in the Earth. It is of special interest to find any relationships between regional variations in  $Q$  and regional variations in velocity and anisotropy such as those being found in recent tomographic studies of lateral variations of elastic properties in the earth (Clayton and Cromer, 1983; Nataf et al, 1984; Woodhouse and Dziewonski, 1984). Moreover, accurate estimation of yields of nuclear explosions also requires knowledge of attenuation properties of the mantle.

This study is an attempt to obtain a frequency dependent  $Q$  model for the mantle underlying the northern shield areas of Eurasia. We have used estimates of  $t^*$  from short and long period observations over the 0.01 to 10 Hz band. Details of the  $t^*$  measurements are in Der et al (1985) and Lees et al (1985) (hereafter referred to as Paper I and Paper II, respectively).

Previous work on the frequency dependence of  $Q$  includes regional studies across the 0.5 to 4 Hz band, especially with respect to differences between the Eastern and Western United States (Lay and Helmberger, 1981; Der et al, 1982a; Der and Lees, 1984). At longer periods, Sipkin and Jordan (1979) have found that multiple ScS waves required a frequency dependence of  $Q$  in the western Pacific. Spanning frequencies across the larger seismic band of 0.01 to 10 Hz, several specific frequency and depth dependent  $Q$  models of the Earth have been proposed (Lundquist and Cormier, 1980; Anderson and Given, 1982) based on temperature and pressure dependent physical models of anelastic attenuation. The common feature of these models is that  $Q$  increases with frequency in most of the seismic band and the depth dependence is such that the upper mantle low  $Q$  zone is confined to shallower depths at shorter wave

periods, while it extends to greater depth in the long period band. The model of Anderson and Given (1982) also introduces a broad low  $Q$  region above the core-mantle boundary and assumes absorption in pure compression in various parts of the Earth. The existence of low  $Q$  regions in the Earth near the core-mantle boundary has been the subject of extensive debate (Teng, 1968; Mula and Mueller, 1980; Mula, 1981; Doornbos, 1983). Another controversial subject is the presence and location of any losses in compression (Sailor and Dziewonski, 1978), although the relative contribution of such mechanisms to the total of anelastic attenuation for seismic waves is generally thought to be low. The observational studies of Lay and Helmberger (1981) and Der et al (1979) did not indicate any need for invoking losses in compression in the upper mantle under the United States, and most existing other data can be fit satisfactorily without assuming any losses in compression.

The results of this study are generally consistent with those of previous work. We find that attenuation under the Eurasian shield is frequency dependent, with higher  $Q$  at higher frequencies. At all frequencies between 0.01 and 10 Hz,  $t^*$  is lower than the long period global averages from free oscillation measurements. The model with the best fit has  $Q$  generally increasing with depth. The data do require a low  $Q$  zone between 100 and 200 km depth and suggest a another low  $Q$  zone several hundred kilometers thick at the base of the mantle.

### **The $Q$ Model**

In Papers I and II the results of a variety of mutually complementary data analysis methods utilizing relative amplitudes, waveform modeling, and spectral methods were presented. In the case of frequency dependent  $Q$  these various approaches will derive different kinds of information from the data, and their interrelationship must be understood. In an attenuating environment, the relative amplitudes of band-limited phases are proportional to  $\exp[-\pi f t^*(f)]$ , the factor by which the amplitude of any

individual spectral component is reduced. The waveforms and spectral ratios, on the other hand, are mostly shaped by the apparent  $t^*$ ,  $\bar{t}^*$ , which for a limited frequency band, may be written as:

$$\bar{t}^* = t^* + f(dt^*/df).$$

Since the apparent  $t^*$  is less affected by amplitude fluctuations due to random heterogeneities in the Earth and is thus easier to measure, more apparent  $t^*$  measurements were made than absolute ones. The absolute  $t^*$  will then have to be obtained by using sets of the solutions of the differential equation above that agree with all the measured apparent  $t^*$ , and available absolute  $t^*$  as well, in some optimum sense.

In using a variety of methods we attempted to reduce the chances of methodology related biases and by using averages of measurements we tried to minimize the effects of scatter in the results which is so typical of all kinds of geophysical data. Generally, the observed variance of the data dictates the amount of data needed to establish results with a desired confidence limit. Unfortunately, as the results of the previous two parts of this paper show, the scatter in the data is much worse than one would like it to be, even in the long period band. A risky practice prevalent in numerous studies of earthquake source mechanisms using band limited data is to model seismograms in the time domain by using complex source mechanisms in which the number of parameters is dangerously close to the degrees of freedom available from the band limited data themselves. Clearly, by including enough parameters anything can be fit, and  $Q$  can be easily traded off with source properties. We have purposely tried to avoid this problem by canceling the sources in comparing  $S$  and  $SS$  and multiple  $ScS$  amplitude levels for a large number of events, rather than attempting to derive detailed source models for fewer events. This way, we feel that we made a cruder, but more robust statement about the amplitude loss in these phases even though the outcome may appear to be less aesthetically pleasing to the reader than those from many detailed

waveform studies.

The selection of the types of measurements we have made was also dictated by the nature of the data themselves. At the high frequency end of the spectrum, up to 10 Hz, P waves constitute the only kind of teleseismic data available. S waves usually do not contain detectable energy above 2 Hz even for high Q paths. At frequencies in the 0.1 to 2 Hz range a variety of measurements on both P and S waves can be utilized. In this band we may investigate any deviations from the assumption  $t_S^* = 4 t_P^*$  since both P and S waves are observable. At frequencies below 0.1 Hz it is not possible to do this since the amplitudes and spectra of long period P waves are quite insensitive to Q and any Q related changes are masked by other effects. Therefore, at the long period end of the spectrum we had to rely exclusively on analyses of multiple S and SeS waves.

An important, but as yet largely unknown factor in all studies of Q is the effect of scattering on body wave spectra, amplitudes, and waveforms. The various types of measurements utilized in our study are affected in various degrees by scattering. According to recent theoretical and numerical studies, the spectra of short period body waves are relatively less affected by scattering than waveforms and amplitudes (Frankel and Clayton, 1984; McLaughlin et al, 1984). Thus spectra will tend to be more determined by anelasticity, while waveforms and amplitudes will be diagnostic of both the anelastic and scattering losses. This seems to be supported by the fact that analyses spectral shapes generally give higher Q values than those of waveforms and wave amplitude. We may consider, therefore, spectral Q estimates as upper limits on Q, while those from waveforms (rise times for instance) will result in lower limits. We believe that scattering losses, while not negligible, are smaller than the anelastic losses that occur in shear deformation. This contention is supported by regional and global studies where a 4:1 ratio between  $t_S^*$  and  $t_P^*$  explains both the spectral shapes and amplitude data, while if scattering were dominant this would not be true (Lay and Helmberger, 1981; Der et al, 1982b). A 4:1 ratio between  $t_S^*$  and  $t_P^*$  also implies small, if any, losses in compression, (Sailor and Dziewonski, 1978; Anderson and Given, 1980).

To reduce the effects of increased variance in the data due to scattering we have used averaged values of  $t^*$  in all of our work. General problems associated with the direct estimation of  $t^*(f)$  from short period body wave spectra are discussed in more detail by Der and Lees (1984) in a companion paper included in this report.

Figure 1 summarizes the values of  $t^*$  that we obtained for high and low frequencies using a variety of seismic arrivals and techniques in Papers I and II. In interpreting these results we shall keep the precautions concerning the limitations of the various kinds of measurements discussed above in mind.

The Q model of Anderson and Given (1982) was used as the starting point in developing a  $Q(f)$  model to fit the observations plotted in Figure 1 and outlined above. The Anderson and Given model is an average model for the whole earth, which is mostly oceanic, and thus we can anticipate that modifications will be needed to make it consistent with our shield data set. The model is based on the physically plausible idea that attenuation is an activated process, and thus Q varies with depth to correspond to variations in temperature and pressure. However, we are not requiring our model to conform to any particular absorption band parameterization since it is likely that a number of attenuation mechanisms occur in the earth, and that the mechanisms may vary with depth, pressure, temperature, composition, and other such factors.

To obtain  $t^*$  from the Q models at different frequencies, a raytracing program was used with the P-velocity model KCA (King and Calcagnile, 1976) and the S-velocity model SNA (Grand and Helmberger, 1984). Both of these velocity models are developed from data crossing high velocity shield regions and are consistent with the observations in Papers I and II. More details about the KCA and SNA velocity models are in Papers I and II, respectively. We have also assumed no bulk attenuation and thus  $t_S^* = 4t_P^*$ . As we noted above, while we have not found any evidence in this work to support the presence of appreciable bulk attenuation in the mantle, this is still an area open to active investigation.



Figure 2 shows the frequency dependent Q model for the Eurasian shield, EURS, that we developed to fit the observations listed above and shown in Figure 1. Table 1 contains a listing of the Q model. Figure 3 shows  $t^*$  and  $\bar{t}^*$  predicted by our Q model for direct S or P at 60°, superposed on the observations shown in Figure 1. Clearly, the model is a smoothed, simple fit to the data. Many details of the model can not be well resolved, and our intention was merely to find a plausible model that fits the available data. Nevertheless, the resultant model has some specific properties that are required by the observational analyses. As expected, Q generally increases with frequency, and it also increases with depth for each frequency. There is a low Q layer between 100 and 200 km; this is required by the spectral ratios between the branches of the short period P wave triplications. It is not clear whether the broadening of the low Q zone at 100 to 200 km is required by the long period data. However, the upper mantle Q's are still high in an overall global context. It is interesting that the data seem to require this low Q layer while the observed extent of the triplication branches of the same high frequency P arrivals do not necessarily require any kind of low *velocity* layer for P waves in the upper mantle (King and Calcagnile, 1976; Paper I). The EURS model also has a low Q layer at the base of the mantle because the amplitudes of long period multiple S arrivals give  $t_S^* \sim 2.5$  to 3 seconds while multiple ScS arrivals give  $t_S^* \sim 4.2$  seconds. The exact values of Q and thickness of this layer are not well resolved since the long period ScS arrivals tend to be poor in continental regions (Sipkin and Jordan, 1980).

Figures 4 and 5 show  $t_S^*$  and  $t_{ScS}^*$  for the EURS Q model as a function of epicentral distance and frequency. If Q was constant throughout the earth,  $t^*$  would be directly proportional to travel time and smoothly increase with distance. However, this work is consistent with observations that  $t^*$  is fairly constant with distance in the 30 to 80° distance range (Der and McElfresh, 1977; Shore, 1983). This is because arrivals at shorter distances have traveled more obliquely through the upper mantle, sampling more of the upper mantle low Q than arrivals at greater distances which travel more steeply

through the upper mantle but have a much longer path through the high  $Q$  lower mantle. The large difference in  $t^*$  values for  $S$  and  $ScS$  is due to the substantial low  $Q$  layer above the core mantle boundary which is sampled by the  $ScS$  waves, but not by  $S$  at distances of less than  $80^\circ$ .

### Discussion

The main conclusion of this work is that  $Q$  is clearly frequency dependent under the Eurasian shield.  $Q$  increases with frequency between 0.01 and 10 Hz which explains why  $S$  and even  $SS$  waves with frequencies around 1 Hz are observed for teleseismic paths across the Eurasian shield.  $Q$  generally increases with depth, consistent with other observations of fairly constant  $t^*$  with epicentral distances of  $30$  to  $80^\circ$ . Spectral ratios between branches of the  $P$  wave triplications across the high frequency 1 to 8 Hz band require a low  $Q$  layer between 100 and 200 km depth. Amplitude data from long period multiple  $ScS$  arrivals also suggest a low  $Q$  layer at the base of the mantle. The shifts in  $Q$  with depth in the model for  $Q$  under the Eurasian shield, EURS, are consistent with attenuation as an activated process which is influenced by the temperature and pressure in the earth. EURS was developed to satisfy the observations as simply as possible; we have not added the additional constraint of parameterizing the model to fit a Minster and Anderson (1981) absorption band as it seems more reasonable that a number of attenuation mechanisms operate in the earth, and that the dominant mechanisms of attenuation may vary with temperature, pressure, composition, and other such factors.

It is interesting to compare our results for attenuation under a shield with available results for attenuation under tectonic regions. Der and Lees (1984) have found for short period data that there is a  $t_P^*$  differential between the Eastern (relatively shield-like) and Western (tectonic) United States of around 0.2 seconds. Furthermore, their results strongly suggest that this differential continues out to longer periods. The pre-

iminary results for attenuation in the long period band under tectonic regions in Paper II of this study also suggest a shield-tectonic  $t^*$  differential at long periods, with  $\Delta t_S^* \sim 2$  seconds, or  $\Delta t_P^* \sim 0.5$  seconds, around 0.05 Hz. This suggests that  $t^*(f)$  models for shield and tectonic regions are parallel, and even diverging at low frequencies, over the band of frequencies of seismic body waves.

This work suggests several other studies that should be undertaken. To further refine the model for  $t^*$  under Eurasia, short period data is needed to define the extent of the low Q layer at the base of the mantle. Additional analyses of long period data are also needed, both of the multiple ScS phases and of the individual branches of the SS phases which were used in SS/S amplitude ratios to estimate  $t_S^*$  under the shield region. This work is also an excellent starting point for studies of attenuation under tectonic regions. Since tectonic regions seem to have higher  $t^*$ 's than the shield regions, many Q estimates will have to be based on differences relative to shield regions, perhaps simply as limiting bounds if a phase is seen in one region and not in the other. In the continuation of this project, we are addressing many of these questions.

### Acknowledgements

We gratefully acknowledge the assistance of Lisa Anderson in this research. We have benefited from discussions with Drs. Keith McLaughlin and Robert R. Blandford.

## References

- Anderson, D.L. and R.S. Hart (1978). Q of the Earth, *J. Geophys. Res.*, **83**, 5869-5872.
- Anderson, D.L., and J.W. Given (1982). Absorption band Q model for the earth, *J. Geophys. Res.*, **87**, 3893-3904.
- Clayton, R.W. and R.P. Cromer (1983). A tomographic analysis of mantle heterogeneities from body wave travel times, *EOS*, **64**, 776.
- Der, Z.A. and A.C. Lees (1984). Methodologies of estimating  $t^*(f)$  from short period body waves and regional variations of  $t^*(f)$  in the United States. (*Submitted to the Geophys. J. R. A. S.*)
- Der, Z.A., and T.W. McElfresh (1977). The relationship between anelastic attenuation and regional amplitude anomalies of short-period P waves in North America, *Bull. Seism. Soc. Am.*, **67**, 1303-1317.
- Der, Z.A., T.W. McElfresh, and C.P. Mrazek (1979). Interpretation of short-period P-wave magnitude anomalies at selected LRSM stations, *Bull. Seism. Soc. Am.*, **69**, 1149-1160.
- Der, Z.A., T.W. McElfresh, and A. O'Donnell (1982a). An investigation of the regional variations and frequency dependence of anelastic attenuation in the mantle under the United States in the 0.5-4 Hz band, *Geophys. J. R. Astr. Soc.*, **69**, 67-100.
- Der, Z.A., W.D. Rivers, T.W. McElfresh, A. O'Donnell, P.J. Klouda, and M.E. Marshall (1982b). Worldwide variations in the attenuative properties of the upper mantle as determined from spectral studies of short-period body waves, *Phys. Earth Planet. Int.*, **30**, 12-25.
- Der, Z.A., A.C. Lees, V.F. Cormier and L.M. Anderson (1985). Frequency dependence of Q in the mantle underlying the shield areas of Eurasia, Part I: analyses of short and intermediate period data, included in this report.
- Doornbos, D.J. (1983). Present seismic evidence for a boundary layer at the base of the mantle, *J. Geophys. Res.*, **88**, 3498-3505.
- Frankel, A. and R.W. Clayton (1984). A finite-difference simulation of wave propagation in two-dimensional random media, *Bull. Seism. Soc. Am.*, **74**, 2167-2186.
- Given, J.W. and D.V. Helmberger (1980). Upper mantle structure in northwestern Eurasia, *J. Geophys. Res.*, **85**, 7183-7194.
- King, D.W. and G. Calcagnile (1976). P-wave velocities in the upper mantle beneath Fennoscandia and western Russia, *Geophys. J. R. astr. Soc.*, **46**, 407-432.
- Lay, T. and D.V. Helmberger (1981). Body wave amplitude patterns and upper mantle attenuation variations across North America, *Geophys. J. R. astr. Soc.*, **66**, 691-726.
- Lees, A.C., Z.A. Der, V.F. Cormier, M.E. Marshall and J. Burnetti (1985). Frequency dependence of Q in the mantle underlying the shield areas of Eurasia, Part II: analyses of long period data, included in this report.

- Lundquist, G.M., and V.F. Cormier (1980). Constraints on the absorption band model of  $Q$ , *J. Geophys. Res.*, **85**, 5244-5265.
- McLaughlin, K.L., L.M. Anderson and Z.A. Der (1984). Investigation of seismic waves using 2-D finite difference calculations, submitted to *Geophys. J. R. astr. Soc.*
- Minster, J.B. and D.L. Anderson (1981). A model of dislocation-controlled rheology for the mantle, *Philos. Trans. R. Soc. London*, **299**, 319-356.
- Mula, A.H.G. (1981). Amplitudes of diffracted long-period P and S waves and the velocities and  $Q$  structure at the base of the mantle, *J. Geophys. Res.*, **86**, 4999-5011.
- Mula, A.H.G. and G. Muller (1980). Ray parameters of diffracted long-period P and S waves and the velocities at the base of the mantle, *Pure Appl. Geophys.*, **118**, 1270-1290.
- Nataf, H.-C., I. Nakanishi and D.L. Anderson (1984). Anisotropy and shear-velocity heterogeneities in the upper mantle, *Geophys. Res. Lett.*, **11**, 109-112.
- Sailor, R.V. and A.M. Dziewonski (1978). Measurements and interpretation of normal mode attenuation, *Geophys. J. R. astr. Soc.*, **53**, 559-581.
- Shore, M.J. (1983). Short period P-wave attenuation in the middle and lower mantle of the earth, *VSC-TR-83-7*, VELA Seismological Center, Alexandria, Virginia.
- Sipkin, S.A., and T.H. Jordan (1979). Frequency dependence of  $Q_{ScS}$ , *Bull. Seism. Soc. Am.*, **69**, 1055-1079.
- Sipkin, S.A., and T.H. Jordan (1980). Regional variations of  $Q_{ScS}$ , *Bull. Seism. Soc. Am.*, **70**, 1071-1102.
- Teng, T. (1968). Attenuation of body waves and the  $Q$  structure of the mantle, *J. Geophys. Res.*, **73**, 2195-2208.
- Woodhouse, J.H. and A.M. Dziewonski (1984). Mapping the upper mantle: three-dimensional modeling of earth structure by inversion of seismic waveforms, *J. Geophys. Res.*, **89**, 5953-5986.

Table I

Parameters for the EURS Q Model

Depth (km)	$V_s$ (km/sec)	$Q_s$ Frequency (Hz)						
		0.01	0.03	0.1	0.3	1.0	3.0	10.0
0.1	3.5000	252.	270.	291.	317.	445.	600.	800.
15.	3.5000	252.	270.	291.	317.	445.	600.	800.
15.	3.7500	216.	230.	248.	266.	365.	495.	665.
20.	3.7500	216.	230.	246.	266.	365.	495.	665.
20.	4.8000	216.	230.	246.	266.	365.	495.	665.
38.	4.8000	218.	230.	248.	266.	365.	495.	665.
50.	4.7900	218.	230.	246.	266.	365.	495.	665.
75.	4.7750	216.	230.	246.	266.	365.	495.	665.
100.	4.7750	216.	230.	246.	266.	365.	495.	665.
100.	4.7750	123.	130.	138.	148.	200.	290.	380.
125.	4.7750	123.	130.	138.	148.	200.	290.	380.
150.	4.7750	123.	130.	138.	148.	200.	290.	380.
175.	4.7100	123.	130.	138.	148.	200.	290.	380.
200.	4.6300	123.	130.	138.	148.	200.	290.	380.
200.	4.6300	123.	130.	138.	148.	200.	700.	950.
225.	4.6400	123.	130.	138.	148.	200.	700.	950.
240.	4.6580	123.	130.	138.	148.	200.	700.	950.
240.	4.6580	123.	130.	138.	148.	530.	700.	950.
250.	4.8700	123.	130.	138.	148.	530.	700.	950.
275.	4.6950	123.	130.	138.	148.	530.	700.	950.
280.	4.7000	123.	130.	138.	148.	530.	700.	950.
280.	4.7000	123.	130.	138.	389.	530.	700.	950.
300.	4.7200	123.	130.	138.	389.	530.	700.	950.
320.	4.7360	123.	130.	138.	389.	530.	700.	950.
320.	4.7360	123.	130.	356.	389.	530.	700.	950.
325.	4.7400	123.	130.	356.	389.	530.	700.	950.
350.	4.7550	123.	130.	356.	389.	530.	700.	950.
360.	4.7590	123.	130.	358.	389.	530.	700.	950.
360.	4.7590	123.	330.	356.	389.	530.	700.	950.
375.	4.7650	123.	330.	356.	389.	530.	700.	950.
405.	4.7800	123.	330.	356.	389.	530.	700.	950.
408.	5.0000	307.	330.	356.	389.	530.	700.	950.
425.	5.0500	307.	330.	356.	389.	530.	700.	950.
450.	5.0900	307.	330.	358.	389.	530.	700.	950.
475.	5.1400	307.	330.	356.	389.	530.	700.	950.
500.	5.1900	307.	330.	358.	389.	530.	700.	950.
525.	5.2400	307.	330.	358.	389.	530.	700.	950.
550.	5.2900	307.	330.	358.	389.	530.	700.	950.
575.	5.3450	307.	330.	358.	389.	530.	700.	950.
600.	5.3950	307.	330.	358.	389.	530.	700.	950.
625.	5.4450	307.	330.	356.	389.	530.	700.	950.
659.	5.5000	307.	330.	356.	389.	530.	700.	950.
660.	5.9100	565.	650.	860.	1310.	2145.	3555.	5825.
675.	5.9800	565.	650.	860.	1310.	2145.	3555.	5825.
700.	8.0500	565.	650.	860.	1310.	2145.	3555.	5825.
725.	8.1300	585.	650.	860.	1310.	2145.	3555.	5825.
750.	6.2000	585.	650.	860.	1310.	2145.	3555.	5825.
775.	8.2200	565.	650.	880.	1310.	2145.	3555.	5825.
800.	8.2400	585.	650.	880.	1310.	2145.	3555.	5825.
825.	8.2600	585.	650.	860.	1310.	2145.	3555.	5825.
850.	8.2750	585.	650.	860.	1310.	2145.	3555.	5825.
875.	8.2900	565.	650.	860.	1310.	2145.	3555.	5825.
900.	6.3050	565.	650.	860.	1310.	2145.	3555.	5825.
925.	6.3200	565.	850.	880.	1310.	2145.	3555.	5825.

950.	6.3350	565.	650.	860.	1310.	2145.	3555.	5825.
975.	6.3500	565.	650.	860.	1310.	2145.	3555.	5825.
1000.	6.3650	565.	650.	860.	1310.	2145.	3555.	5825.
1025.	6.3850	565.	650.	860.	1310.	2145.	3555.	5825.
1050.	6.4050	565.	650.	860.	1310.	2145.	3555.	5825.
1071.	6.4075	565.	650.	860.	1310.	2145.	3555.	5825.
1171.	6.4686	565.	650.	860.	1310.	2145.	3555.	5825.
1271.	6.5270	565.	650.	860.	1310.	2145.	3555.	5825.
1371.	6.5831	565.	650.	860.	1310.	2145.	3555.	5825.
1471.	6.6371	565.	650.	860.	1310.	2145.	3555.	5825.
1571.	6.6891	580.	705.	1055.	1920.	3860.	8000.	16155.
1671.	6.7394	580.	705.	1055.	1920.	3860.	8000.	16155.
1771.	6.7882	580.	705.	1055.	1920.	3860.	8000.	16155.
1871.	6.8357	580.	705.	1055.	1920.	3860.	8000.	16155.
1971.	6.8822	580.	705.	1055.	1920.	3860.	8000.	16155.
2071.	6.9277	580.	705.	1055.	1920.	3860.	8000.	16155.
2171.	6.9728	580.	705.	1055.	1920.	3860.	8000.	16155.
2271.	7.0171	79.	90.	119.	179.	289.	476.	772.
2371.	7.0614	79.	90.	119.	179.	289.	476.	772.
2471.	7.1056	79.	90.	119.	179.	289.	476.	772.
2571.	7.1501	79.	90.	119.	179.	289.	476.	772.
2671.	7.1949	79.	90.	119.	179.	289.	476.	772.
2741.	7.2267	79.	90.	119.	179.	289.	476.	772.
2771.	7.2265	79.	90.	119.	179.	289.	476.	772.
2871.	7.2256	79.	90.	119.	179.	289.	476.	772.
2891.	7.2254	79.	90.	119.	179.	289.	476.	772.

## Figure Captions

**Figure 1.** Summary of  $t^*$  observations reported in Der et al (1985) and Lees et al (1985). Each box is labeled with the phases and method of analysis used. The sizes of the boxes are representative of the range of variations of the observations.

**Figure 2.** The EURS Q model. Each line is a plot of Q versus depth for a different frequency.

**Figure 3.** Plot of  $t^*$  and  $\overline{t^*}$  for direct S or P at  $60^\circ$  as predicted by the EURS Q model, superimposed on the  $t^*$  observations of Figure 1.

**Figure 4.** Plot of  $t^*$  versus epicentral distance for direct S waves, assuming the SNA shear velocity model (Given and Helmberger, 1980) and the EURS Q model.

**Figure 5.** Plot of  $t^*$  versus epicentral distance for direct ScS waves, assuming the SNA shear velocity model (Given and Helmberger, 1980) and the EURS Q model.



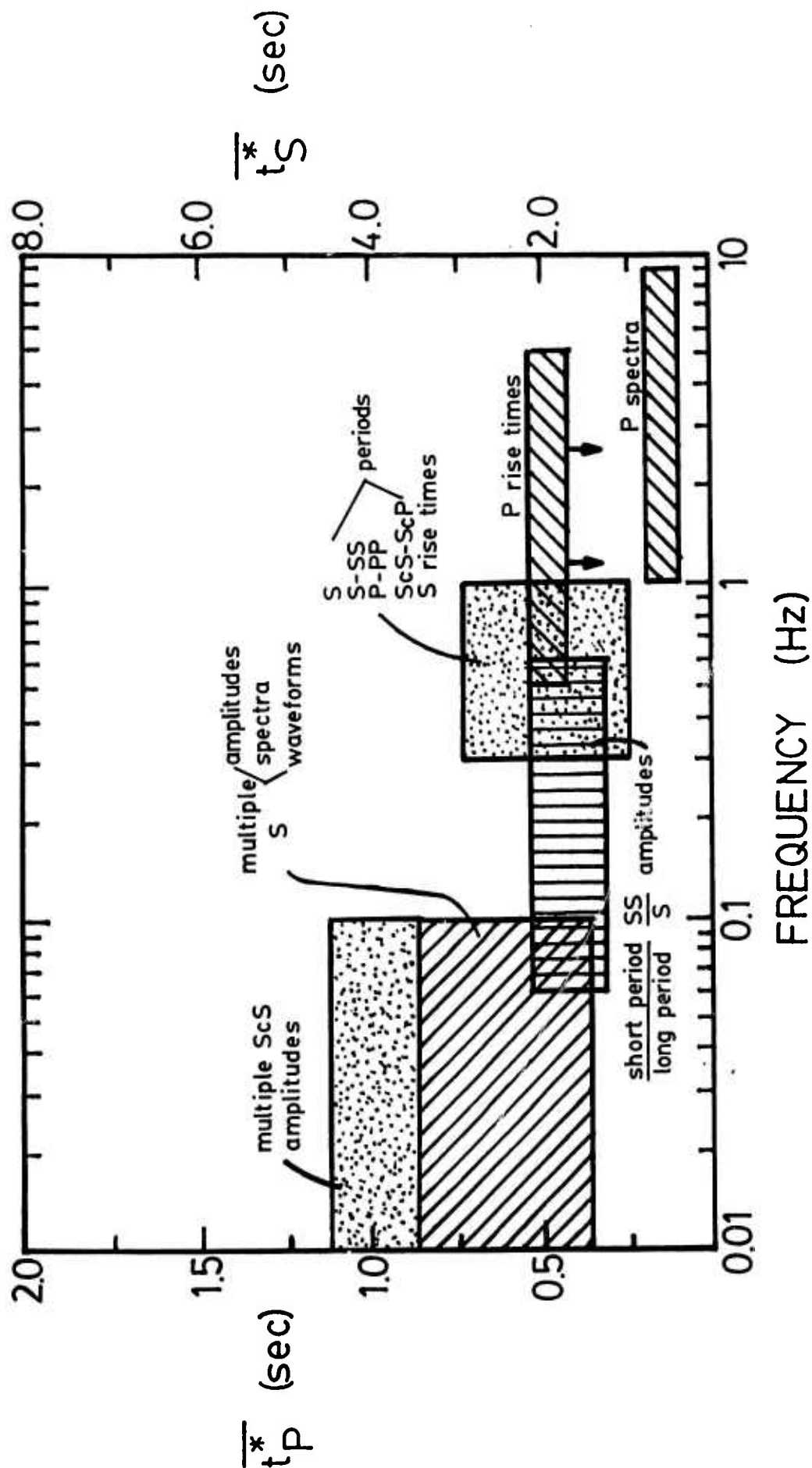


Figure 1

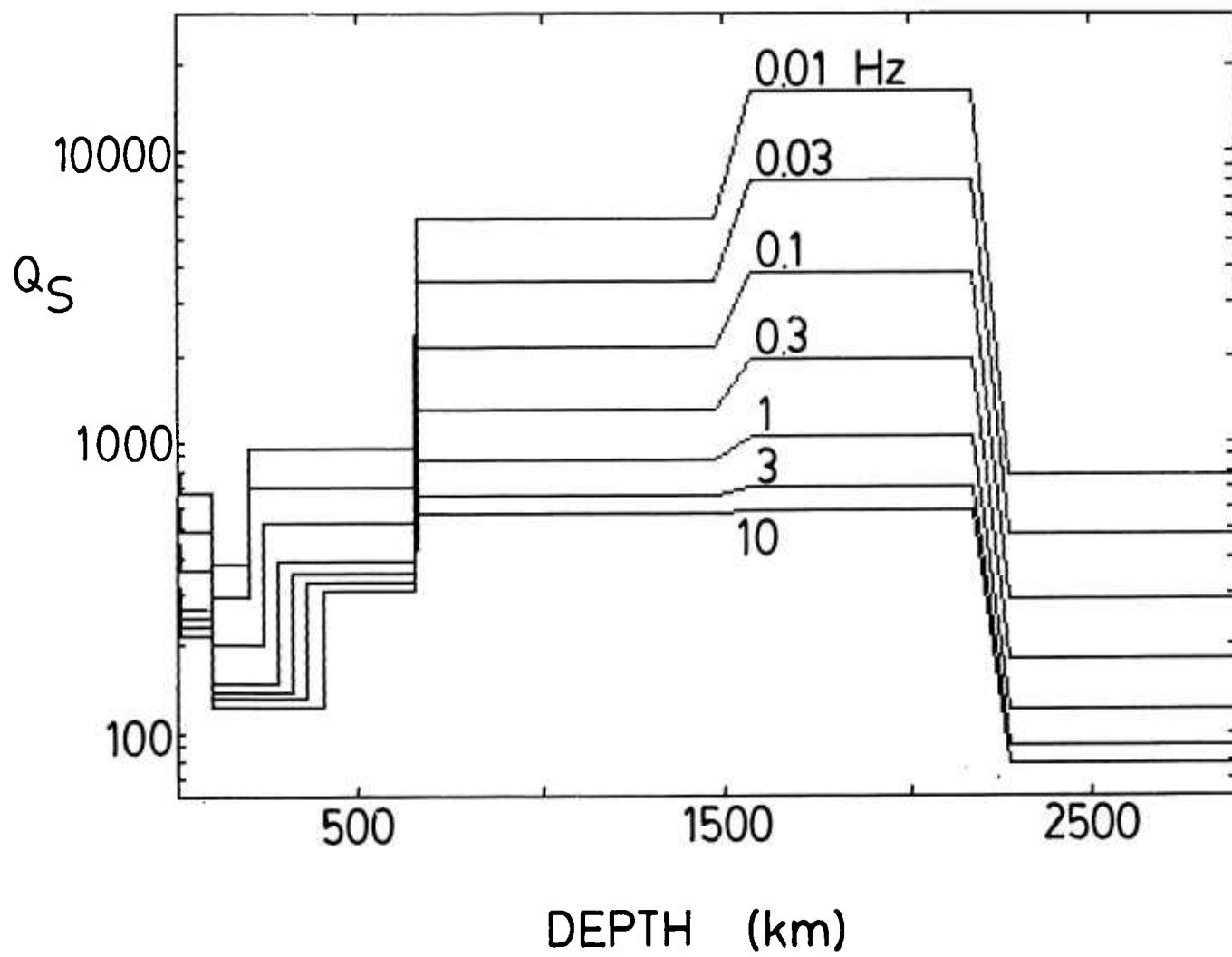


Figure 2

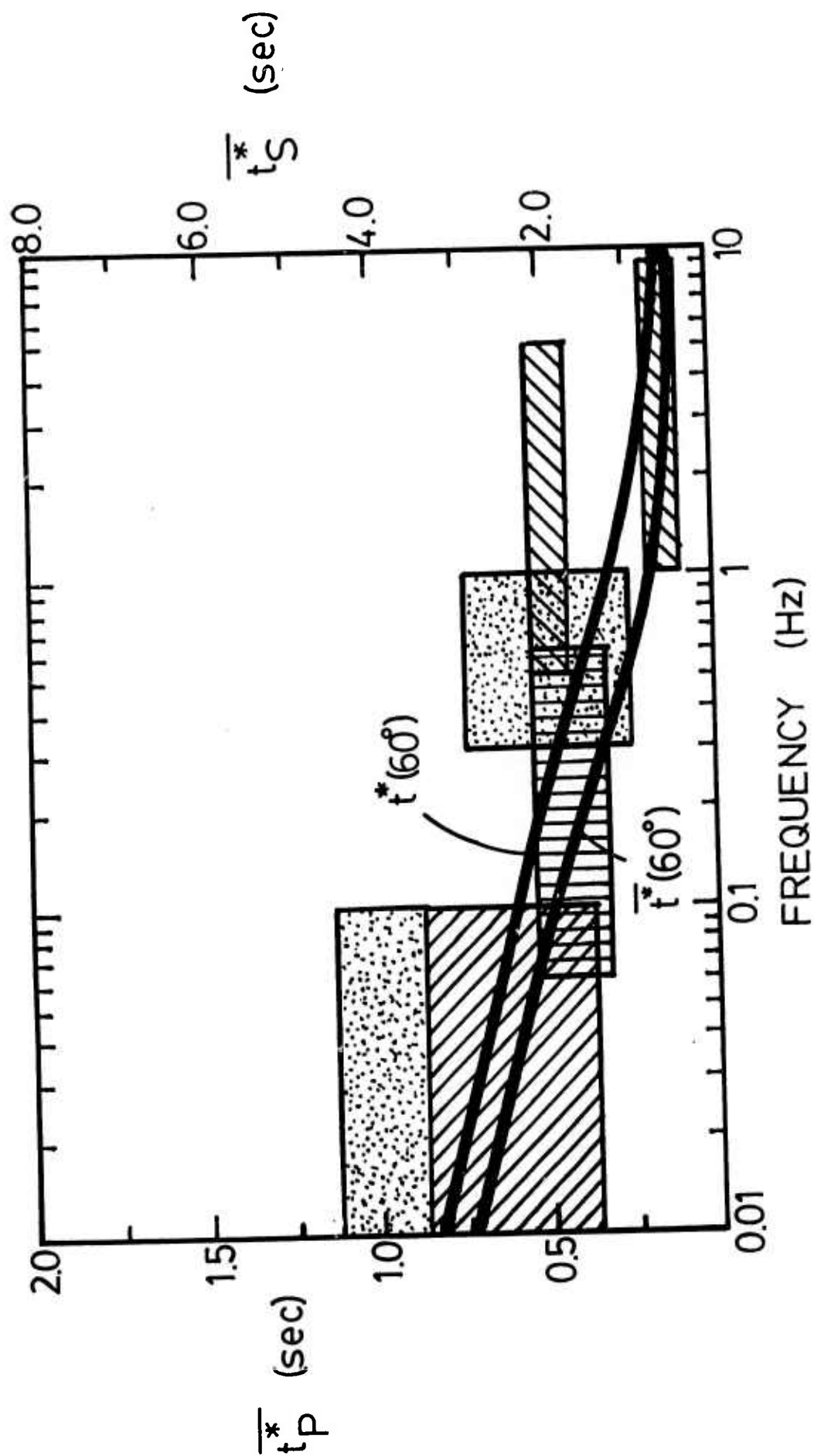


Figure 3

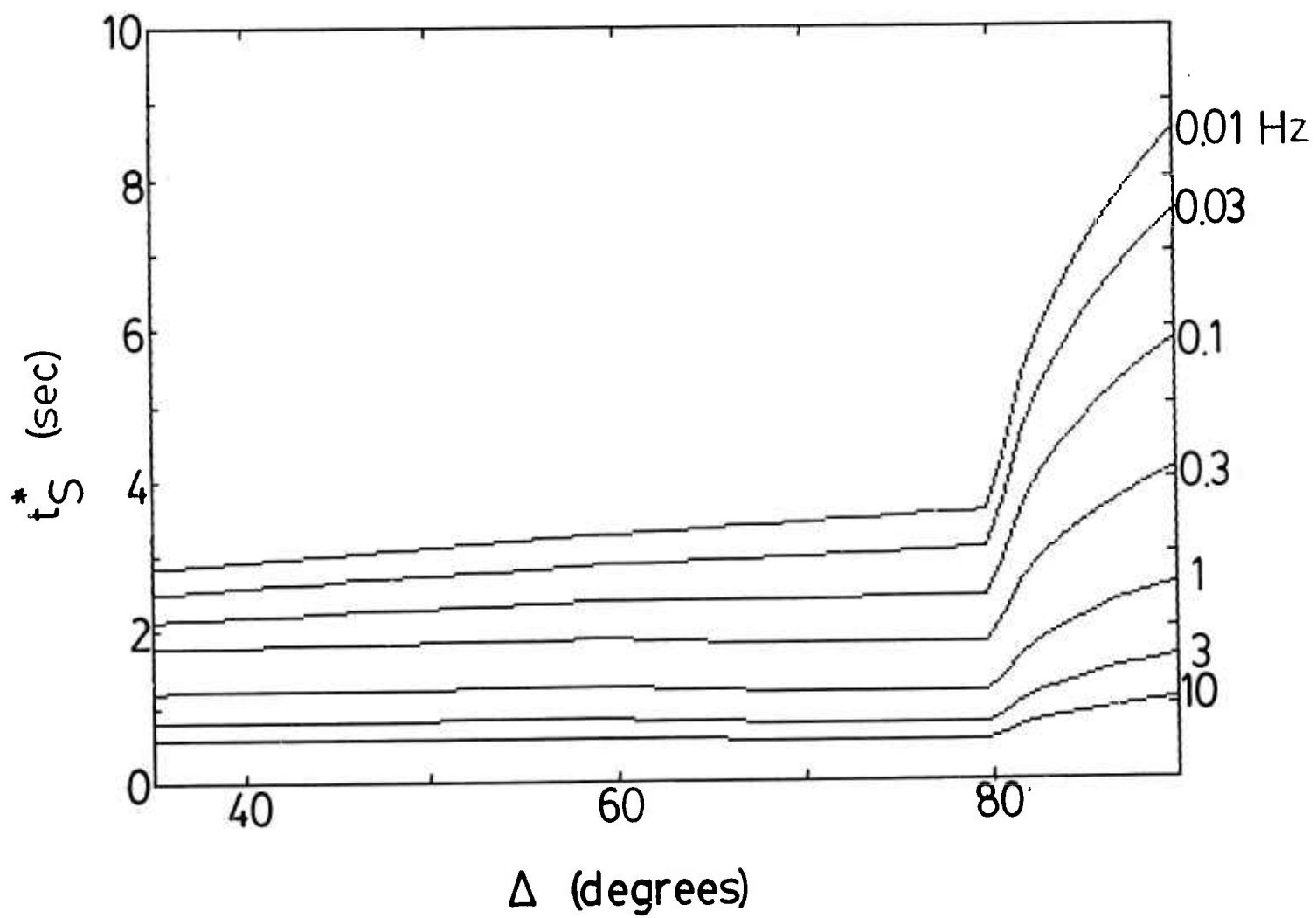


Figure 4

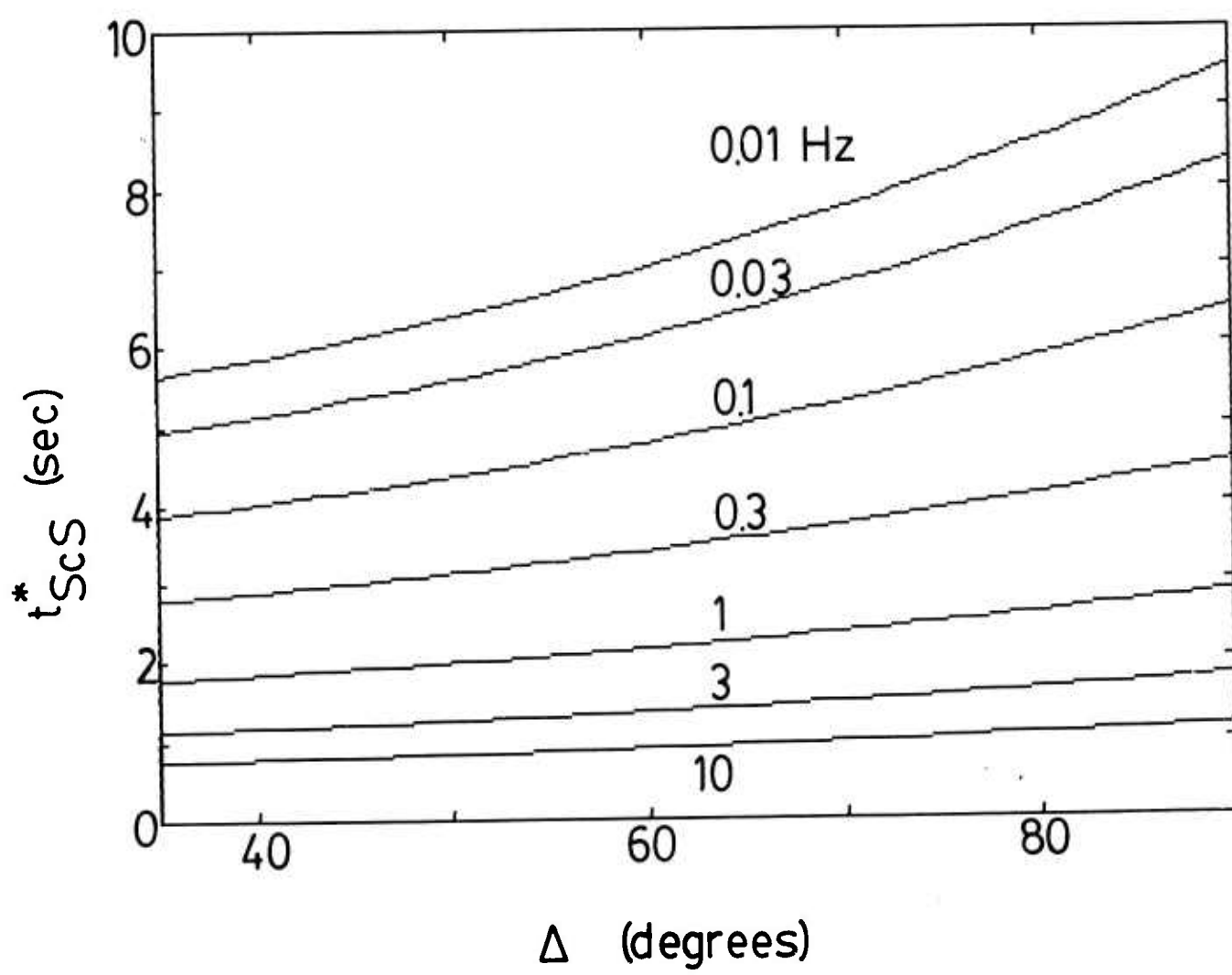


Figure 5

**Methodologies for Estimating  $t^*(f)$  from Short Period Body Waves  
and Regional Variations of  $t^*(f)$  in the United States**

Zoltan A. Der and Alison C. Lees

Teledyne Geotech  
314 Montgomery Street  
Alexandria, Virginia 22314

13 July 1984

revised 30 November 1984

submitted to *Geophys. J. Roy. astr. Soc.*

## Abstract

In this paper we discuss some aspects of estimating  $t^*$  from short period body waves and present some limits on  $t^*(f)$  models for the central and southwestern United States (CUS and SWUS). We find that for short period data, with frequencies above 1 or 2 Hz, while the average spectral shape is stable, the smaller details of the spectra are not; thus, only an average  $t^*$ , and not a frequency-dependent  $t^*$ , can be derived from such information. Also, amplitudes are extremely variable for short period data, and thus a great deal of data from many stations and azimuths must be used when amplitudes are included in attenuation studies.

The predictions of three pairs of models for  $t^*(f)$  in the central and southwestern United States are compared with time domain observations of amplitudes and waveforms and frequency domain observations of spectral slopes to put bounds on the attenuation under the different parts of the country. A model with the  $t^*$  values of the CUS and SWUS converging at low frequencies and differing slightly at high frequencies matches the spectral domain characteristics, but not the time domain amplitudes and waveforms of short period body waves. A model with  $t^*$  curves converging at low frequencies, but diverging strongly at high frequencies matches the time domain observations, but not the spectral shapes. A model with nearly-parallel  $t^*(f)$  curves for the central and southwestern United States satisfies both the time and frequency domain observations.

We conclude that use of both time and frequency domain information is essential in determining  $t^*(f)$  models. For the central and southwestern United States, a model with nearly-parallel  $t^*(f)$  curves, where  $\Delta t^* \sim 0.2$  seconds, satisfies both kinds of data in the 0.3-2 Hz frequency range.

## Introduction

In the last several years, there has been considerable progress in the study of attenuation in the mantle, including much work on the frequency dependence of  $Q$  across the seismic band. There is now a profusion of frequency dependent  $t^*$  models in the literature and in various research reports. Many of these have been derived from P wave spectra with heavy reliance on the details of the spectral shapes, especially at low frequencies. Others are derived from broad-band studies of time domain amplitudes and waveforms without using spectral information. A number of these studies have also shown that the anelastic attenuation is higher for paths crossing the upper mantle under the western United States than for paths under the central and eastern United States, and several pairs of models for frequency dependent  $t^*$  have been proposed for such paths.

There are differences and inconsistencies among the results mentioned above, often due to interpretation of only one aspect of the data or from use of inappropriate methods of data analysis. Thus, in the first part of this paper, we wish to point out some of the pitfalls of working with short period data by discussing the use and limitations of time domain and spectral domain information for the determination of  $t^*(f)$  in the 0.3-2 Hz range. Short period time domain amplitude data is subject to substantial variability, so large amounts of data must be averaged over a range of azimuths in order to draw significant conclusions. The site dependent fluctuations in the P wave spectral shapes are such that they preclude the reliable determination of the functional forms of  $t^*(f)$  from spectra of short period P waves arriving from a limited range of azimuths to any single station or a moderate sized array.

In the second part, we attempt to constrain the differences in  $t^*(f)$  between the central United States (CUS) and the southwestern United States (SWUS) by examining spectral and amplitude data for short period P and S waves in the two regions. Three



pairs of models for the two regions are examined, two with  $t_{CYS}^*(f)$  and  $t_{SWS}^*(f)$  converging at low frequencies and diverging at different rates at high frequencies, and one where  $t_{CYS}^*(f)$  and  $t_{SWS}^*(f)$  are nearly parallel. We find that the quasi-parallel model best matches both the spectral and amplitude data.

### Use of Time and Frequency Domain Information in Determining $t^*$

A variety of mutually complementary techniques are available for determining  $t^*(f)$  from such time and frequency domain information as changes in amplitudes, waveforms, and frequency spectra of body waves. At a constant frequency,  $t^*$  can be determined from the change in amplitude of a phase (relative to another phase or an assumed source), where

$$A = e^{-\pi f t^*}. \quad (1)$$

The waveforms and spectral ratios, on the other hand, are mostly shaped by the apparent  $t^*$ ,  $\bar{t}^*$ , which for a limited frequency band, may be written as:

$$\bar{t}^* = t^* + f (dt^* / df). \quad (2)$$

$\bar{t}^*$  can be determined directly from spectral measurements or spectral ratios:

$$\bar{t}^* = \frac{-1}{\pi} \frac{d(\ln A)}{df}. \quad (3)$$

Since the  $t^*(f)$  for given paths in the Earth probably represent superpositions of elementary absorption bands it is unlikely that they would correspond in their functional forms to any simple absorption band model although they are often modeled as such. Therefore, we chose to leave the functional forms unspecified and to be solely determined from the data.

Short period body wave amplitudes and waveforms are characterized by strong variations associated with small changes in the positions of the sources and receivers.

Since such changes are obviously not related to intrinsic attenuation, care must be taken when interpreting short period body wave data in terms of anelasticity and extensive use of statistical techniques is necessary. A significant advance in the understanding of these variations was made by Frasier & Filson (1972). They expressed the spectra of teleseismic P waves  $P_{ij}$  at an array as the product

$$P_{ij} = S_i T_j, \quad (4)$$

where the  $S_i$  are source amplitude spectra and  $T_j$  are the path response spectra. The attenuation factor along the path can be separated from the rest of  $T_j$  such that (4) may be written as

$$P_{ij} = S_i R_j e^{-\pi f t^*(f)}, \quad (5)$$

where  $f$  is frequency,  $R_j$  is the site response function (which includes all path effects except for the intrinsic attenuation), and the frequency dependent parameter  $t^*(f)$  is the ratio of the travel time and the average  $Q$  along the path.

Our ability to determine  $t^*(f)$  depends on how the parameters in (5) are behaving. A reasonable starting hypothesis with regards to  $t^*(f)$  is that it probably does not vary rapidly with small perturbations of the raypath. Below, we consider the effects of the parameters  $S_i$  and  $R_j$ .

The source spectrum,  $S_i$ , is assumed to be known in many studies of  $Q$  as there is a trade-off between the assumed source spectrum and the resultant  $t^*(f)$  model. Nevertheless, there is considerable disagreement as to some of the most basic properties of the source, even in the case of nuclear explosions. The high frequency falloff rate of far-field explosion spectra is probably between  $\omega^{-2}$  and  $\omega^{-3}$  (Mueller & Murphy 1971; von Seggern & Blandford 1972; Lay *et al* 1984). We favor a falloff rate less than  $\omega^{-3}$ , otherwise many teleseismic  $Q$  estimates from P waves would become negative (Der *et al* 1982b).

The site response spectrum,  $R_j$ , is responsible for the strong variations of P waveforms and amplitudes between closely spaced receivers at arrays (Mack 1969; Frasier & Filson 1972; Chang & von Seggern 1980). The physical causes of these variations are focusing and defocusing due to lateral heterogeneities in the Earth, local conversions to Rayleigh waves, and the like. Only in rare instances can the site effects be adequately modeled by the responses of plane-parallel layering. Since the nature of the site response function strongly influences estimates of  $Q$  and thus the choice of methodology for estimating  $t^*$ , we shall discuss its properties in some detail. The first important property of  $R_j$  is that at most sites it is strongly dependent on the slowness vector (azimuth-distance) of the arrival. The variations in the waveforms due to variations in the slowness vector are random and so can easily be separated from  $Q$  effects. Another important property of the site response function is that in the spectral domain its average slope is quite stable over a reasonably wide frequency range in the short period band, although there is considerable variation in the details of the individual spectral shapes. Figure 1 is a histogram of relative  $t^*$  measurements in the 0.5-4 Hz band between sets of pairs of sensors at NORSAR for 10 arbitrarily chosen seismic events at various azimuths. The standard deviation of this  $\Delta t^*$  population is 0.06 seconds, which indicates that this measurement, which reflects the variations in the gross shapes of the spectra, is quite stable across NORSAR. In practical terms, it means that only 5% of the measured values of  $\Delta t^*$  differ by more than 0.12 seconds from the average. This explains the fact that apparent  $t^*$  measurements, which characterize the broad-band gross spectral shapes in terms of a single parameter  $\bar{t}^*$  (per equation (3)), are usually comparable in various published studies (Fraser & Filson 1972; Nojonen 1975; Der & McElfresh 1977). Using the empirical formula  $\Delta m_b \sim 1.35\Delta t^*$  (Der *et al* 1979),  $\Delta t^* = 0.06$  seconds translates into  $\Delta m_b \sim 0.08$ . The actual variation of  $\Delta m_b$  as measured from amplitude variations is about 0.4 magnitude units, demonstrating that the average spectral shapes are more stable than the signal amplitudes. Of course, this experiment does not rule out the possibility of azimuthal bias in

attenuation estimates from limited source regions, but the statistics above indicate that this bias is probably not large in most cases.

Let us now investigate the stability of the details of the spectral shapes across an array. In Figure 2, sets of intersensor spectral ratios at NORSAR are shown for NTS and Kazakh nuclear explosions; use of ratios cancels out the source spectra. While the shapes of spectral ratios below 4 Hz are similar for the same pairs of sensors and test sites, as expected from above, the strong variations in these ratios with frequency indicates that details in the spectral shapes at any given site are unstable for arrivals from a limited source region. This result is not surprising, since waves propagated through media with random velocity variations commonly reveal variations in details of their spectra while the gross shapes are relatively constant after propagating roughly the same distance (Frankel & Clayton 1984). Moreover, even if one assumes a flat layered medium for a crustal structure, it would change the details in the spectral shapes, while leaving the overall slope relatively constant. Some studies, such as those of Lundquist & Samowitz (1981, 1982) did not consider the possibility of site related distortion and yielded quite improbable variations in  $t_p^*(f)$ . For instance, it is easy to see that applying this method to the data at NORSAR shown in Figures 2a and b would result in strong variations in  $t^*(f)$  values for neighboring raypaths, both of which do not seem very likely.

These problems with the details of spectral shapes can be reduced by either averaging measurements from P waves arriving from many azimuths (Der *et al* 1982a) or averaging the spectral shapes across arrays (Bache 1984). Figure 3 shows two examples of the average spectral shape of Soviet explosions as recorded at NORSAR over the 1-7 Hz band. Only spectral amplitudes within two orders of magnitude of the maximum amplitude and with a signal-to-noise power ratio of greater than 4 have been retained to assure that the data are significant and not affected by the gain ranging of the NORSAR instruments (Bungum 1983). The bounds are 95% confidence limits. Several  $t^*$  models, discussed later in this paper, are superimposed on each figure, and

it is clear that within the variance of the data a number of  $t^*$  models can describe the spectra. In a more extensive study, Bache (1984) stacked spectra at the United Kingdom arrays for suites of Soviet nuclear explosions and found that the stacked spectral ratio shapes can be fitted to a variety of different  $t_P^*$  models in the absence of constraints at lower frequencies. Thus, at least for the path from the Russian shield to northern Europe, while the averaged spectra are inconsistent with  $t^*$  models that are strongly frequency dependent at high frequencies, the variance in the spectral shapes is such that we cannot distinguish between a  $t^*$  which is independent of frequency and a  $t^*$  which varies slowly with frequency in the 1-7 Hz band.

The apparent  $t^*$  measurements, which are a reasonably stable estimate of the average  $t^*$  in the short period band, must thus be connected in some way to other kinds of data to define  $t^*(f)$ . A feasible approach is to combine apparent  $t_P^*$  measurements with short period S analyses and any available, reliable absolute  $t^*$  estimates in the intermediate and long period bands (Der *et al* 1982a). S waves are especially suitable for this type of study; observationally,  $t_S^* \sim 4t_P^*$  (Der *et al* 1980; Lay & Helmberger 1981; Der *et al* 1982a), so for a given path length, S waves are much more sensitive to the effect of Q than are P waves. Although several studies of Q indicate that some losses in compression may occur in the Earth (Sailor & Dziewonski 1978; Anderson & Given 1982), the need for such refinements requires further observational verification.

It must be pointed out that because of the focusing effects it would also be unreasonable to expect a good correlation between the apparent  $t^*$  measured from spectral slopes, and the body wave amplitudes measured at single sites from limited source regions. It is easy to imagine scenarios in which the body wave arrivals are systematically focused or defocused for most azimuths. The amplitudes of P waves are even more severely affected by the factor  $R_j$  than are the spectral shapes. It is not uncommon to see systematic variations in P wave amplitude between sensors exceeding a factor of 4-5 across large arrays for all arrivals from a limited source region (Chang & von Seggern 1980). Again, it may be hoped that azimuthal averaging will reduce such

biases. At any rate, amplitude patterns of P waves arriving from a limited range of azimuths have very little, if anything, to do with Q at individual recording sites (Butler 1984). In addition to variance due to focusing and defocusing across an array, scattering is an important phenomenon which is part of the  $t^*$  measurements, though it is difficult to separate the scattering and intrinsic components of attenuation (Richards & Menke 1983; Bache 1984; McLaughlin & Anderson 1984). This again points to the need to average amplitude and spectral measurements in estimating  $t^*$ , though there is much work still to be done on the effect of scattering contributions on  $t^*$ . Nevertheless, it is possible to distinguish among various types of  $t^*(f)$  models by combining amplitude, waveform, and spectral observations for both P and S waves in the short period band as illustrated below.

### **Constraints on $t^*(f)$ Models for the Central and Southwestern United States using Observations of Short-Period P and S Waves**

Several pairs of frequency dependent Q models have been proposed to explain the differences in observed short period P and S wave amplitudes, waveforms, and spectra between the central and southwestern United States. We shall limit our following discussions to these two regions since they show the largest regional differences in mantle Q structure in the United States, notably larger than the variations found between the eastern and western United States. (Solomon & Toksoz 1970; Der *et al* 1975; Butler & Ruff 1980).

These models fall into two categories. The first group is characterized by  $t^*(f)$  curves that converge to the same value at low frequencies. Such models are based on the idea of an "absorption band shift" where the low frequency limits of the absorption band are constant in all areas and the decrease of  $t_P^*$  (and  $t_S^*$ ) with frequency is determined by a single parameter,  $\tau_m$ . The convergent models proposed by Lay & Helm-

berger (1981) and Butler (1984) are nearly identical and have a strong frequency dependence for paths crossing the mantle under the eastern United States. These models were developed as bounds on the  $t^*$  variations in the United States to fit amplitude data for frequencies  $\leq 1$  Hz, and are used as an example of a strongly convergent model. Another pair of convergent  $t^*(f)$  models was proposed by Hadley & Mellman (1983) to explain the  $t^*$  and  $m_b$  differentials between NTS and RKON. This pair has a weak frequency dependence in order to fit the average apparent  $t_p^*$  estimates from spectral measurements across the United States.

The third pair of  $t^*(f)$  models do not converge at low frequencies and are quasi-parallel throughout the seismic band. This model was proposed by Der *et al* (1982a,b) in order to conform with some reported regional Q differentials at lower frequencies (Solomon & Toksoz 1970; Lee & Solomon 1975). The idea of regional Q differentials over a broad frequency range encompassing both the short and long period bands is further supported by regional variations in the Q estimates derived from long period ScS waves (Sipkin & Jordan 1979; Der *et al* 1984). It also appears to be a more natural choice if attenuation is a thermally activated process, in which case temperature increases in broad regions of the mantle would cause an increase in attenuation in a broad frequency band. Therefore, both theoretical considerations and the available, though few, results on the regional variations of Q in the long period band appear to indicate that regional Q differentials will exist in the long period band and the  $t^*$  curves do not converge. One can reach the same conclusion from short period observations alone, as we shall show below.

In Figure 4a we show graphs of the three  $t^*(f)$  pairs discussed above as models for the frequency dependence of attenuation along shield-to-shield (S-S) and shield-to-tectonic (S-T) types of paths; the corresponding  $\bar{t}^*$  curves are shown in Figure 4b. The convergent models with large and small  $t^*$  differentials at high frequencies are named **CS** (convergent, strong frequency dependence at high frequencies) and **CW** (convergent, weak frequency dependence at high frequencies), respectively; the quasi-parallel

model is named **QP**. Note the substantial variations in the 0.3-2 Hz range of  $\Delta t^*$  and  $\Delta \bar{t}^*$  for the S-S and S-T paths of the different models.

In this study, we are considering the central areas of the United States as part of the "shield"-type environment, while the more attenuating Basin and Range and Cordillerian areas of the United States are included under the label "tectonic". The events studied are deep earthquakes, so the source side of the raypath is not subject to upper mantle attenuation, and is thus considered as "shield", since previous work has shown that the  $t^*$  values for paths originating from deep earthquakes do not differ from those originating from near-surface events on shields (Der *et al* 1982b). We shall also use some results of regional studies of P and S wave amplitude and spectral variations between these two regions (Booth *et al* 1974; Der *et al* 1980, 1982a; Shore 1983; Butler 1984).

Any acceptable pair of  $t^*(f)$  models for shield-to-shield and shield-to-tectonic paths must satisfy a number of time domain and spectral constraints derived from observations. In this study, we look at the results of analyses of short period data from WWSSN and LRSM stations in the United States. Though the WWSSN and LRSM instruments have slightly different responses, the results from the different studies are similar. In the time domain, the CUS-SWUS contrast is about a factor of 2 or 3 in P-wave amplitudes around 1-2 Hz (Booth *et al* 1974; Butler & Ruff 1980; Der *et al* 1982a), with a slight increase of the average periods in the WUS to 0.9 seconds as compared to 0.7 seconds in the EUS (Der *et al* 1982a). S waves around 0.3-1 Hz have amplitudes that average 6-10 times larger in the CUS than in the SWUS as seen by typical short period instrumentation (Lay & Helmberger 1981; Der *et al* 1982a). For these S wave amplitude ratios, the effects of sediment amplification are unimportant and the large differentials must thus be attributed to lateral variations of mantle Q (Der *et al* 1982a). Depending on the observed S wave period seen in the CUS, which presumably shows the original source pulse with less modification due to Q, there is a varying amount of pulse broadening in the S waves seen in the SWUS. If the S wave has a high frequency



character in the CUS the S wave period increases considerably in the SWUS for the same event, sometimes from 1 second to more than 3 seconds. If the source has a low frequency character no great change in the pulse shape is evident (Der *et al* 1980). This is in agreement with the results of numerical experiments on broad-band and narrow-band signals (Der & McElfresh 1980).

In the spectral domain, estimates of  $t_p^*$  for the shield-to-tectonic type of path are around 0.45 seconds and for shield-to-shield paths the value is around 0.2 seconds (Der & McElfresh 1976, 1977; Der *et al* 1984), consistent with the differential in  $\bar{t}_p^*$  between the CUS and the SWUS of around 0.2-0.25 seconds (Der & McElfresh 1977; Der *et al* 1982a; Shore 1983) in the short period band. The differential in apparent  $t_s^*$  is about 3 to 4 times that of  $t_p^*$  (Der *et al* 1980, 1982a; Lay & Helmberger 1981), thus supporting the idea that most differential Q losses occur in shear deformation. Table 1 presents a summary of these time and frequency domain constraints for P and S waves. Figure 5 shows representative S waves at CUS and SWUS WWSSN stations, with the appropriate gain factors noted next to the waveform. The difference in both amplitude and period between S waves from the same event arriving in the CUS and the SWUS is quite striking.

It is also interesting to consider how the regional variations of  $t^*$  correlate with other geophysical properties. As others have noted there seems to be a substantial correlation between the  $t^*$  variations discussed above and the travel time delays across the United States as reported by Cleary & Hales (1966), Herrin & Taggart (1968), and Sengupta & Julian (1976). The major features of their results include large delays in the Basin and Range and SWUS, early arrivals through the CUS shield region, and slightly late arrivals along the Atlantic seaboard and in New England, very similar to the variations in  $t^*$  that were outlined above. Heat flow and the available electrical conductivity data have also been found on a broad scale to follow similar patterns across the United States (Roy *et al* 1972; Gough 1984). These correlations of  $t^*$  variations with travel time anomalies, heat flow, and thermal conductivity are consistent

with the idea that temperature is an important parameter in the physics of attenuation mechanisms.

Now, we investigate how the models in Figure 4 fit the variety of observations given in Table I. Figures 6, 7, and 8 show simulated waveforms for the three  $t^*(f)$  pairs for a variety of source pulse durations. The Ohnaka pulse (Hermann & Kijko 1983) was used for the source function since this type of waveform does not produce some of the peculiar looking waveforms which can result from the corners of the triangular or trapezoidal source pulses that are commonly used in calculating such synthetics. The source is then convolved with both a WWSSN short period instrument response and the appropriate  $t^*(f)$  to model the P and S waveforms. The period of each waveform and the amplitude ratio of each pair of waveforms is also shown in the figures.

From Figures 6, 7, and 8, it is clear that the three  $t^*(f)$  models have substantially different effects on the waveforms. There are significant differences in both the S-S/S-T amplitude ratios and the amount of waveform spreading predicted by the three models. The amplitude and period variations in these figures were used to judge the fit of the various models to the time domain constraints outlined above. To judge the fit of the models to spectral constraints we use the apparent  $t^*$  graphs shown in Figure 4b.

The **CW** model, with  $t^*$  convergent at low frequencies and small differences in  $t^*$  at higher frequencies was designed to fit the observed  $\bar{t}^*$  differentials around 1 Hz, and thus it is consistent with the spectral domain constraints. However, the model fits neither the observed P or S wave amplitudes or periods. Because this model has high values of  $t^*$  in the 0.5 to 2 Hz range, it produces relatively long period synthetics, even for a source modeled as an impulse. The shortest period shield-shield P and S waves that this model predicts are 0.75 and 2.6 seconds, respectively, while much shorter period P and S waves are observed at central United States WWSSN stations. This model also predicts S-S/S-T amplitude ratios for P and S waves of around 1.3, much less than observed, especially for S waves. In the **CW** model,  $t^*(f)$  varies rapidly with

frequency around 1 Hz to give the desired  $\Delta \bar{t}^*$  differential. Thus, while  $\Delta \bar{t}^*$  is large,  $\Delta t^*$  is relatively small as seen in Figures 4a and b, which explains the relatively small amplitude ratios.

The **QP** and **CS** models are both consistent with the observed S-S/S-T amplitude ratios for P and S waves. However, a much longer source duration is needed by the **CS** model relative to the **QP** model to produce the appropriate S-S periods. Within the considerable scatter of the data, both models also agree with the difference in period of P and S arrivals between the shield-shield and shield-teetonic paths, again, for the appropriate initial S-S periods. The **CS** model tends to predict a much larger increase in period between spreading of pulses which arrive in a teetonic region and those which arrive in a shield region than observed, though the model cannot be ruled out when the variation in the data is considered.

The major differences between the **QP** and **CS** models appear when the spectral data, or the relative  $\bar{t}^*$ s are considered. The **CS** model predicts  $\Delta \bar{t}_P^* \sim 0.7$  seconds or  $\Delta \bar{t}_S^* \sim 2.9$  seconds around 1 Hz, about three times the observed values. These very large  $\bar{t}^*$  differentials are due to the large  $t^*$  differentials and the substantial frequency dependence around 1 Hz in this model. On the other hand, the **QP** model predicts  $\Delta \bar{t}_P^* \sim 0.2$  seconds or  $\Delta \bar{t}_S^* \sim 0.8$  seconds, in reasonable agreement with the observations.

While the **QP** model is consistent with the data, it can still be refined. The  $t^*$  curves could be somewhat more divergent around 1 Hz, slightly increasing the model predictions of the S-S/S-T amplitude ratios and of  $\Delta \bar{t}^*$ .

This comparison of the short period time and spectral domain data with the predictions of different pairs of  $t^*$  models emphasizes the importance of utilizing both the time domain and spectral information in developing a  $t^*$  model. The analyses above mostly constrain the differentials in the  $t^*(f)$  for the two types of paths, but allow a considerable variation in the absolute values in  $t^*(f)$  at low frequencies. These values have to be determined independently in the long and intermediate period bands.

## Summary and Conclusions

In this paper, we have discussed the importance of utilizing both time and spectral domain information in developing  $t^*$  models and the limitations in using the various kinds of data. For short period data, while the average spectral shape is stable, the small details of the spectra are not; thus, such information can only be used to generally constrain  $t^*$  and not to fit a specific model to the data. Also, amplitudes are very variable for short period data as evidenced from array recordings; thus to use short period amplitude data in attenuation studies, a great deal of data from many stations and azimuths is needed to have confidence in the results.

To put bounds on the attenuation under the central and southwestern United States, we compared the amplitude, waveform, and  $\Delta t^*$  predictions of three models with observations from short period P and S waves. The models included two where the values of  $t^*$  for the S-S and S-T paths converged at low frequencies, with strong and weak frequency dependence at the high frequencies, respectively, and one where the  $t^*$  curves for the two paths are roughly parallel. Even given the considerable scatter in the amplitude and waveform data, the observations ruled out the two convergent models. The convergent model with the small  $t^*$  differential at high frequencies was consistent with observed differentials in apparent  $t^*$  between the eastern and western United States, but did not predict large enough amplitude or period variations between the EUS and the WUS. The convergent model with the large  $t^*$  differential correctly predicted the observed amplitude ratios and waveform period differentials between the EUS and WUS, but predicted a much larger  $\Delta t^*$  between the two regions than is observed. The quasi-parallel model provides a reasonable fit to both the time and frequency domain observations.

From the above analyses, we conclude that models which converge towards low frequencies are not acceptable representations of attenuation under the United States,

and thus that a shifting absorption band model may not be appropriate for modeling regional variations in attenuation. Actually, it may not be physically reasonable to model attenuation with a single broad absorption band of prescribed shape, as it is generally assumed that the net  $t^*(f)$  is the result of superposition of many elementary absorption bands. This work also demonstrates the importance of making full use of both time and frequency domain data in developing  $t^*$  models and that the differences among the manifestations of the various alternative models are quite distinct in the short period band.

### **Acknowledgements**

The authors gratefully acknowledge the assistance of Jim Burnetti, Pamela Klouda, Peggy Marshall, and Tom McElfresh. This research was supported by the Defense Advanced Research Projects Agency and monitored by the Air Force Office of Scientific Research, under contract number F49620-83-C-0040.

## References

- Anderson, D.L. & Given, J.W., 1982. Absorption band Q model for the earth, *J. Geophys. Res.*, **87**, 3893-3904.
- Bache, T.C., 1984. Q and its effects on short period P waves from explosions in central Asia, *SAI-84/1589*, Science Applications, Inc., La Jolla, CA.
- Booth, D.C., Marshall, P.D. & Young, J.B., 1974. Long and short period P-wave amplitudes from earthquakes in the range  $0^{\circ}$ - $114^{\circ}$ , *Geophys. J. R. astr. Soc.*, **39**, 523-537.
- Bungum, H., 1983. Power spectral bias sources and quantization levels, in NORSAR Scientific Report No. 2-82/83, Semiannual Technical Summary 1 October 1982 - 31 March 1983, ed. L.B. Tronrud, 65-71.
- Butler, R., 1984. Azimuth, energy, Q, and temperature: Variations on P wave amplitudes in the United States. *Rev. Geophys. Space. Phys.*, **22**, 1-36.
- Butler, R. & Ruff, L., 1980. Teleseismic short-period amplitudes: source and receiver variations, *Bull. Seism. Soc. Am.*, **70**, 831-850.
- Chang, A.C. & von Seggern, D.H., 1980. A study of amplitude anomaly and  $m_b$  bias at LASA subarrays, *J. Geophys. Res.*, **85**, 4811-4828.
- Cleary, J. & Hales, A.L., 1966. An analysis of the travel times of P waves to North American stations, in the distance range  $32^{\circ}$  to  $100^{\circ}$ , *Bull. Seism. Soc. Am.*, **56**, 467-489.
- Der, Z.A., Masse, R.P. & Gurski, J.P., 1975. Regional attenuation of short-period P and S waves in the United States, *Geophys. J. R. astr. Soc.*, **40**, 85-106.
- Der, Z.A. & McElfresh, T.W., 1976. Short-period P wave attenuation along various paths in North America as determined from P wave spectra of the SALMON nuclear explosion, *Bull. Seism. Soc. Am.*, **66**, 1609-1622.
- Der, Z.A. & McElfresh, T.W., 1977. The relationship between anelastic attenuation and regional amplitude anomalies of short-period P waves in North America, *Bull. Seism. Soc. Am.*, **67**, 1303-1317.
- Der, Z.A. & McElfresh, T.W., 1980. Time domain methods, the values of  $t_P^*$  and  $t_S^*$  in the short-period band and regional variations of the same across the United States, *Bull. Seism. Soc. Am.*, **70**, 921-924.

- Der, Z.A., MeElfresh, T.W. & Mrazek, C.P., 1979. Interpretation of short-period P-wave magnitude anomalies at selected LRSM stations, *Bull. Seism. Soc. Am.*, **69**, 1149-1160.
- Der, Z.A., Smart, E. & Chaplin, A., 1980. Short-period S wave attenuation in the United States, *Bull. Seism. Soc. Am.*, **70**, 101-126.
- Der, Z.A., MeElfresh, T.W. & O'Donnell, A., 1982a. An investigation of the regional variations and frequency dependence of anelastic attenuation in the mantle under the United States in the 0.5-4 Hz band, *Geophys. J. R. astr. Soc.*, **69**, 67-100.
- Der, Z.A., Rivers, W.D., MeElfresh, T.W., O'Donnell, A., Klouda, P.J. & Marshall, M.E., 1982b. Worldwide variations in the attenuative properties of the upper mantle as determined from spectral studies of short-period body waves, *Phys. Earth Planet. Int.*, **30**, 12-25.
- Der, Z.A., Lees, A.C., Anderson, L.M., Burnetti, J.A., Marshall, M.E., MeElfresh, T.W. & Wagner, R., 1984. Frequency dependence of Q in the mantle underlying the shield areas of Eurasia, *AL-84-1*, Teledyne Geotech, Alexandria, VA.
- Frankel, A. & Clayton, R.W., 1984. A finite difference simulation of wave propagation in two-dimensional random media. (Submitted to the Bull. Seism. Soc. Am.).
- Frasier, C.W. & Filson, J., 1972. A direct measurement of the earth's short-period attenuation along a teleseismic ray path, *J. Geophys. Res.*, **77**, 3782-3787.
- Gough, D.I., 1984. Mantle upflow under North America and plate dynamics, *Nature*, **331**, 428-433.
- Hadley, D.M. & Mellman, G.R., 1983. Estimation of  $\delta m_b$  from  $\delta t^*$  measurements, (Topical Report), *SGI-R-83-093*, Sierra Geophysics, Redmond, WA.
- Hermann, R.B. & Kijko, A., 1983. Modeling some empirical vertical component  $L_g$  relations, *Bull. Seism. Soc. Am.* **73**, 157-171.
- Herrin, E. & Taggart, J., 1968. Regional variations in P travel times, *Bull. Seism. Soc. Am.*, **58**, 1325-1337.
- Lay, T. & Helmberger, D.V., 1981. Body wave amplitude patterns and upper mantle attenuation variations across North America, *Geophys. J. R. astr. Soc.*, **66**, 691-726.
- Lay, T., Helmberger, D.V. & Harkrider, D.G., 1984. Source models and yield-sealing relationships for underground nuclear explosions at Amchitka Island, *Bull. Seism. Soc. Am.*, **74**, 843-862.

- Lee, W.B. & Solomon, S.C., 1975. Inversion schemes for surface wave attenuation and  $Q$  in the crust and upper mantle, *Geophys. J. R. astr. Soc.*, **43**, 47-71.
- Lundquist, G.M. & Samowitz, I.R., 1981. Inversion for  $U^*(f)$ , *SGI-R-81-052*, Sierra Geophysics, Redmond, WA.
- Lundquist, G.M. & Samowitz, I.R., 1982. Relative attenuation properties for 12 paths about the Kazakh test site, *SGI-R-82-064*, Sierra Geophysics, Redmond, WA.
- Mack, H., 1969. Nature of short-period P wave signal variations at LASA, *J. Geophys. Res.*, **74**, 3161-3170.
- McLaughlin, K.L. & Anderson, L.M., 1984. Stochastic dispersion of seismic waveforms due to scattering and multipathing (abstract), *Earthquake Notes*, **55**, 27.
- Mueller, R.A. & Murphy, J.R., 1971. Seismic characteristics of underground nuclear detonations, *Bull. Seism. Soc. Am.*, **61**, 1675-1692.
- Noponen, I. 1975. Compressional wave-power spectrum from seismic sources, *ISNB-45-0538-7*, Institute of Seismology, University of Helsinki, Contract AFOSR-72-2377 (Final Report).
- Richards, P.G. & Menke, W., 1983. The apparent attenuation of a scattering medium, *Bull. Seism. Soc. Am.*, **73**, 1005-1021.
- Roy, R.F., Blackwell, D.D. & Decker, E.R., 1972. Continental heat flow, in *The Nature of the Solid Earth*, ed. E.C. Robertson, McGraw-Hill Inc., New York, 506-543.
- Sailor, R.V. & Dziewonski, A.M., 1978. Measurements and interpretation of normal mode attenuation, *Geophys. J. R. astr. Soc.*, **53**, 559-581.
- Sengupta, M.K. & Julian, B.R., 1976. P-wave travel times from deep earthquakes, *Bull. Seism. Soc. Am.*, **66**, 1555-1579.
- Shore, M.J. 1983. Short period P-wave attenuation in the middle and lower mantle of the earth, *VSC-TR-83-7*, VELA Seismological Center, Alexandria, Virginia.
- Sipkin, S.A. & Jordan, T.H., 1979. Frequency dependence of  $Q_{ScS}$ , *Bull. Seism. Soc. Am.*, **69**, 1055-1079.
- Solomon, S.C. & Toksoz, M.N., 1970. Lateral variation of attenuation of P and S waves beneath the United States, *Bull. Seism. Soc. Am.*, **60**, 819-838.



von Seggern, D.H. & Blandford, R.R., 1972. Source time functions and spectra from underground nuclear explosions, *Geophys. J. R. astr. Soc.*, **31**, 83-97.

Table I

S Waves			
period for shield-to-shield paths (seconds) $T_{S-S}$	period for shield-to-tectonic paths (seconds) $T_{S-T}$	amplitude ratios for shield-to-shield and shield-to-tectonic paths $A_{S-S}/A_{S-T}$	$\Delta t^*$
1.3	2.5	8	0.6-0.8
1.8	3	5	
2.3	3.4	3.5	

P Waves			
period for shield-to-shield paths (seconds) $T_{S-S}$	period for shield-to-tectonic paths (seconds) $T_{S-T}$	amplitude ratios for shield-to-shield and shield-to-tectonic paths $A_{S-S}/A_{S-T}$	$\Delta t^*$
0.7	0.9	2-3	0.2-0.25

References in the text.

Since the typical period of S waves with shield-to-shield paths varies among events, the S wave part of the table includes periods for S-T paths and relative amplitude ratios corresponding to three different predominant periods for S-S paths.

**Figure 1.** Relative  $t^*$  between subarrays at NORSAR for ten teleseismic events.

**Figure 2a.** Intersensor spectral ratios for a set of NTS nuclear explosions at NORSAR.

**Figure 2b.** The same as Figure 2a, except that the intersensor spectral ratios are for a set of Kazakh explosions at NORSAR.

**Figure 3.** Array averaged power spectra at NORSAR of (a) a Soviet peaceful nuclear explosion on 24 November 1972 and (b) a Kazakh explosion on 10 July 1973. The bounds are 95% confidence limits. Theoretical spectra derived using a von Seggern-Blandford (1972) source model and various  $t^*$  models are superimposed on the averaged spectra. The other  $t^*$  models used in this figure are the quasi-parallel (QP), weakly convergent (CW), and strongly convergent (CS) models, all for shield-to-shield (S-S) paths. These  $t^*$  models are shown in Figure 4a.

**Figure 4.** (a)  $t^*(f)$  and (b)  $\bar{t}^*(f)$  models discussed in the text and used for the waveform synthetics in Figures 6, 7, and 8.  $t_S^* = 4t_P^*$  has been assumed.

**Figure 5.** Short period S waveforms from WWSSN stations in the United States. For each event noted on the left, a waveform is shown from a station in the central United States (center) and a station in the southwestern United States (right). For each waveform, the station designation, the short period instrument orientation, the instrument gain in thousands, and the period of the S phase are shown listed from top to bottom. The CUS/SWUS S wave amplitude ratio  $[A_S = (A_{S_z}^2 + A_{S_N}^2 + A_{S_E}^2)^{1/2}]$  is noted between each pair of waveforms for the cases where all three components were available at both stations.

**Figure 6.** Synthetic P and S waveforms corresponding to the S-S and S-T paths for the QP  $t^*$  model shown in Figure 4a and a short period WWSSN instrument response. The source pulses are shown on the left; all of the time series are longer than shown, so that none of the source or synthetic pulses have been truncated. The S-S/S-T peak-to-peak amplitude ratio is shown between each pair of waveforms, and the period is written below each waveform in italics.

**Figure 7.** Synthetic P and S waveforms corresponding to the S-S and S-T paths for the CS  $t^*$  model shown in Figure 4a and a short period WWSSN instrument response. The source pulses are shown on the left; all of the time series are longer than shown, so that none of the source or synthetic pulses have been truncated. The S-S/S-T peak-to-peak amplitude ratio is shown between each pair of waveforms, and the period is written below each waveform in italics.

**Figure 8.** Synthetic P and S waveforms corresponding to the S-S and S-T paths for the CW  $t^*$  model shown in Figure 4a and a short period WWSSN instrument response. The source pulses are shown on the left; all of the time series are longer than shown, so that none of the source or synthetic pulses have been truncated. The S-S/S-T peak-to-peak amplitude ratio is shown between each pair of waveforms, and the period is written below each waveform in italics.

# RELATIVE $t^*$ MEASUREMENTS ACROSS NORSAR

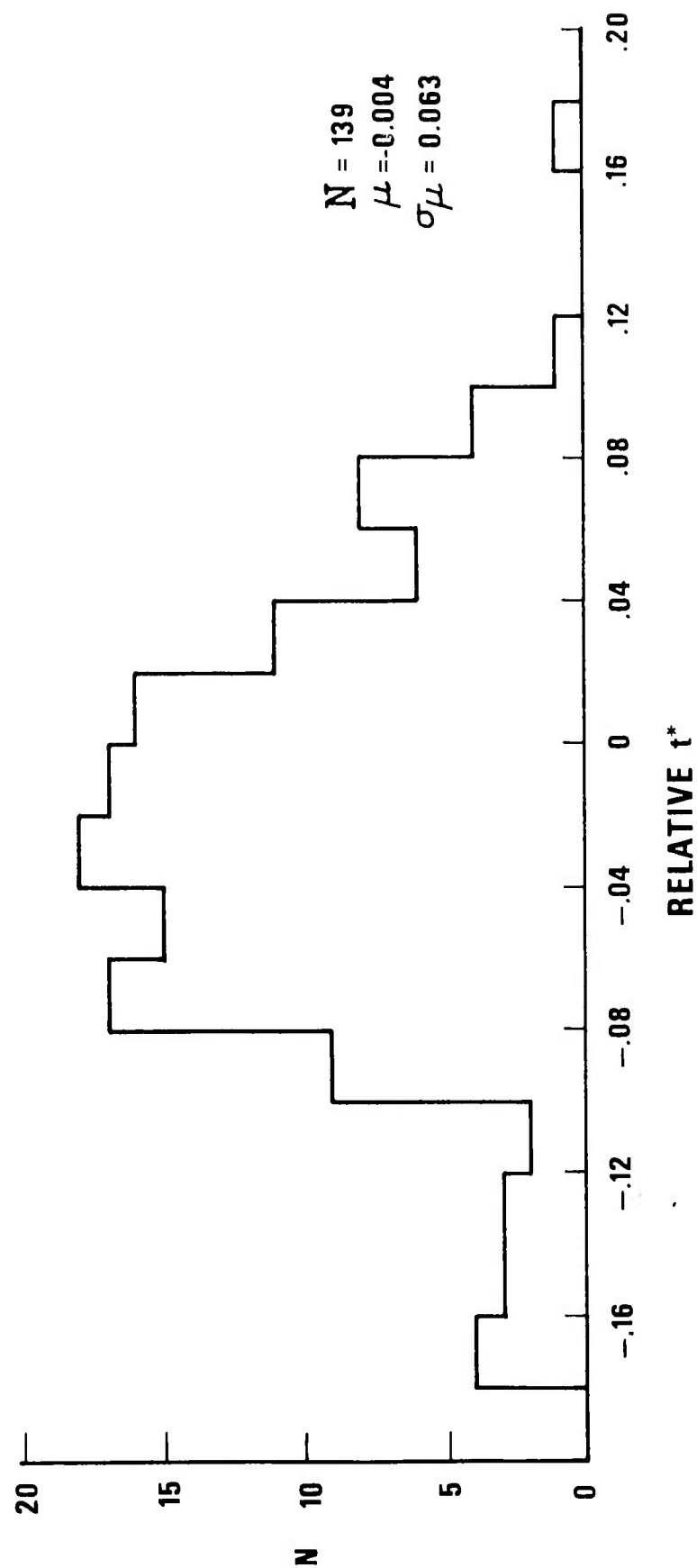


Figure 1

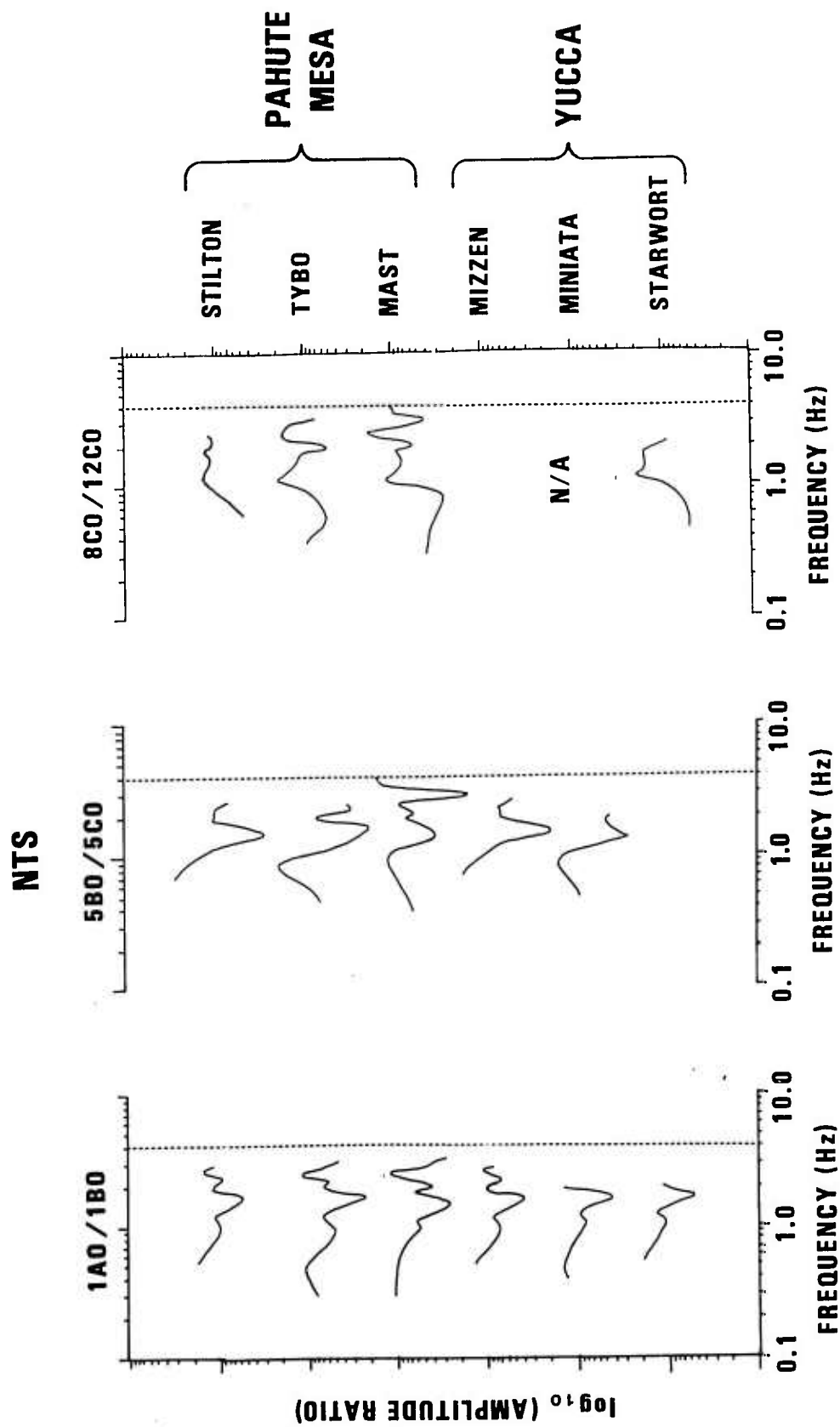


Figure 2a

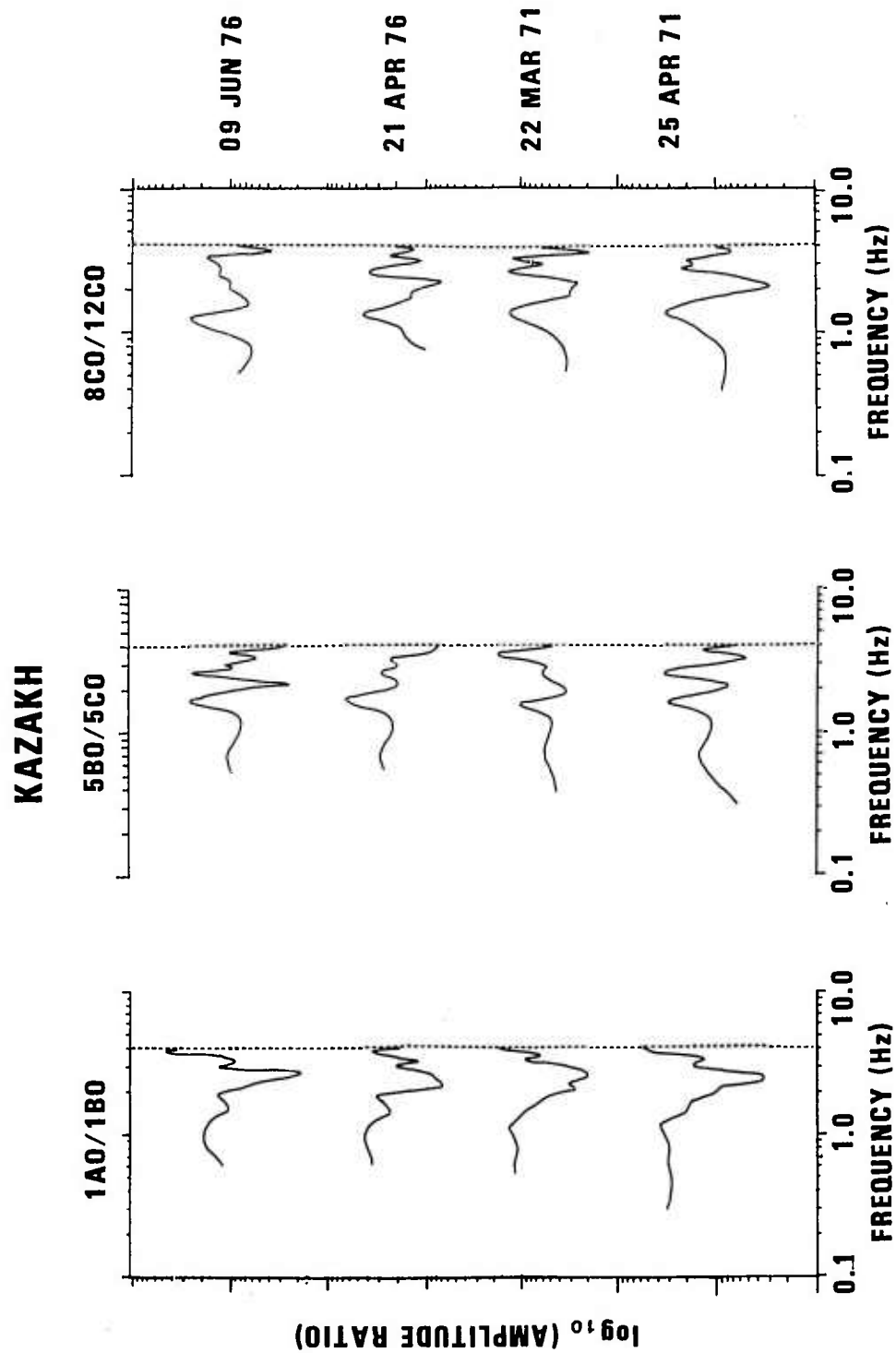
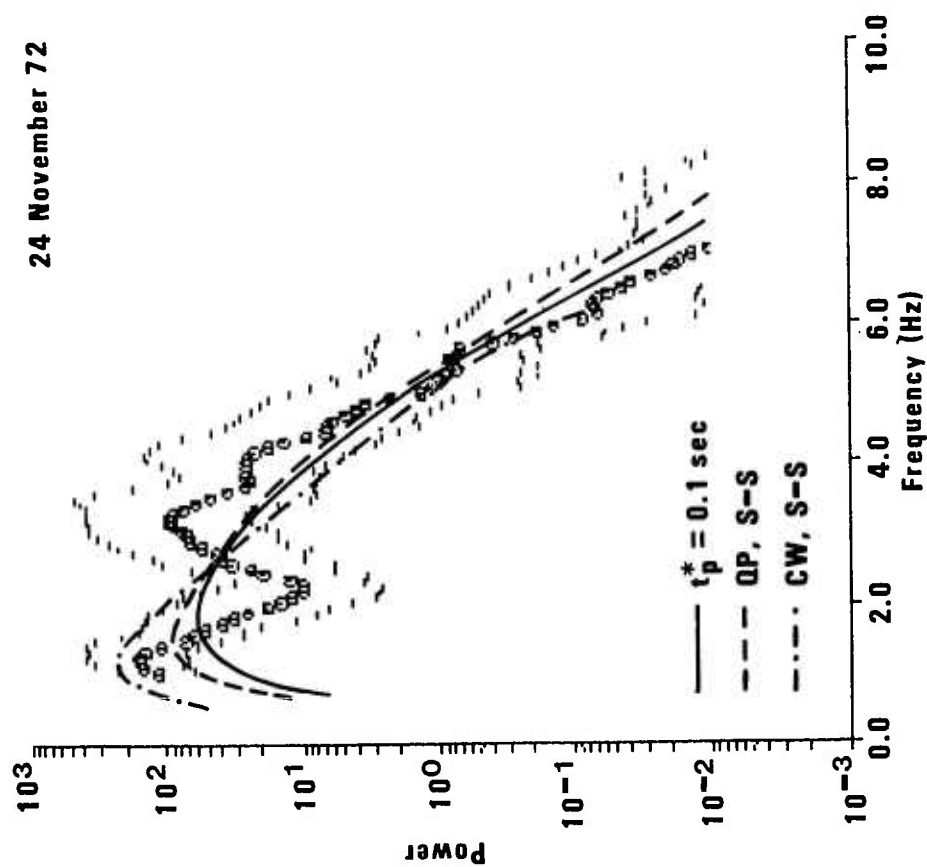


Figure 2b

(a)

24 November 72



(b)

10 July 73

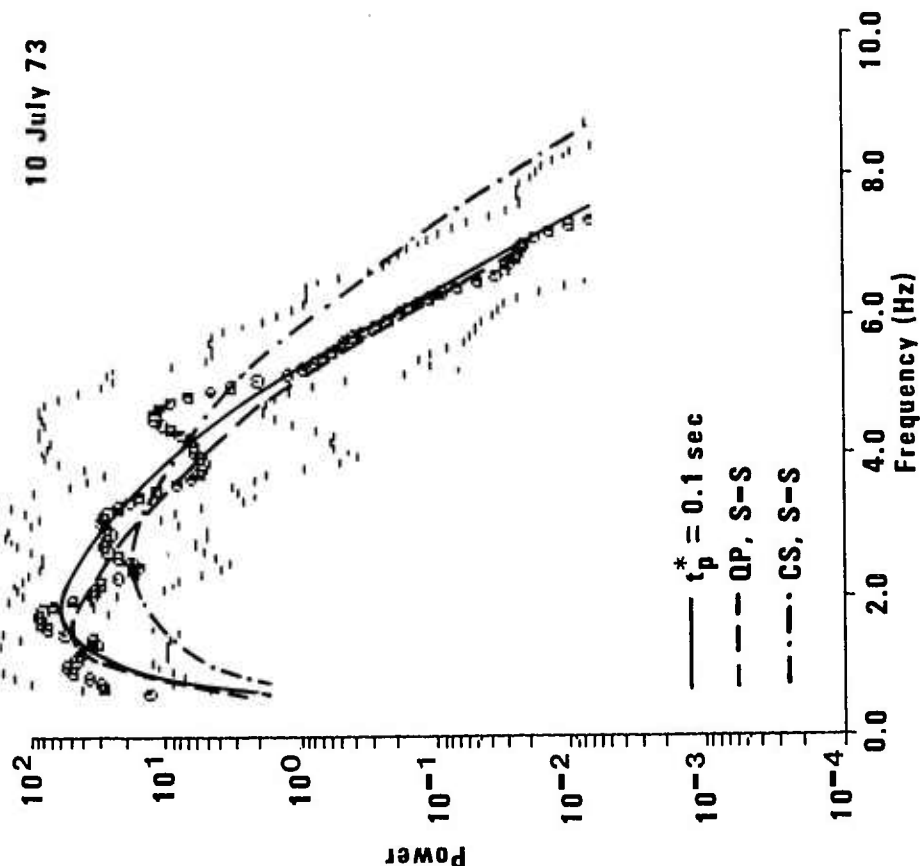


Figure 3

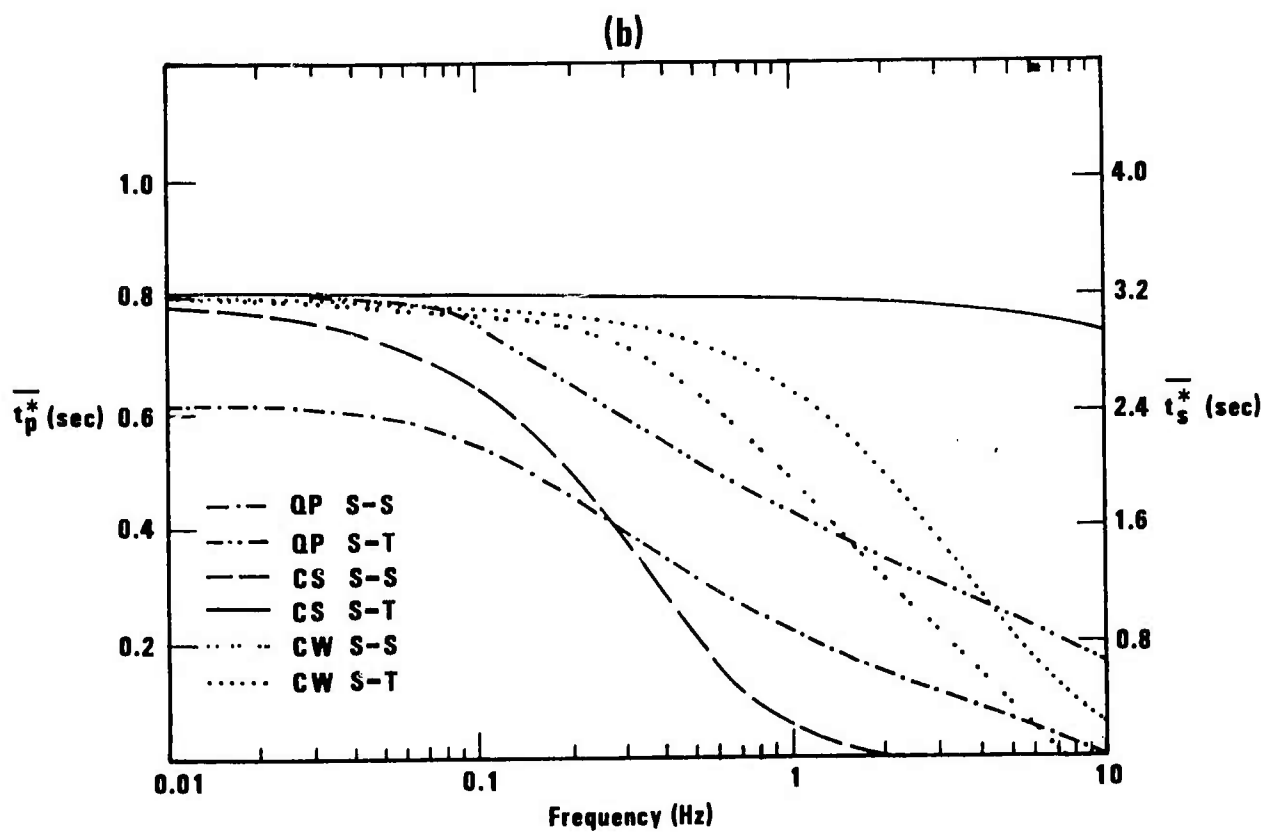
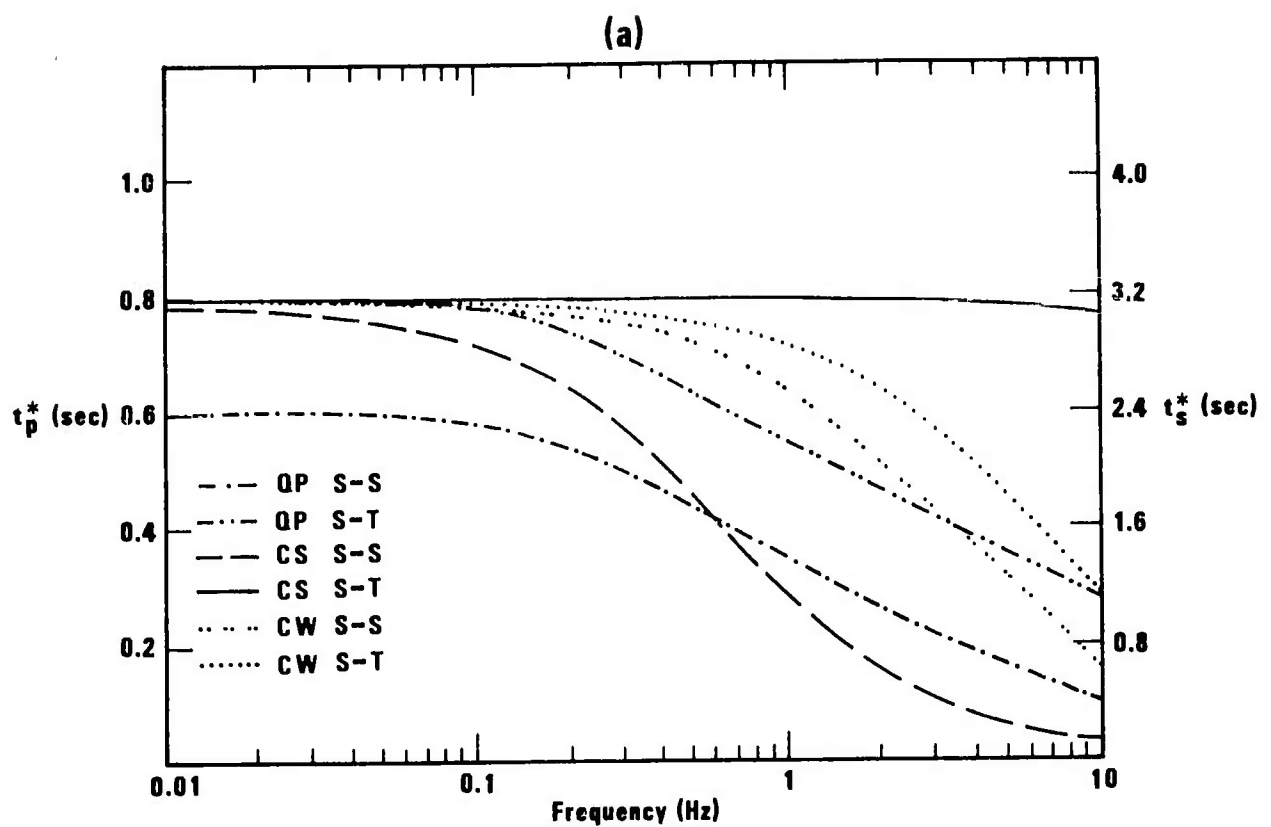
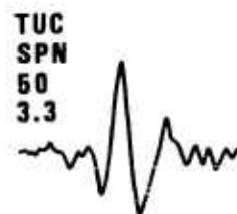


Figure 4



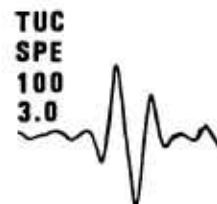
10 NOV 63  
01:00:38.8  
9.2S, 71.4W  
600 km,  $m_b$  5.6



9 DEC 64  
13:35:42.4  
27.5S, 63.2W  
586 km,  $m_b$  5.9



9.8



9 DEC 64  
13:35:42.4  
27.5S, 63.2W  
586 km,  $m_b$  5.9



6.4



3 NOV 65  
01:39:03.1  
9.1S, 71.4W  
593 km,  $m_b$  6.2



12



18 MAR 64  
04:37:26.9  
52.5N, 153.6E  
438 km,  $m_b$  5.6



6.8



18 MAR 64  
04:37:26.9  
52.5N, 153.6E  
438 km,  $m_b$  5.6



6.5



Figure 5

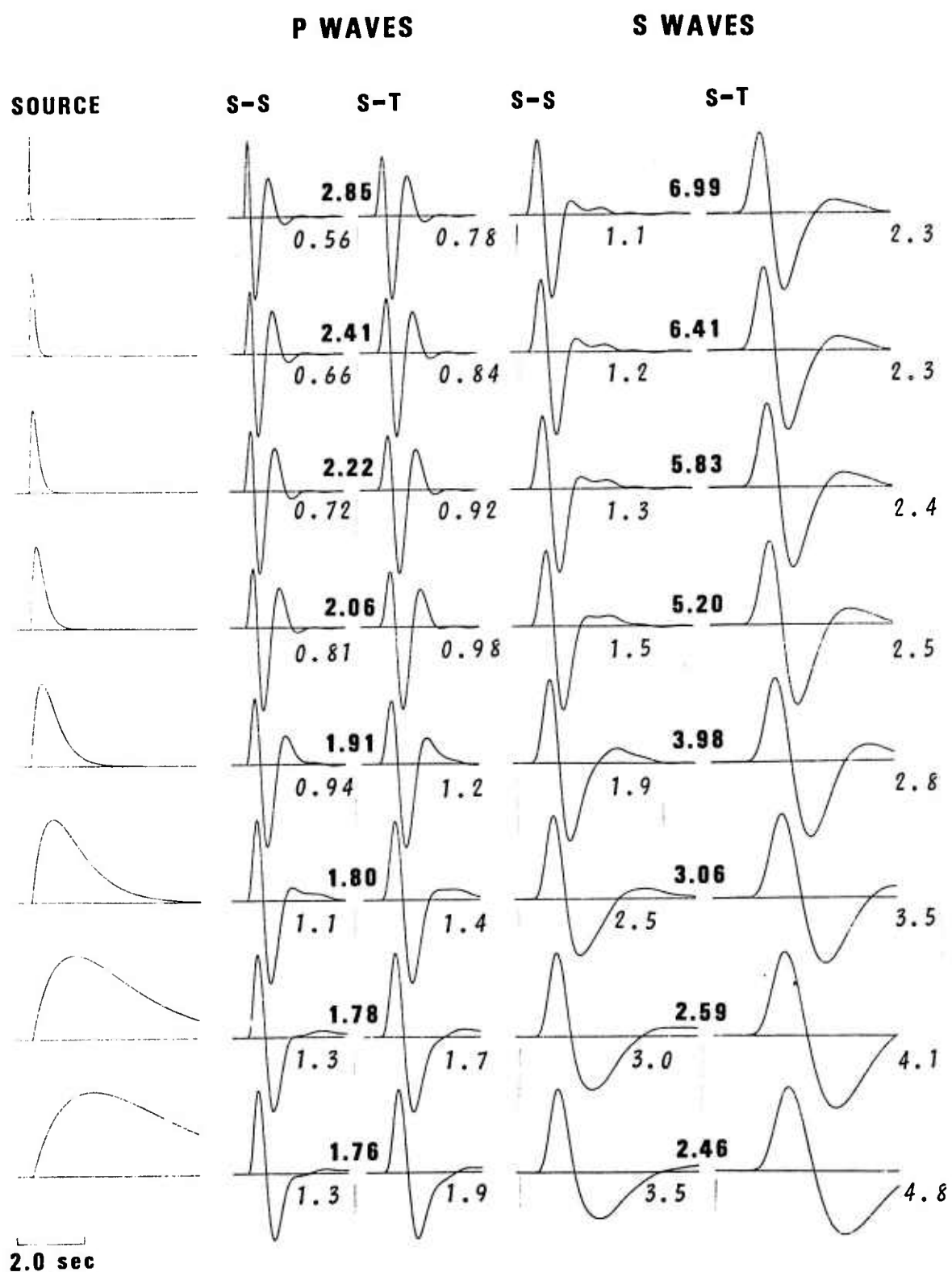


Figure 6

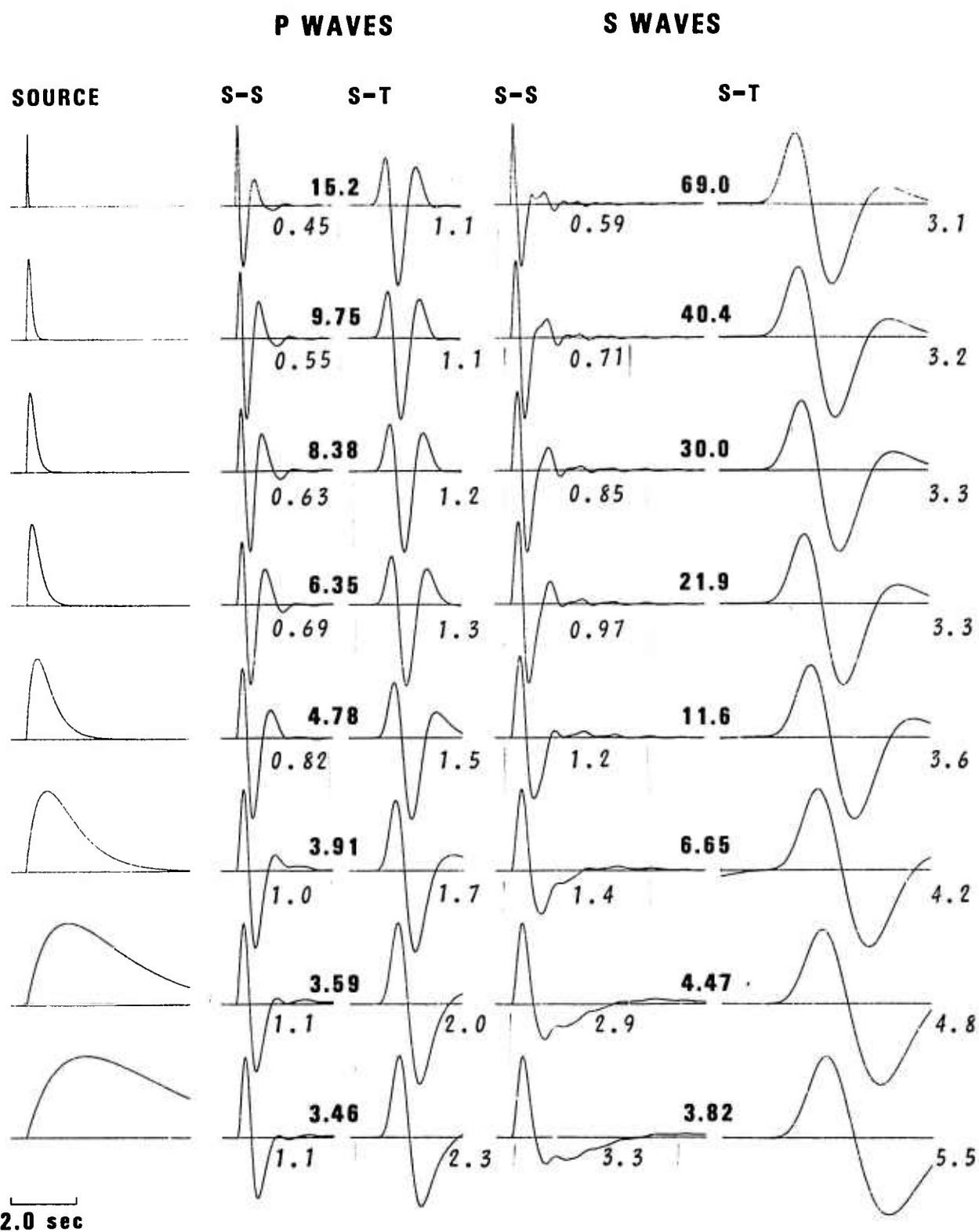


Figure 7

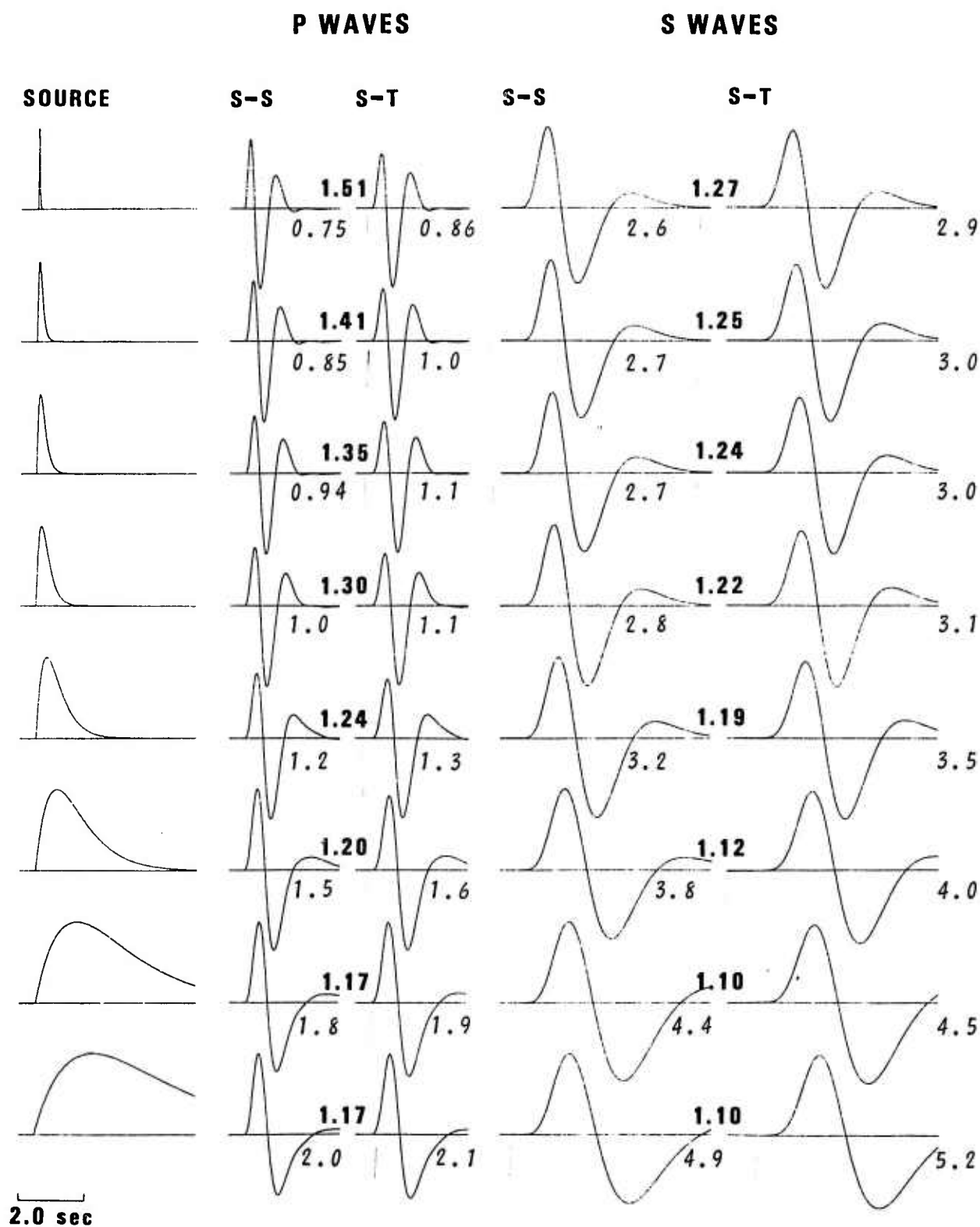


Figure 8